Università degli Studi di Cassino e del Lazio Meridionale
Corso di Dottorato in Metodi, Modelli e Tecnologie per l'Ingegneria
Dipartimento di Ingegneria Elettrica e dell'Informazione

Design, development and validation of an automated and integrated measurement system for neuromotor performance assessment.

Chiara Carissimo

chiara.carissimo@unicas.it

In Partial Fulfillment of the Requirements for the Degree of
PHILOSOPHIAE DOCTOR in
Electrical and Information Engineering

20/10/2023

TUTOR
Prof. Luigi Ferrigno
Prof. Alessandro Marino

COORDINATOR
Prof. Fabrizio Marignetti

UNIVERSITÀ DEGLI STUDI DI CASSINO E DEL LAZIO MERIDIONALE

CORSO DI DOTTORATO IN METODI, MODELLI E TECNOLOGIE PER L'INGEGNERIA

Date: **20/10/2023**

Author: **Chiara Carissimo**

Title: **Design, development and validation of an automated and integrated measurement system for neuromotor performance assessment.**

Department: **DIPARTIMENTO DI INGEGNERIA ELETTRICA E DELL'INFORMAZIONE**

Degree: **PHILOSOPHIAE DOCTOR**

"Memore del tuo proposito, tieni sempre davanti agli occhi il punto di PARTENZA. I risultati raggiunti, conservali; ciò che fai, fallo BENE; non arrestarti; ma anzi, con corso veloce e passo leggero, con piede SICURO, che neppure alla polvere permette di ritardarne l'andare, AVANZA confidente e lieta nella via della beatitudine che ti sei assicurata."

Chiara d'Assisi

Contents

List of Figures

List of Tables

Chapter 1

Introduction

The sustainable development of the planet is one of the widely discussed topics on the United Nations table: issues like protecting the environment and the rights and health of humanity are among the 17 goals of the 2030 Agenda [1]. It is a single-action programme that aims to use all forces at play to accept and win sustainable world challenges. Nothing and no one can be left behind in a world experiencing rapid digitisation and technological development. Technology should not dominate humanity, but be an innovative tool used intelligently to improve its life and that of the Earth. The goals under discussion include a focus on safeguarding the health and wellness of all and for all. This becomes the ground for boosting the already ongoing process of health digitisation also known as E-Health. In particular, it is a process involving networked resources, solutions and information technology applied to health and healthcare, to promote the prevention, diagnosis and monitoring of diseases and reduce bureaucratic processes by improving the accessibility of healthcare facilities [2].

E-health is a recent application field and requires medical and engineering expertise aiming at a common vision: a new concept of medicine and an easiness of interaction among patient, doctor and medical facilities.

Areas of interest are plentiful: electronic medical records, wearable sensors, remote assistance devices, and robotic or automated systems for the

administration of medical care or treatment.

These can play a crucial role in removing travel-related barriers in healthcare facilities and allowing personalised predictive diagnoses.

In this context, the development and consolidation of telemedicine systems are gaining wide interest and deployment in a rapidly ageing world. According to the World Health Organisation (WHO), the combination of declining birth rates and increasing life expectancy will result in one in six people being over 60 by 2030 [3]. Telemedicine can make healthcare easier and more available to all [4], as doctors can provide healthcare services remotely using information and communication technology (ICT) [5] (e.g. using video conferencing, medical imaging). A decisive boost to the spread of telemedicine was also provided by the COVID-19 pandemic when people in many countries were forced into isolation and social distancing. This also restricted recurrent monitoring, as in the case of diabetes patients [6], the possibility of access to rehabilitation facilities [7], and the monitoring of disease onset or progression. An integrated networked service system would allow doctors not only to monitor clinical parameters and the progress of customised treatment plans remotely or in real-time, but also to reduce geographical distances to specialised structures, reducing crowding and queues in hospitals [8]. One area where telemedicine is widely applied and rapidly developing is Neurodegenerative Disease (NDD) field. As life expectancy increases, the number of people affected by NDDs rises as well. Currently, NDDs affect more than 30 million people worldwide, the largest percentage is represented by the over-60 population. Among the most prevalent NDDs, are Alzheimer's disease (AD), Parkinson's disease (PD), and Amyotrophic Lateral Sclerosis (ALS) [9]: all of them are characterised by a continuous decline in cognitive and/or motor functions.

Particularly, Parkinson's is one of the most common disorders and it especially affects the aged population. PD is characterised by non-motor symptoms such as sensory disorders, cognitive impairment, mood disturbances, and motor symptoms like a Freezing of Gait, different types of

tremor, bradykinesia, rigidity, and dyskinesia [10].

At present, to make a diagnosis neurologists administer motor tasks and, based on the obtained results, assign a score according to a standardised Unified Parkinson's Disease Rating Scale (UPDRS) [11] and to assess the disease progression they use Hoehn and Yahr (HY) scale [12]. Classical diagnostic methods have a subjective component that could lead to misdiagnoses, especially in the early stages of the disease, when symptoms are mild and not always visible. In addition to clinical examinations, it is possible to perform more in-depth analyses such as magnetic resonance imaging, computed tomography and genetic tests, which are often expensive and limited to a few centres distributed throughout the territory, which make use of high-performance machines. Furthermore, patients have routine checkups by attending specialised medical centres, which constitutes a stressful activity. For these reasons, telemedicine systems and the development of a precision medicine approach could be essential in ensuring monitoring and medical care, reducing stress and travel difficulties for patients and caregivers and associated technologies could give objective diagnoses more cheaply. To have continuous monitoring and obtain remote data, objective methods and suitable instrumentation are needed. Devices already used in these applications are wearable, mini-invasive, accurate, low-cost, and easy to use by the patient in autonomous or semi-autonomous modes. As concerns the measuring devices for motor symptoms, some different sensors and techniques can be used to detect and capture human movements.

In this scenario, combining technical skills and medical expertise to make healthcare easier and available to everyone [4] becomes challenging.

Based on the motivations and requirements addressed in this chapter, this thesis proposes the design and development of an automatic measurement system capable of monitoring and acquiring information on neuromotor deficits and the implementation of data analysis algorithms to derive disease severity indices and adherence to pharmacological treatment. The proposal is divided into 3 main steps:

i) Identification and comparison of accurate, easily integrated, non-invasive compact measuring devices to acquire reliable information on human movement. Analysis of metrological performance and Identification of the minimum characteristics these devices must have to perform well in the chosen field of application, are fundamental tasks.

ii) Development and implementation of specific algorithms to analyse time series of raw data and derive motion information. The adopted algorithms must be generalisable and applicable not only to a medical context but also to a sports one.

iii) Application and review of points (i) and (ii) to real-life case studies: characterisation and classification of pathological movements in the medical field, analysis of medication adherence in people with Parkinson's disease, analysis of coordination abilities in the sports field.

This study paves the way for the realisation of digital architecture capable of objectively evaluating data acquired in real-time during normal daily life activities. The idea is to converge in the future to a multipurpose automatic measurement system to be used in many different contexts and enforce the E-health development.

Chapter 2

State of the art

In recent decades, life expectancy has increased due to improvements in health care and treatment. However, the ageing of the population will have a significant impact on the socio-economic structure of society in terms of social welfare and healthcare needs. New strategies and technologies need to be developed to meet the growing demand for health care and services in a way that is accessible to all and affordable. Remote monitoring can be a concrete answer to these needs: in recent years, scientific interest in this topic has grown in the medical [5] and sporting fields [13]. This monitoring idea allows data acquired during normal daily activities to be obtained and gives specialised staff continuous control over the health status of patients or athletes, depending on the application. To get remote data to allow medical staff to have continuous monitoring of patients or healthy people, objective methods and suitable instrumentation are needed. Monitoring devices should be accurate, mini-invasive, and easy to wear or adopt in autonomous or semi-autonomous modes. As concerns the measuring devices for motor symptoms, there are different sensors and techniques that can be used to capture human movements. Firstly, optical measurements [14] are widely used for the advancements in image processing and their easiness of use. In NDD applications, for example, the leap motion system is used

in [15] to detect upper limb motor skills in Parkinson's disease. In another work [16], the authors describe how markerless depth camera systems can be used to estimate upper-limb joint angles accurately. It is shown how, compared to reference methods, correlation coefficients around 0.99 can be obtained. The depth camera system has economic and easy to use in movement detection applications, but it presents occlusion issues during upper limbs' joint movement or their possible field-of-view sudden exit [14].

Another research work proposed a magnetic, low-cost, and scalable system to monitor the evolution of PD [12]. In particular, the system focused on two parameters: tremor and hands trajectory, and an anchored magnetic measuring system are used to assess the position of the hand in a 3D limited space and a single accelerometer, with a sampling frequency of 100 Hz to detect tremor. In this application, the space to perform movements is reduced to the size of the measurement domain.

In order to simplify the measurement system and converge towards simpler hardware solutions, the usage of wearable sensors [17] could be a viable solution. The smaller and simpler the adopted sensors, the heavier and more complex the processing algorithms to get movement recognition. The small sizes of these devices allow integrating them into clothing, watches or contact lenses [18], so the people's vital signs, during normal daily activities, can be constantly monitored in a non-invasive way. These devices and their integration enable the development of a telemedicine and telehealth approach. Wearable sensors guarantee a continuous and objective measurement of movement, overcoming the limitations found in classical diagnostic methods used for movement assessment. For example, in the sports field tapping test (TT) is used for evaluating coordination abilities [19]: the subject is asked to perform the exercise by doing as many taps as possible. The number of taps is counted by an operator observing the test. This evaluation can be influenced by subjective components. To try to overcome this limitation in work [20], the use of wearable sensors for the objective assessment of the TT was introduced. In particular, the authors demonstrate

how reliable results can be obtained by combining wearable technology and specific algorithms. Cameras combined with wearable sensors can also be used to identify movements during sports activities such as football. In the paper [21], it is shown how this measurement system can be developed to extrapolate information during a football training session, in particular features such as ball-foot impact, end of the kick, and lending of kick leg. The first measurement set-up to test the system and the algorithm was performed in a controlled environment. Wearable sensors are also widely used to assess pathological movements in people with neurodegenerative diseases. Currently, the diagnosis is carried out by neurologists, who administer motor tasks and, on the basis of the obtained performance, assign scores according to the standardized scale UPDRS (Unified Parkinson's Disease Rating Scale); to evaluate the progression of the disease the Hoehn and Yahr (HY) scale is used [22]. In [23], the percentage of misdiagnosis in the case of atypical Parkinsonian symptoms and essential tremor is assessed to be approximately 25%.

Therefore, it becomes valuable to find a device that can obtain objective and accurate measurements of movement and help specialists in motor assessment, physical activities as well as in the diagnosis of movement disorders. One promising solution is represented by Inertial Measurement Units (IMUs), whose typical equipment is made up of a multi-axis accelerometer, a multi-axis gyroscope and a multi-axis magnetometer. Such sensors are capable of acquiring information about acceleration and angular velocity which could be used to estimate the orientation. Inertial devices are generally low cost, networked, low power, and provide quite accurate measurements for monitoring and managing the pathology. In the field of human body motion capture, inertial sensors are the most widely adopted. The rapidity with which sensor technology advances makes their use suitable for the objective measurement of parameters that well describe human movement. In particular, these devices have been used for the detection and diagnosis of PD. For example, authors in this work [24] used inertial sensors to acquire data

during activities such as walking and tapping; thanks to the development of specific data analysis techniques, they were able to identify PD with an accuracy of 62%. Result that can grow by improving the algorithms or identifying other sensors. These technologies also represent a valuable tool for monitoring older adults, e.g. in the review [25] it can be observed how wearable sensors can be adopted to make fall detection or fall risk detection in elderly persons. It is emphasised that for each application, the choice of device, the positioning, the choice of measurement parameters and the development of the analysis process are important. For fall risk, the sensors most widely used in the literature are accelerometric sensors placed in the lower back.

Hence, while remote telemedicine is already spreading widely, the search for discriminating, sensitive and specific algorithms to obtain health status from raw data is still ongoing. In this direction, wearable sensors and artificial intelligence can represent an interesting solution for the objective and quantitative evaluation of body movement. These issues are widely addressed in the literature, and so there are different measurement systems used to capture and classify motion. As an example, in [26], the authors presented the results of a pilot study to evaluate the possibility of using accelerometer data, acquired with a sampling rate of 100 Hz, and a camera to video record movement activity, to find and study motor complications in patients with PD. They used a Support Vector Machine (SVM) classifier to estimate the severity of tremor, bradykinesia, and dyskinesia from accelerometer data. Another application is described in [27], where the authors want to distinguish PD tremor from Essential tremor. They used six Inertial Measurement Units (IMUs) placed on several patient's body parts and, for the classification, they implemented different machine learning algorithms, i.e. neural networks, SVM, k-nearest neighbour, decision tree, random forest, and gradient boosting; the best performance was obtained with SVM technique achieving 89% accuracy. Papadopoulos et al. [28] focused their work on the problem of automatically detecting PD

tremors from IMU data collected in the wild via a smartphone. They introduced a new dataset of accelerometer recordings from both PD patients and healthy subjects, captured outside laboratory conditions. To acquire tremor annotations for each user, they used the widely recognized Unified Parkinson's disease rating scale (UPDRS) [11]. Their method operates on accelerometer signals only during phone call events and the authors used a Multiple-Instance Learning approach for movement disorders classification. The sampling rate used to acquire the data depends on the mobile phone used by the individual subjects. In the aforementioned works, the authors used different machine learning algorithms to classify PD movement disorders: to perform accurate tests, it is always necessary to collect enough data in different operating conditions. Therefore, the involved patients have to repeat the required tasks more than once on different days, at home or in a clinical environment [29], so it takes time before a validated dataset is created. Artificial intelligence algorithms combined with inertial sensors are also applied for the recognition of activities in everyday life and sports. In particular, in the work [30] a measurement system characterised by five IMUs placed in different parts of the body is used. The aim is to train neural networks for the recognition of activities such as sitting, standing, descending stairs, running, walking, jumping, etc. The authors demonstrate how comparing different deep learning models yields performance over 95%. The analysis and processing of the data acquired by the sensors represent two important steps in the measurement process. In addition to the implementation and training of artificial intelligence algorithms, a valuable contribution in the field of motion detection is also made by the development of specific algorithms able to extract information characterising motion. In the paper [31] the authors validate an algorithm for step detection, in particular, they develop an algorithm based on continuous wavelet transform (cwt). The aim of this study was therefore to validate an acceleration-based gait detection algorithm for PD patients and older adults in both laboratory and home environments.

Wearable sensors and data analysis techniques can also be valuable measurement systems in remote monitoring applications. Particularly, inertial measurement units (IMUs) paired with other devices, such as smartphones and smartwatches, can provide information on the participant's habitual behaviour and context (e.g. indoor or outdoor) [32]. For example, in the case of patients with NDD, real-time monitoring can help to check for pathological movements and objectively track medication intake time (e.g. via a smartwatch) [33]. Besides monitoring of ageing and age-related conditions like PD, inertial sensor can be used to assess the presence of motor fluctuations related to medication [34]. The authors in [35] aimed to identify medication ON and OFF states by analyzing acceleration and angular velocity signals acquired by two sensors placed on the knee and ankle of people with PD, during various activities of daily living. To classify the two states, a Long Short-Term Memory network (LSTM) was trained, achieving 73-77% accuracy. In [36], the authors analyze the acceleration signals acquired from a wrist sensor in a free-living environment. A Convolution Neural Network (CNN) was implemented to classify the 'ON', 'OFF' and 'DYSKINESIA' states and results showed that the three states were identified with an accuracy of 65.4%. Even in sports, real-time monitoring with wearable sensors can also provide athletes with real-time feedback on the techniques used in their respective sports, thus helping them to perform efficiently. In this article [37], authors review the key technologies (IMU sensors, communication technology, data fusion and data analysis techniques) used in this type of application. A study of the literature shows how the spread of wearable technologies and data analysis algorithms has involved not only applications of the sporting field but also those of medical interest, to identify measurement tools capable of providing objective information on human movement. The motivation behind the development of this thesis lies in the idea of designing and developing an automatic measurement system characterised by a network of sensors and algorithms that is non-invasive, low-cost and capable of measuring movement by providing synthetic indices that give

quantitative information. The challenge is to achieve a measurement system that is flexible, and reliable and combines new sensor technologies and data analysis techniques that are also suitable for remote or real-time monitoring.

Chapter 3

Inertial Measurement Unit Simulator

Recently, there has been a growing need for wearable devices to detect body movement objectively. These devices are widely used for monitoring movement disorders in patients with NDDs [38] and for analysing and controlling movement during sports training [37]. The detection analysis of NDDs by means of low-cost sensors and suitable classification algorithms is a key point of the widely spreading telemedicine techniques. The choice of suitable sensors and the tuning of analysis algorithms require a large amount of data, which could be derived from a wide experimental measurement campaign involving voluntary patients. This process requires a prior approval phase for the processing and the use of sensitive data in order to respect patient privacy and ethical aspects. An alternative consists of structuring, implementing, validating, and adopting a software simulator, especially for the initial stage of the research. To this aim, this chapter proposes the development, validation, and usage of a software simulator able to generate movement disorders-related data, both for healthy and pathological conditions. The study focuses on a specific case, i.e. Parkinson's disease-related tremor, one of the main disorders of the homonym pathology.

3.1 The research motivation

To have large amounts of data, it is necessary to involve people who are willing to take part in specific experimental campaigns. To optimize the algorithm development, a large amount of data is generally needed: it could be obtained from a large campaign of experimental measurements involving volunteer patients, although it is not always easy to implement [39]. A possible solution could be to use data that is available publicly, but in this case, the data generation process has already been performed and very often the available information is not sufficient for a complete analysis. To try to overcome these limitations, the development and validation of a pathological motor pathology simulator able to generate motion and tremor data fully compliant with real measurements made by IMU devices was proposed. The ability to select the sensor capacity, metrological characteristics and noise contribution, as well as the resolution of the sensing system and the type of motor pathology to be simulated, makes the developed simulator a widely applicable tool, as it allows algorithms to be characterised with an arbitrary level of measurement data quality and to generate data for a customisable time period, avoiding the limitations inherent in already available datasets.

The aims that encouraged the simulator's development were several:

- the development of a widely-applicable simulator having a two-fold purpose, consisting of replicating the metrological features of several IMU devices and adding signal features to acceleration and angular velocity data to create pathological conditions in terms of movement disorders;
- a classification performance assessment which considers measuring device features as variable parameters instead of classical machine learning hyper-parameter optimization; accordingly, the simulator allows engineers to choose their favourite trade-off combination between device cost (and related measurement performance) and classification

accuracy;

- the building of arbitrarily large datasets, eventually composed of hybrid data, i.e. mixing different measuring devices and obtaining a balanced and cost-effective set-up to propose for physical deployment.

3.2 The proposed software tool architecture

Figure 3.1 shows the block diagram of the movement disorder simulator. Three inputs are required to generate pathological movements: IMU characteristics, real inertial data related to a specific trajectory, and pathology characteristics. In the first case, once the real device to be simulated has been identified (in this case, a nine-axis IMU), it is necessary to define the metrological characteristics of the simulated sensor. For this, it is necessary to set parameters related to i) hardware characteristics, ii) noise, and iii) environmental factors [40].

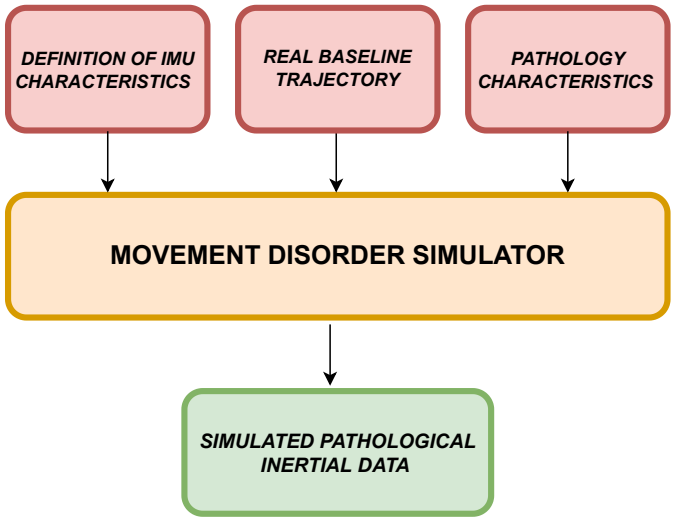

Figure 3.1: The Block Diagram Simulator [39]

With regard to the i) category, several parameters can be defined:

- the vertical resolution of the analog-to-digital converter (r_{ADC}), which influences the digitisation process of the acquired data;
- the axis misalignment value for the three-axis IMU considered (a_{MIS});
- the constant bias value (b_{VAL}), which influences all measurements by altering their average value and which is generally attributable to hardware defects.

As far as ii) category is concerned, the sensor measurements could also be affected by several random noises (rnd_{NOISE}):

- white noise;
- random walk, i.e. the amount of Brownian noise;
- bias instability, which concerns the level of pink or flicker noise in the measurement.

The simulator makes it possible to define which subset of them should be used to take into account the metrological performance of the considered sensor.

Finally, with regard to the effects of the environment (third category), the following quantities can be set:

- bias temperature (b_{TEMP}), defined as the difference from the predefined operating temperature;
- temperature scaling factor (sf_{TEMP}), which considers the error due to variations in the operating temperature.

$$IMU_{MODEL} = f(r_{ADC}, a_{MIS}, b_{VAL}, rnd_{NOISE}, b_{TEMP}, sf_{TEMP}); \quad (3.1)$$

In eq. 3.1, the function f, taking as input the aforementioned parameters, provides a model (IMU_{MODEL}), needed to perturb the nominal trajectory. At this stage, the real baseline trajectory has to be considered. Accordingly, two possible solutions are theoretically available: acquire such data from the field or generate them digitally. In the case of trajectory generation, eq. 3.2 has to be considered. It deals with imposed coordinates and orientation (subscript "q" stands for "quaternion" values) and the found IMU model. The second solution is more general since it allows generating data considering whatever IMU model where the information required by eq. 3.1 is available. As regards the first solution, adopted in the paper for the experimental validation, it is strictly important that the acquisition from the field is performed with a reference IMU, i.e. a device that has far better metrological performance than the ones it is needed to simulate. In this way, the acquired trajectory can be assumed as ideal.

$$T(t) = g(\vec{x}, \vec{y}, \vec{z}, \vec{x_q}, \vec{y_q}, \vec{z_q}, \vec{w_q}, IMU_{MODEL}); \tag{3.2}$$

Finally, having identified the pathology to be simulated, it is necessary to provide a mathematical description of the main objective motor effects provoked by the pathology, to be used as baseline trajectory perturbation.

$$p(t) = h(fr, a, T, n); \tag{3.3}$$

Applying eq. 3.3, it is possible to get the perturbed and pathological trajectory. The parameters of the h-function are: frequencies (fr), amplitudes (a), perturbed trajectory (T), and eventual adding noise sources (n) that could be defined by the pathology itself.

The simulator output, outputting IMU typical quantities, is characterized by simulated pathological inertial data, expressed as a 9-axis matrix, containing acceleration, angular velocity, and magnetic field as time-domain profiles.

To implement the h-function, it was necessary to consult and study the literature on movement disorders in Parkinson's disease. For example, in works [41, 42], the characteristics of tremor in terms of typical frequency ranges, typical energy in the frequency domain and accelerometer waveforms during a tremor event were consolidated.

3.3 Measurement Set-Up

In this application, the proposed simulator is specifically employed to reproduce inertial data characterizing PD, particularly tremors occurring in the upper limbs during a linear trajectory in a 3D space. A validation procedure is carried out to evaluate its suitability to faithfully generate IMU data in nominal conditions, i.e. without the disease effects by comparing generated data with real ones.

Two different sensors are used for the evaluation:

- SBG Ellipse-E (SBG) made by SBG Systems company (Figure 3.2 a) [43];
- MetaMotionR (MMR) made by mbientlab company (Figure 3.2 b) [44].

Figure 3.2: IMU devices used for validation: (a) SBG Ellipse-E; (b) MetaMotionR

Regarding the SBG Ellipse-E [43], it is a compact device with a high-performance Inertial Navigation System (INS). It includes a MEMS-based IMU and runs an enhanced Extended Kalman Filter (EKF), that fuses inertial and aiding information in order to obtain accurate real-time orientation

and navigation data. It is capable to supply data in output with a maximum frequency of 1000 Hz [43]. The other considered sensor is the MetaMotionR (MMR) [44], which is a wearable device capable to offer real-time and continuous monitoring of motion and environmental sensor data. In this case, the maximum frequency of data output is 100 Hz. It is widely used for scientific studies on patients in clinical settings. Each sensor has an onboard tri-axis accelerometer, a gyroscope, and a magnetometer with a 16-bit A/D converter. Table 3.1 shows the measurement parameters used to set the devices.

Table 3.1: Sensors' main parameters

	SBG Ellipse-E	**MetaMotionR**
Sample Rate	1000 Hz	100 Hz
Resolution	$16bit$	$16bit$
Accelerometer Range	$\pm 16g$	$\pm 16g$
Gyroscope Range	$\pm$ 1000°/s	$\pm$ 2000°/s
Accelerometer Noise Density	57 $\mu g/\sqrt{\text{Hz}}$	180 $\mu g/\sqrt{\text{Hz}}$
Gyroscope Noise Density	0.0025 °/s/ $\sqrt{\text{Hz}}$	0.0070 °/s/ $\sqrt{\text{Hz}}$

3.3.1 Characterisation and experimental validation of the simulator

The aim of the current subsection is to carry out static and dynamic tests with real IMU sensors to validate the simulator's capability to generate IMU-like data and to assess its basic performance. The idea is to compare the real data acquired during movement tests with simulator inertial results in order to evaluate their measurement compatibility, i.e. to state if data differences are only due to random factors characterizing the sensor's measurements uncertainty or if specific biases or deterministic phenomena intervene during the measurement process. The usage of two IMU sensors

is due to the need to have a reference instrument (namely, SBG) that feeds the simulator (providing inertial data from real baseline trajectory), and a second IMU sensor (MMR), whose data, acquired during such a trajectory, should be compatible with those obtained from the simulator, programmed to generate MMR-like data.

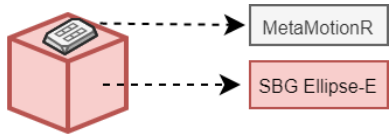

Figure 3.3: SBG and MMR measurement configuration

Subsequently, dynamic tests are performed: the sensor couple is placed on the back of an operator's hand (to assume a position that is typical of smart-watch devices' placement) and several movements in the 3D space are performed. During the test phase, inertial data from SBG and MMR are collected and subsequently used in the validation process, as shown in Figure 3.4. The simulator receives as input the inertial data from SBG. It perturbs the input inertial data using MMR characteristics (Table 3.1), to obtain simulated IMU values as output. As an example, Figure 3.5 displays the simulated accelerometer and angular velocity data during one of the horizontal movements.

3.3.2 Experimental validation results

To verify the reliability of the simulation results, two suitable figures of merit are identified: Pearson's correlation coefficient and Root Mean Square Error (RMSE), described by eqs. 5.1, 4.2, respectively. They are adopted to evaluate the similarity degree between simulated and real acquired data.

$$\rho_{xy,\%} = \frac{E[(X - \mu_x)(Y - \mu_y)]}{(\sigma_x \sigma_y)} * 100; \tag{3.4}$$

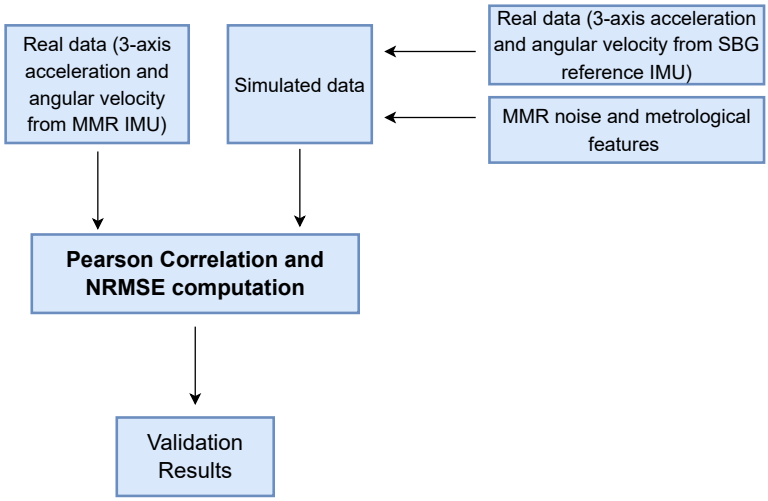

Figure 3.4: Block diagram to perform the validation procedure[39]

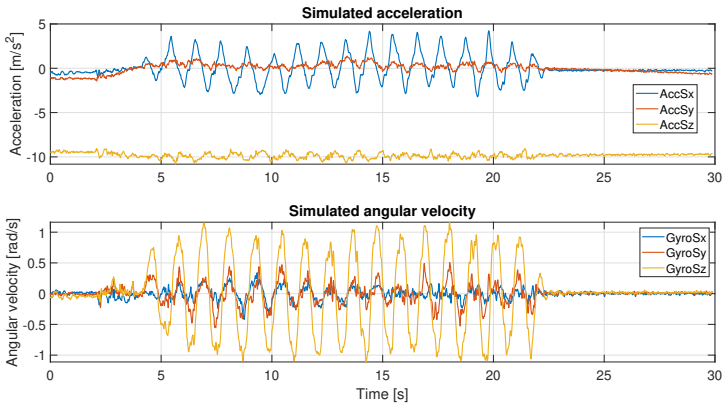

Figure 3.5: Simulated acceleration and angular velocity recording during horizontal movement [39]

$$RMSE_{\%} = \sqrt{\frac{1}{n}\Sigma_{i=1}^{n}(X_i - Y_i)^2} * 100; \tag{3.5}$$

In eqs. 5.1, 4.2, X corresponds to MMR signal samples, while Y repre-

sents the simulated inertial data. As for eq. 5.1, σ_x and σ_y are the standard deviations of X and Y, while the mean values of X and Y are represented by μ_x and μ_y, respectively; E is the expectation operator.

Before computing these parameters, it is necessary to normalize data. Min-max normalized method [45] is considered.

In Tables 3.2 3.3, the obtained results are described, considering angular velocity and acceleration data, respectively. The results are distinguished axis by axis and consider the absolute value (**abs**) of the signal. Qualitatively, the results can also be seen in the Figures 3.6, 3.7, where simulated IMU data are superimposed on the real one. Under defined operating conditions, the simulator is able to reproduce inertial data with a high level of reliability.

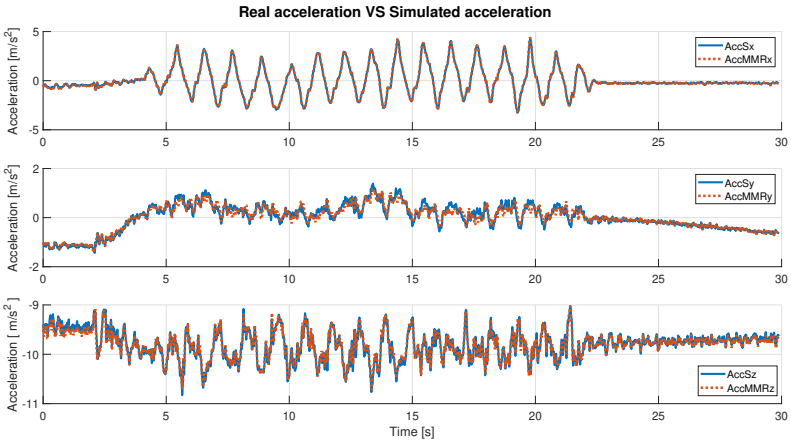

Figure 3.6: Real Acceleration Data VS Simulated Acceleration Data

Under any condition the Pearson's coefficient is greater than 94% in angular velocity comparison, instead, it is greater than 97% in acceleration comparison, axis by axis, while it slightly decreases when the **abs** is considered. In detail, it is possible to observe that for the acceleration data (Table 3.3), the best value is obtained along the x-axis (99.88%), while in

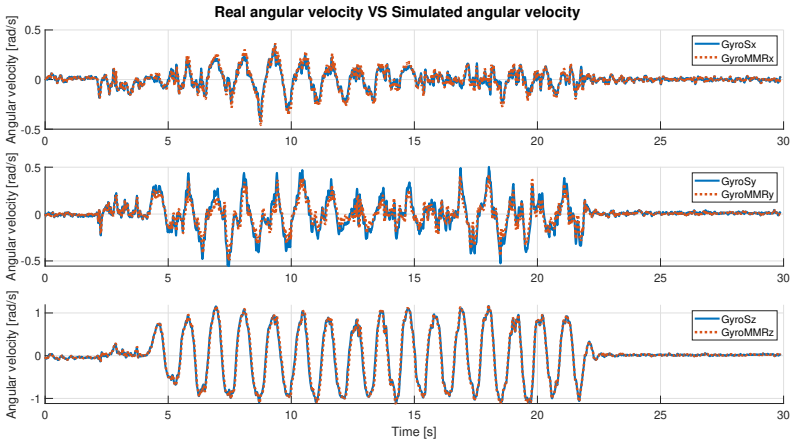

Figure 3.7: Real Angular Velocity Data VS Simulated Angular Velocity Data

the case of the gyroscope (angular velocity, Table 3.2) is obtained along the z-axis (99.35%). Considering the correlation results in terms of the absolute value of the signal, the highest value is obtained in the case of the simulated angular velocity and it is greater than 98%.

Table 3.2: Pearson's correlation and RMSE computed for real and simulated angular velocity data

	Pearson's Correlation [%]	**RMSE** [%]
x	95.70	3.51
y	94.30	4.98
z	99.35	2.77
abs	98.38	4.40

The RMSE is generally bounded from above by 6% (5.66% for acceleration along y-axis). As the best-observed values, for angular velocity data, the lower RMSE is 2.77% achieved on the z-axis while for acceleration data the

Table 3.3: Pearson's correlation and RMSE computed for real and simulated acceleration data

	Pearson's Correlation [%]	**RMSE** [%]
x	99.88	0.99
y	97.21	5.66
z	97.94	4.59
abs	93.64	4.43

lowest error is observed in accordance with the x-axis and it is equal to 0.99%. Finally, the error computed on the absolute value, in either case, is slightly greater than 4%. These results show a high compatibility level between simulated and real data.

3.4 The genearation of pathological movements

Among Parkinson's motor disorders, tremor is diagnosed in more than 70% of patients. To the best of our knowledge, there is no objective method to distinguish different types of tremors, but neurologists use patient history and physical examinations evaluated through UPDRS metric [46]. PD tremor is the most recognized sign and, although it could not be life-threatening, it surely influences normal daily activities and reduces patients' quality of life [47]. Objective measurements and classification systems, such as the joint use of IMU and Machine Learning algorithms, can be valuable tools to help clinicians make an increasingly accurate diagnosis. In this section, data associated with PD tremors, generated by means of the proposed simulator, are reported and discussed.

3.4.1 Adopted tremor typologies

Among the many possible typologies of tremor, this article focuses on the most common three types of hand tremor: resting tremor (RT), postural

tremor (PT), and kinetic tremor (KT); Table 3.4 summarises their main features [48].

Table 3.4: Adopted types of tremors: main features

Types of tremor	Clinical Features
Rest Tremor	RT occurs when there aren't voluntary movements and the limbs are at rest and supported against gravity.
Postural Tremor	PT is define as an action tremor, it is occurs when a position is maintained against gravity.
Kinetic Tremor	KT is an action tremor, which appears during voluntary movement

To replicate the pathological typical assessment movements, three reference tests are identified from the UPDRS document [11].

- Test for the identification of postural tremor of the hands: the subject's arms are stretched out in front of the body with the palms down, the wrist should be straight and the fingers should not touch;
- Test for the identification of kinetic tremor of the hands: this test uses the finger-to-nose technique. Specifically, the subject starts with the arm outstretched and must then perform at least three finger-nose movements with each hand extending as far as possible until it touches the examiner's finger;
- Test for identification of resting tremor: the subject is sitting quietly in a chair with hands resting on the arms of the chair and feet resting on the floor. This position should be held for 10 seconds without any other direction.

These tasks are administered by the neurologist in classical examinations. The replication of such tasks for our purposes has been carried out by performing the following phases.

- Before generating the pathological tests, baseline tests for each task are carried out. The operator placed the SBG sensor on the top of the hand and performed the tests as described in the guide. This first collection of data is considered free of any pathology.

- Subsequently, tremors to these traces are added: they are modeled analytically as multisine signals whose frequency and amplitude range [11] are derived from [42] and added to the baseline perturbed traces (the MMR-like signals are always generated using the simulator). On each baseline inertial trace, several 2-second pathological tremors disjoint intervals are superimposed for each axis. For each test, 1000 trials of 60 seconds duration were generated, each containing five 2-second tremor time segments. Tremor is generated for each interval randomly in terms of frequency and amplitudes, although within the recommended values, in order to generate a widely general dataset.

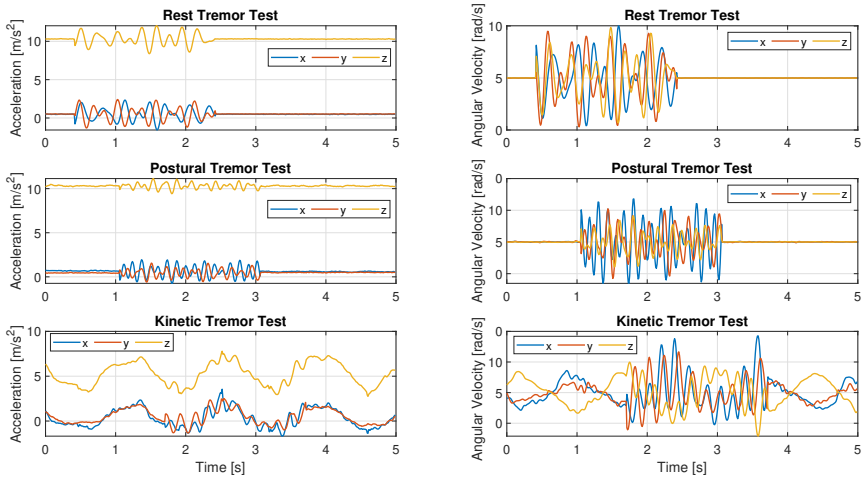

Figure 3.8: Simulated pathological data:
acceleration data on the left; angular velocity data
for the same tests on the right

Figure 3.8 displays an example of simulated accelerometer and gyroscope data for all considered tasks.

3.5 Tremor classification results

In this section, a tremor classification approach is proposed and it is based on pathological data generated by the aforementioned validated simulator. In detail, the adopted machine learning tool is described at first and the obtained classification results are reported.

3.5.1 The machine learning tool

The classification phase is run by adopting an ML algorithm fed with the generated dataset. Among all available ML techniques in Matlab^{TM} environment, the Fine Tree (FT) tool has been chosen as a result of preliminary tests where training accuracy had been adopted as a figure of merit. FT must be able to distinguish four classes: no tremor (Class 1), rest tremor (Class 2), postural tremor (Class 3), and kinetic tremor (Class 4). To recognize tremor and voluntary movement, 11 features are selected. Such choice is derived from the literature related to classification in human activity and motor symptoms' framework [42, 49, 50].

Among these, 8 features belong to time domain processing:

- Mean [49];
- Averange [49];
- Square sum of data under 25 percentile;
- Squared sum of data under 75 percentile;
- Low pass energy (below 2 Hz signal energy, to identify voluntary movement) [50];

- High pass energy (over 2.5 Hz signal energy, to identify involuntary movement) [50];
- Lag of First Autocorrelation Peak (to find the dominant frequency of the involuntary movement) [42];
- Height of First Peak in Autocorrelation (to discriminate periodic movements from aperiodic ones) [42];

while 3 features are related to frequency domain [51]:

- Maximum frequency in the spectrum;
- Sum of amplitude values of frequency components below 5 Hz;
- Number of peaks in the same frequency spectrum interval;

All features are calculated over a 2-second window, with 1 s overlap between consecutive windows [42]. For good performance of the ML algorithm, it is necessary to normalize the features input data: before moving on to classification a dataset normalization is carried out by means of a Z-score feature scaling method [52].

The classification stage involves two main analyses. The first analysis adopts one only dataset, where 70% of the data is used to train the tool, while the remainder is used for the test phase. Part of the first step is also to look for the effects of reducing/increasing the measurement axes for the accelerometer and/or gyroscope, i.e. to consider smaller amounts of data, on the classification performance.

A second analysis concerning a different goal: to test the algorithm on data deriving from different sensors with respect to those used in the training phase and to calculate the obtained performance in order to establish possible relations between metrological features of sensors acquiring training data (that can be performed once) and those related to instrumentation gathering test data (eventually, in real-time). This second test is particularly relevant since we would like to understand if low-cost IMU sensors

could be adopted for real-time monitoring, regardless of the adopted sensors to train the classification algorithm. To take account of the performance obtained during the test phase, Accuracy, Precision, Recall, and F1-score are calculated.

3.5.2 Classification performance

To analyze the obtained classification results, it is needed to define three specific figures of merit, namely Precision, Recall, and F_1-Score. They are reported in eqs. 3.6–3.8, respectively.

$$Precision(p) = \frac{TP}{TP + FP}; \tag{3.6}$$

$$Recall(r) = \frac{TP}{TP + FN}; \tag{3.7}$$

$$F_1 - Score(F_1) = 2\frac{p * r}{p + r}; \tag{3.8}$$

$$Accuracy = \frac{TP + TN}{TP + TN + FP + FN}; \tag{3.9}$$

where TP, TN, FP, FN represent true positive, true negative, false positive, and false negative cases in their common definition, respectively.

The total number of samples is around 10000. As stated before, 70% of them have been used for training and the remaining ones for testing. We present results in two distinct ways: confusion matrices and aggregate values by the adopted figures of merit. In detail, Figure 3.9 reports the obtained confusion matrices for two distinct cases regarding the adopted acquired data for training and testing: accelerometer values only (subfigure 3.9.a) and the joint use of accelerometer and gyroscope data (subfigure 3.9.b).

As widely known, the better the performance, the greater the value on the confusion matrix main diagonal. A very high TP positive rate is

obtained for all classes and particularly for classes 2 and 3.

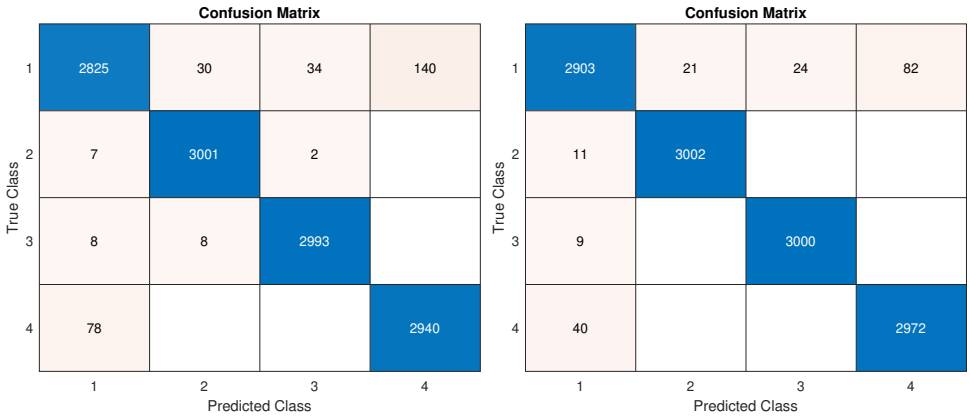

(a) (b)

Figure 3.9: Confusion Matrix of test phase: (a) Considering acceleration data from all axis; (b) Considering acceleration and angular velocity data from all axis

Table 3.5: Classification performance results computed on acceleration data only (considering all axis)

Class\Metrics	p	r	F_1
No Tremor (1)	96.81%	93.27%	95.01%
Postural Tremor (2)	98.75%	**99.70%**	**99.22%**
Rest Tremor (3)	**98.81%**	99.47%	99.14%
Kinetic Tremor (4)	95.45%	97.42%	96.43%
Test Accuracy		97.46%	

Such results are confirmed by Tables 3.5–3.6 where the highest value for each figure of merit is reported in bold. A fast comparison between the cited tables proves how the joint adoption of accelerometer and gyroscope data slightly increases performance values.

In detail, the best improvement is obtained in the *recall* parameter in the case of Class 1, where 93.27% is obtained with accelerometer data only

Table 3.6: Classification performance results computed on acceleration and gyroscope data (considering all axis).

Class\Metrics	p	r	F_1
No Tremor (1)	97.98%	95.81%	96.88%
Postural Tremor (2)	**99.31%**	99.63%	**99.47%**
Rest Tremor (3)	99.21%	**99.70%**	99.45%
Kinetic Tremor (4)	97.31%	98.67%	97.99%
Test Accuracy		98.45%	

Table 3.7: Classification performance results in different employment conditions for accelerometer and gyroscope.

	accelerometer x-axis only			**accelerometer xz-axes**		
Class\Metrics	p	r	F_1	p	r	F_1
No Tremor (1)	96.24%	91.15%	93.62%	97.19%	91.19%	94.09%
Postural Tremor (2)	**97.91%**	98.17%	98.04%	98.52%	**99.70%**	**99.11%**
Rest Tremor (3)	97.49%	**99.27%**	**98.37%**	**98.75%**	99.44%	99.09%
Kinetic Tremor (4)	94.21%	97.25%	95.71%	93.77%	97.81%	95.75%
Test Accuracy		96.71%			97.03%	
	accelerometer and gyroscope: x-axis			**accelerometer and gyroscope: xz-axes**		
Class\Metrics	p	r	F_1	p	r	F_1
No Tremor (1)	97.57%	92.77%	95.11%	96.54%	94.78%	95.65%
Postural Tremor (2)	**97.92%**	98.41%	**98.16%**	**98.58%**	99.20%	98.89%
Rest Tremor (3)	97.32%	98.61%	97.96%	98.55%	**99.40%**	**98.98%**
Kinetic Tremor (4)	95.95%	**98.94%**	97.42%	97.19%	97.51%	97.35%
Test Accuracy		97.19%			97.72%	

(Table 3.5) while 95.81% is achieved with the additive support of gyroscope data. Taking the test accuracy as an aggregate performance index, a 0.99% (from 97.46% to 98.45%) improvement is achieved by increasing data sources.

A specific mention is deserved by Table 3.7. In order to exploit as fewer data as possible, and remain in the first classification step, we analyzed the effect of reducing the data amount by limiting the number of acquisition axes both for accelerometer and gyroscope instruments. Surprisingly, although a general performance worsening is visible, the effect of reducing to one or two axes the data amount does not heavily impact the very high scores got by the defined performance indexes. Performance levels got a few percentage points to decrease, thus still ensuring a good classification accuracy for the

required types of tremors. Still, training and testing are performed on the same dataset, although subdivided in the aforementioned way.

3.6 Classification performance stability under data quality variation

Another key factor we would like to explore is the possibility to have datasets generated from different sensors for training and testing phases, respectively. In particular, it is desirable to understand how the parameters of the sensors could affect the classification results whenever an uneven set of data is fed to the classifier during the learning phase and the following test. The results presented in this section aim to check if the most common situation is viable for the application purposes, i.e. the best accurate sensors are available to train and tune the classifier, but less accurate devices are generally available during normal monitoring activities due to cost constraints and the large variety of IMU sensors available on the market. In any case, to have a full report of the possible cases, several training/testing combinations are considered. In detail:

a. Training and testing with data coming from the same high-performance sensor (best/best);

b. Training with high-performance sensor data and testing with lower-level sensor data (best/worst);

c. Training with lower-level sensor data and testing with high-performance sensor data (worst/best).

d. Training and testing with data coming from the same lower level sensor data (worst/worst);

In all combination tests data from the three-axis accelerometer and three-axis gyroscope are considered. Although in Section 3.5.2 we proved how

the reduction of involved axes does not critically reduce the performance indexes, here we aim at analyzing a different effect, and therefore, to avoid possible joint causes, we restored the original maximum number of available data, specifically in terms of sensors' axes. The results and performances in the best condition (case (a)) are described in the subsection 3.5.2. The results obtained in test (c) show the case of low-quality data training and high-quality data testing. Comparing Table 3.8 with best case (Table 3.6), it is possible to observe a general performance drop: in particular for Class 3 of index *recall* a decrease of 19.81% is recorded (from 99.47% to 79,66%), while the test accuracy goes down by 11.34% (from 98.45% to 87.11%). These results are also visible in Figure 3.10b where a test confusion matrix is shown. In the case worst/worst (d) it can be seen that by training and testing the network with the same lower-level sensors data, the test phase performances are similar to those obtained in case (a), indeed the difference between tests accuracy is 0.93% (for details, see Table 3.9 and Figure 3.10c).

Table 3.8: Classification performance results computed on acceleration and gyroscope data: in the training phase 8 bit sensors are used, while for the test phase 16-bit sensors (worst/best).

Class\Metrics	p	r	F_1
No Tremor (1)	89.85%	78.28%	83.67%
Postural Tremor (2)	82.17%	**98.81%**	**89.72**%
Rest Tremor (3)	**96.81%**	79.66%	87.40%
Kinetic Tremor (4)	83.10%	91.73%	87.20%
Test Accuracy		87.11%	

A broader discussion of the case best/worst test results is necessary. Firstly, performance degradation is visible comparing confusion matrix in Figure 3.9 with the one shown in the Figure 3.10a. The worst results are recorded for the identification of Classes 2 and 3 especially. Both classes, in most cases, are wrongly predicted as Class 1.

The aforementioned results are confirmed by indexes computed and re-

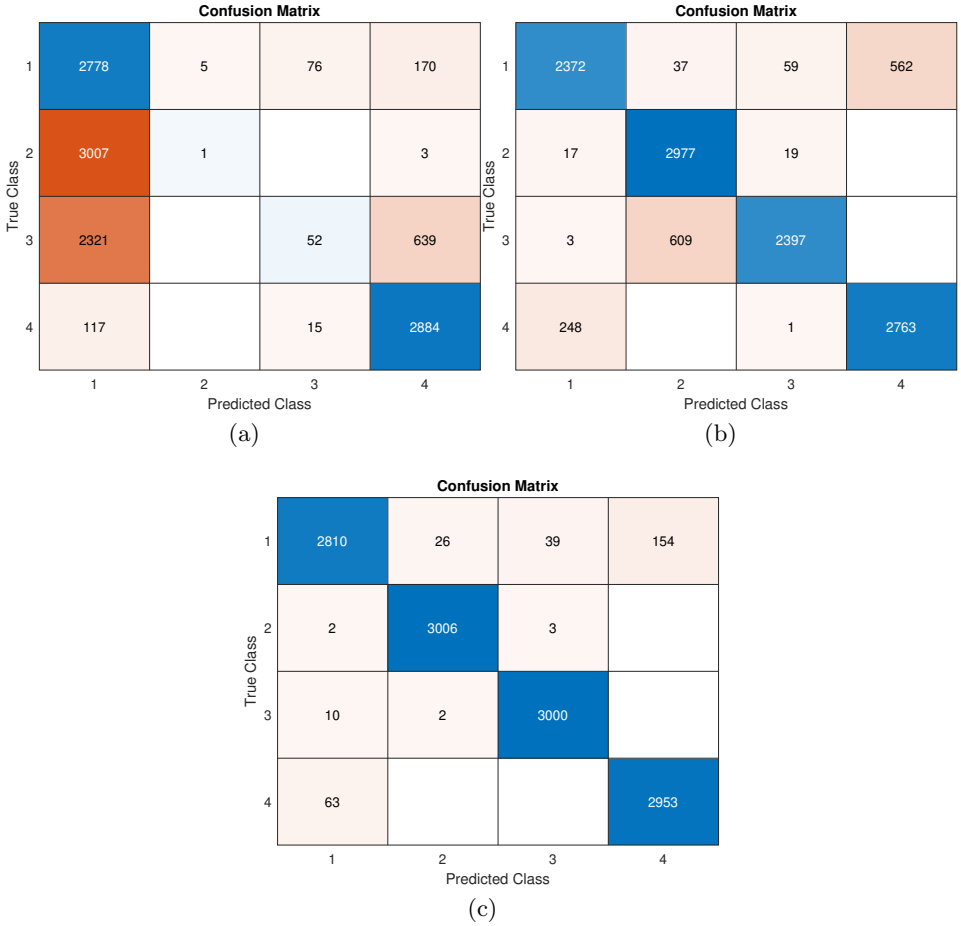

Figure 3.10: Confusion Matrix of test phase: (a) test data according to best/worst specifications; (b) test data according to worst/best specifications;(c) test data according to worst/worst specifications.

Table 3.9: Classification performance results computed on acceleration and gyroscope data: in the training phase and test phase 8 bit sensors 10% worse noise are used (worst/worst)

Class\Metrics	p	r	F_1
No Tremor (1)	97.40%	92.77%	95.03%
Postural Tremor (2)	**99.17%**	**99.83%**	**99.45%**
Rest Tremor (3)	98.62%	99.60%	99.11%
Kinetic Tremor (4)	95.04%	97.91%	96.46%
Test Accuracy		97.52%	

ported in Tables 3.10, where a general decline in performance can be seen. Comparing Table 3.10 with Table 3.6 the worst decrease is obtained in F_1 score index especially for Class 2, where radical reduction is recorded. The test accuracy also goes from 98.45% (Table 3.6) to 47.36% (Table 3.10). The highest number of misclassifications is recorded for Classes 2 and 3, with all indices showing values below 17% for class 2 and below 37% for Class 3.

Table 3.10: Classification performance results computed on acceleration and gyroscope data: in the training phase 16 bit sensors are used, while for the test phase 8 bit sensors with 10% worse noise are simulated (best/worst)

Class\Metrics	p	r	F_1
No Tremor (1)	33.78%	91.71%	49.38%
Postural Tremor (2)	16.67%	0.03%	0.07%
Rest Tremor (3)	36.36%	1.73%	3.30%
Kinetic Tremor (4)	**78.03%**	**95.62%**	**85.94%**
Test Accuracy		47.36%	

According to the reported data, we may say that the usage of uneven datasets for training and testing phases is generally not advised, since performance degradation is quite critical. Anyway, there are specific worsening cases, such as only the reduction of the quantization bits (case Table 3.8), where the adoption of different sensors still warrants good performance indexes. In our investigation, the number of quantization bits has a more

negligible effect on the performance than the worsening of all noise levels.

3.7 Final observation

This chapter presents the development, validation, customization, and adoption of a movement disorder simulator, capable of generating reliable acceleration and angular velocity data related to healthy and pathological states for patients possibly affected by Parkinson's disease. In particular, taking into account commercial IMU sensors, the aim of the tool has consisted of generating real-like data to create arbitrarily large datasets to be exploited by researchers in the field of NDD automatic diagnosis to test and tune their classification algorithms. To evaluate the reliability of generated data, a validation set-up was developed and real-acquired and simulated data were compared by means of two suitable figures of merit, which have proved a high agreement level. Subsequently, a classification stage has been developed by using the Fine Tree algorithm on data suitably generated and results have been evaluated through classical performance indexes in the field of Machine Learning. Performance scores generally equal to or greater than 90% have been achieved in most cases, whenever homogeneous (different but acquired with the same sensors) data are adopted for training and testing. Two further analyses are proposed: the effect of the number of axes and sensors (accelerometer, gyroscope) and the adoption of uneven data between training and testing to the classification results. The obtained results show a slight performance worsening when the number of adopted axes decreases and interesting relations between metrological features of the sensors and classification results. This study is intended to give useful information for the choice of proper IMU sensors (metrological aspects) to adopt for NDD monitoring, to prove the suitability of such sensors to acquire useful data for automatic diagnosis of Parkinson's disease based on tremor classification, and, for the adopted classification algorithm, the work is aimed to prove how uneven datasets are generally to be avoided but in

specific cases, acceptable performance can be achieved, whenever only specific features change (e.g., quantization bits). The next validation step of the proposed simulator is to compare its generation with healthy and pathological movements coming from real patients, in order to understand how IMU data should be adapted to different patients' statuses as age, disease gravity and eventually suffered comorbidities.

Chapter 4

Medical field application: IMU sensors to automatically measure movement disorders

The simulator described in the previous chapter allows the designer to locate one or more inertial sensors, generate data by assuming known trajectories, and then analyse performance as measurement parameters change. This preliminary analysis can help test devices in simulation, make comparisons and generate a large amount of data that would be difficult to obtain from experimental campaigns. A large dataset is worthwhile in the testing and validation step of the algorithms before the experimental phase. The study described above identified a commercial IMU, MetaMotionR (MMR), which showed good accuracy for medical applications during simulation. In particular, it was shown how the combination of inertial data, pattern of features, and trained algorithm are suitable for making movement disorders analyses in people with PD. The simulator validation obtained good results, but from

the simulation, it is necessary to verify whether the identified sensors and algorithms achieve the same performance under real conditions. To do this, in this chapter, the tools and algorithms analysed in the simulation phase will be applied to real applications. In particular, the case studies will aim to identify motor disorders and medication adherence in people with PD. Four research questions will be addressed: i) wearable device for Parkinson's disease aided diagnosis; ii) implementation of Machine Learning algorithm to distinguish PD from healthy people; iii) use of the features validated in chapter 3 to identify motor fluctuations in a group of people with Parkinson's disease; iv) investigation of new features for analysing pharmacological adherence.

4.1 The research motivation

The need for continuous monitoring and objective measurements in the medical field is becoming increasingly widespread. Wearable devices can be a concrete answer to these requests. Among the most common neurodegenerative diseases, Parkinson's is one of the main disorders, especially in the aged population. It is characterised by several symptoms whose comprehensive and accurate analysis can lead to a punctual and effective diagnosis. The diagnosis is made by a neurologist who assigns scores on the basis of standardised motor exercises. In the early stages of the disease, symptoms are less visible and less frequent: an automatic measuring instrument at this stage can be a valuable aid for a more accurate diagnosis. A promising solution to detect most motor issues related to Parkinson's disease is represented by Inertial Measurement Units (IMUs), typically including accelerometers, magnetometers and gyroscopes. Their metrological features, such as accuracy, sensitivity and immunity to external disturbances are critical to get a fully functional and discriminant device. Furthermore, the capability to extrapolate pathological states from measurements is a very attractive feature to automatise early warning and fast medical interventions.

4.2 Motor symptoms detection

PD is characterised by motor symptoms such as: a)tremor, b) bradykinesia, c) rigidity, d) Freezing Of Gait and e)dyskinesia and non-motor symptoms like a cognitive impairment, mood disturbances, sensory disorders [53]. Inertial sensors combined with data analysis algorithms are valuable measurement tools able to perform motion disturbance analysis [54]. Such sensors acquire acceleration and angular velocity information that can be fused and used to estimate orientation. This section shows how it is possible to accurately detect various motor symptoms by reducing the number of sensors required and to perform real-time data classification. It is desirable to have an online classifier to reduce the amount of data to be stored and processed to detect pathological conditions at an early stage when symptoms are less visible. Early recognition of these symptoms can help the physician intervene immediately with specific treatments. The idea is to use a single inertial platform to capture the movement of an upper limb, process the acquired data in a lightweight manner, and adopt a trained k-NN algorithm to rapidly classify PD-related motor symptoms. In detail: a) tremor, b) bradykinesia, e) dyskinesia. To perform these tasks, it is first necessary to characterise the adopted platform to verify its metrological characteristics and assess its compliance with the proposed application.

4.2.1 Experimental characterisation

IMU sensor used in the simulation phase described in Chapter 3 was adopted. Specifically, the sensor is the MetamotionR made by Mbientlab, with a wearable-compatible sizes (27mm $\times$ 27mm x 4mm case). The device has a MEMS (Micro-electromechanical systems) technology with on-board sensors such as tri-axis accelerometer, tri-axis gyroscope and tri-axis magnetometer.To estimate the device orientation in space, it is possible to enable sensors fusion modality; all fusion modes provide orientation output as Quaternion or Euler angle [55]. Once the device was identified, a complete

verification of its performance was carried out. In particular, the metrological characterisation concerned the testing of the sensor's ability to recognise movement disorders typical of Parkinson's, i.e. the IMU must provide accurate information on orientation and vibration, both in terms of amplitude and frequency. State and dynamic tests were performed. To acquire data from the MMR device, a Python script was developed from which it is possible to set parameters such as range, and sampling frequency, as well as to establish the connection/disconnection of the sensor and, after execution, to save the measurement data.

Static Tests

The first static measurement set-up is presented in Fig. 4.1. The sensor is placed in a fixed position and by means of the aforementioned script, acceleration data are acquired. Tests are realized in three different range values ($\pm 2g, \pm 8g, \pm 16g$), with a sample rate of 100 Hz.

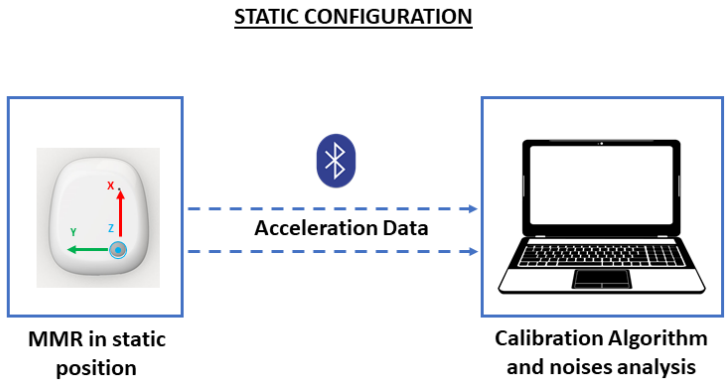

Figure 4.1: Static Configuration for Noise Density Tests [56]

In order to remove typical accelerometer drift, a calibration operation is necessary. Afterwards, for each test, the noise density value is computed for each axis. In eq. 5.1, noise density expression is described:

$$ND_i = \frac{\sigma_i}{\sqrt{f_c/2}}, i \in \{x, y, z\} \tag{4.1}$$

where σ_i is the standard deviation, f_c is the sample rate.

Table 4.1: Noise density acceleration - static estimation

Axis	**Range 2g** $[\mu g/\sqrt{Hz}]$	**Range 8g** $[\mu g/\sqrt{Hz}]$	**Range 16g** $[\mu g/\sqrt{Hz}]$
x	140.70	156.86	173.74
y	142.20	147.65	152.70
z	180.52	223.94	245.72

Table 4.1 displays the noise density results for each operative range and for x, y, z axis. Such characterisation enhances information from datasheet, since in [57] we found values provided for ±8g range and absolute value only. The results obtained in ±8g range are compliant with those described in the datasheet.

Fig 4.2 describes the second static measurement set-up: the IMU device has been anchored in a rigid cube, being parallel to one of its faces. In this configuration rigid 90° rotations are done, to verify the MMR orientation estimation performance. In particular, starting from a first position and applying rigid 90° rotations every 10 s, measurement tests are carried out.

Fig. 4.3 shows how the MMR device correctly records the changes of rotation for each rotation axis. To obtain raw orientation data, the sensor fusion modality is enabled; in particular, "NDoF" [55] fusion mode is chosen, where the fused absolute orientation data is calculated from gyroscope and accelerometer with sample rate of 100 Hz, and the magnetometer with sample rate of 25 Hz. For all sensors, the maximum operative range is set. In this configuration, the MMR output is described by quaternion: to obtain the degree results, data are transformed from quaternion to rotation

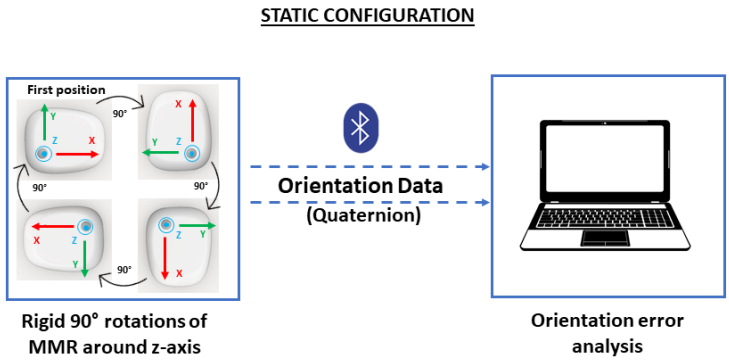

Figure 4.2: Orientation tests in static condition

angles [58].

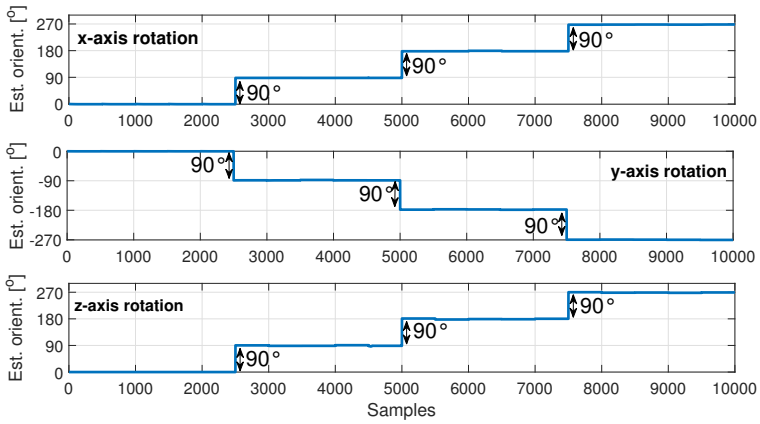

Figure 4.3: The estimated orientation obtained during static tests [56]

For each axis, a normalized orientation error, in static condition, is calculated; in Table 4.2 the results are shown. The lowest percentage error overall is obtained along z axis.

Table 4.2: Percentage Orientation Error - static estimation

Ref. angle	**x** [%]	**y** [%]	**z** [%]
90°	1.98	1.53	0.57
180°	1.68	2.24	0.58
-90°	2.11	0.15	1.03

Dynamic Tests

The dynamic set-up is presented in Fig. 4.4 and it is characterized by a robot manipulator, i.e. a 7-DoF Jaco manufactured by KINOVA company, available in the LAI robotics laboratory of the University of Cassino and Southern Lazio (IT), the MMR sensor and a laptop computer. The MMR has been placed on the robot manipulator's end effector. The communication between the robot and the PC has been performed through the framework ROS (Robot Operating System) on Ubuntu 18.04 version. In this configuration, several tests are realized. Each test is characterized by the imposition of a known trajectory composed of sinusoidal paths with different peak–to–peak amplitude $\{45, 90, 180\}^\circ$ and for different frequencies, i.e. $\{1/8, 1/6, 1/4, 1/2, 1\}$ Hz. The aim of these tests is to verify the capability to retrieve orientation values that are compatible with the imposed ones, i.e. the suitability of the MMR in orientation estimation tasks in presence of a continuous system movement, i.e. the capability to track the orientation of a moving system. Its evaluation can be related to the patient's movements during tests assigned by a specialist in NDD diagnoses. The adopted frequencies are the closest to the natural movement (typical under 2 Hz) that the robotic system could achieve.

The Robot and MMR orientation data are considered and compared; as an example, in Fig. 4.5, an orientation comparison is provided in the case of 90° amplitude and 1/6 Hz frequency sinusoidal trajectory. In particular, the blue line represents the fused sensor data, while the orange one reports

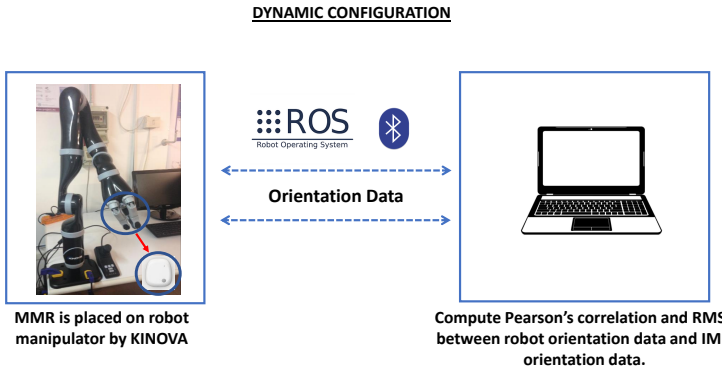

Figure 4.4: Dynamic set-up: robot with MMR placed on the end effector (left) connected to personal computer through ROS (right)

robot orientation. From a qualitative point of view, the compared plots show a good agreement level that must be quantified by means of proper figures of merit.

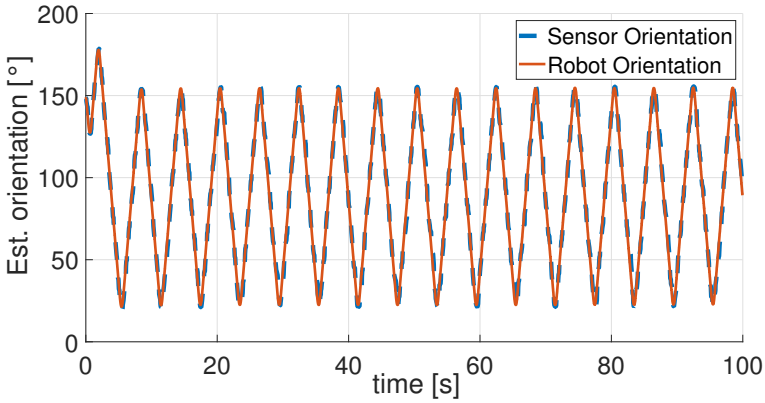

Figure 4.5: Orientation during test with 90° of amplitude and frequency 1/6 Hz, along Y axis [56]

Such an analysis is performed by adopting two indexes: Pearson's correlation and Normalized Root Mean Square Error (NRMSE). The cited metrics are computed according to eqs. 4.2 and 4.3 respectively, where MMR

orientation data are reported in the vector X while robot orientation data are represented by Y.

In Equation 4.2, Pearson's correlation coefficient is described:

$$\rho_{xy,\%} = \frac{E[(X - \mu_x)(Y - \mu_y)]}{(\sigma_x \sigma_y)} * 100 \tag{4.2}$$

where: σ_x and σ_y are the standard deviations of X and Y, μ_x and μ_y are the mean values of X and Y respectively, E is the expectation operator.

In eq. 4.3, Normalised Root Mean Square Error expression is described:

$$NRMSE_{\%} = \sqrt{\frac{1}{n}\Sigma_{i=1}^{n}\frac{(X_i - Y_i)^2}{Y_{max}}} * 100 \tag{4.3}$$

where the subscripts i and max represent the i_{th} element and the maximum value of the corresponding vector.

In Table 4.3, the whole performance indexes are reported by distinguishing them by amplitude cases and considering only the Y axis, because the main motion is performed in this direction (pitch angle changing its value). The previous tests show comparable performance along x, y, z axis directions, therefore here we focused our attention on one axis analysis only. In any condition, Pearson's coefficient has a value greater than 90%; these results confirm the MMR device's capability to accurately estimate the orientation states. The NRMSE is generally upper-limited by 3% in case of amplitudes greater than 45° and 90°, while worse values are experienced when 180° amplitude trajectory is tested, especially due to the limitations of the robot manipulator to apply planned trajectories.

4.2.2 Movement disorders classification

At the beginning of this chapter, movement disorders are described. Tremor, bradykinesia and dyskinesia were chosen to be analysed for classification purposes, given their sensitive incidence in patients with PD. In particular, it is worth remembering that bradykinesia is a slowness of movement

Table 4.3: Characterization in Dynamic Conditions - computed performance indexes

	Amplitude 45°		**Amplitude 90°**		**Amplitude 180°**	
Frequency [Hz]	$\rho_{xy,\%}$	$NRMSE_{\%}$	$\rho_{xy,\%}$	$NRMSE_{\%}$	$\rho_{xy,\%}$	$NRMSE_{\%}$
1/8	99.80	1.26	99.62	2.75	99.74	4.74
1/6	99.48	1.89	99.70	1.86	99.40	5.30
1/4	99.49	1.65	99.55	2.12	98.36	9.28
1/2	97.77	1.83	98.11	2.23	99.40	5.30
1	92.55	1.26	82.41	2.75	93.27	12.19

execution [59], tremor is described as a periodic involuntary movement, while dyskinesia is an uncoordinated, aperiodic involuntary movement [42]. These pathological movements are emulated by one of the authors according to specialists' descriptions and the UPDRS scale indication and used to train and test a machine learning algorithm. This section aims to verify and quantify the capability of the classifier to be discriminant among different movements, acquired by a single IMU device placed on hand palm, and the accuracy of their recognition.

Experimental setup

The experimental set-up is composed of the cited MMR sensor, placed on the hand's palm of one of the authors, being in healthy conditions and emulating the movement disorders. The experimental tests are organised in such a way that there are five different conditions to be classified: 1) Rest, 2) Normal movement, 3) Bradykinesia, 4) Tremor, 5) Dyskinesia.

As regards the dataset building, two different approaches have been followed to populate training and testing datasets. The training data was derived from 5 30-second tests carried out for each of the proposed classes. Except for class "Rest", where no movement has been performed, the remaining tests are composed of a baseline trajectory and a superimposed

pathological condition. The baseline is a linear trajectory in a 3D space, keeping the hand as much parallel as possible to the ground line, to follow a 30 cm path. The superimposed pathological conditions strictly depend on the class to emulate and, particularly:

- Normal movement: no further effects are added to the baseline;
- Bradykinesia: the baseline movement has been voluntarily slowed down with sporadic additions of stopping intervals [60].
- Tremor: a 3-6 Hz oscillation has been superimposed to the baseline in 5-time intervals spaced out by 3 seconds original baseline [61].
- Dyskinesia: a superimposition of a non-periodic movement in non-predictable directions of the space has been added to the baseline [62].

As regards classes Bradykinesia, Tremor and Diskynesia, gravity emulation has been achieved by increasing the described effects, as the mean speed in "Bradykinesia" case, Tremor amplitude in the "Tremor" class and spasmodic movement incidence in the Diskynesia case. Each training repetition has been characterised by a random variation of the pathological severity. All movements can be classified as "reaching" rather than "grasping" activities.

The MMR has been anchored on the hand's palm, and five tests lasting 30 s are carried out for each class. Such data are used to populate the training dataset. Organising data for the test stage has also been necessary to evaluate the algorithm's performance. Several $90s$ tests are realised using the same set-up aforementioned and using a structure described in Fig. 4.6.

For all tests, sample rate of the MMR sensors has been set to $25Hz$; the accelerometer range to $\pm 4g$, while gyroscope range has been fixed to $500°/s$.

Fig. 4.7 displays the acceleration and gyroscope raw data acquired during one of the tests.

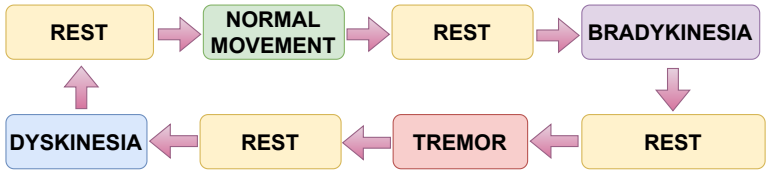

Figure 4.6: Description of final tests structure

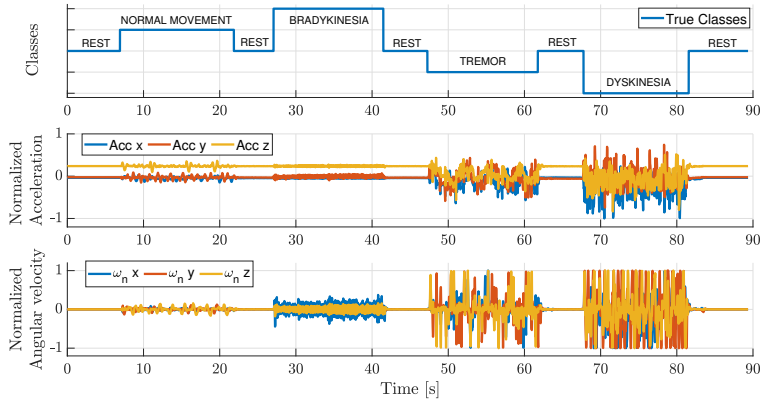

Figure 4.7: Time evolution of acceleration and angular velocity along the coordinate axes during several movement emulations, whose ground truth is reported in the upper figure

Data processing and first obtained results

A k-NN algorithm is implemented for the classification. Among the 11 features validated in the Chapter3, for this study 6 features are selected: 3 belonging to time domain processing [49] (mean, square sum of data under 25 percentile and squared sum of data under 75 percentile) and 3 are in frequency domain [51] (maximum frequency in spectrum, sum of amplitude values of frequency components below 5 Hz, and number of peaks in the same frequency spectrum interval). All features are calculated over a 0.4 s window, with 0.016 s overlap between consecutive windows. A data normalisation process is carried out before inputting acquired data to k-NN network. Min-max feature scaling method is considered: values are shifted

and resized to obtain features values in $[0-1]$ interval. To accomplish such task, it is necessary to apply the eq. 4.4, where $\hat{f}_{i,j}$ is the i_{th} normalised component of feature $\mathbf{f_j}$, while $f_{i,j}$ is its unnormalised version.

$$\hat{f}_{i,j} = \frac{f_{i,j} - min(\mathbf{f_j})}{max(\mathbf{f_j}) - min(\mathbf{f_j})}. \tag{4.4}$$

Once trained, the k-NN network is run on test data. Fig. 4.8 shows the comparison between true classes (blue line) and predicted classes (orange line) during test phase. In correspondence of the transitions (changing one movement to the next one), there are some misclassification cases as well as a small amount of wrong classified windows also affects diskynesia case which is sometimes recognized as tremor: looking at Fig. 4.7, a possible motivation is given by their similarity in time domain signal features both in terms of acceleration and angular velocity. Nevertheless, promising results are obtained in terms of most common indexes adopted for classification performance evaluation, as reported in Table 4.4.

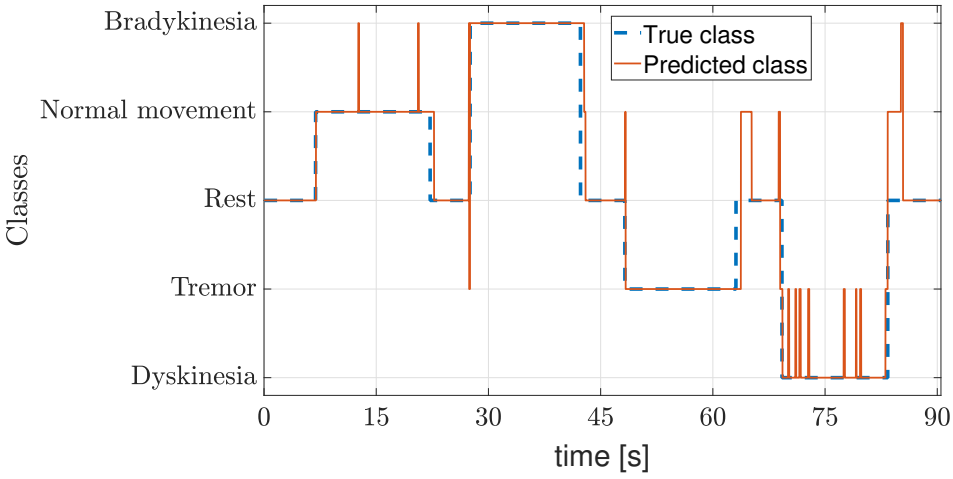

Figure 4.8: True Classes VS Predicted Classes

F1–score coefficients has a value greater always greater than 87%, Recall

Table 4.4: Classification Performance Results

Class	Precision	Recall	F1_score
Rest	1	0.90	0.95
Normal Movement	0.86	0.99	0.92
Bradykinesia	0.99	0.81	0.90
Tremor	0.78	0.98	0.87
Diskinesia	0.93	1	0.97

coefficients overcomes 80% and they are generally greater than 90% for 4 classes over 5. Finally, precision values are very high (greater than 0.85 almost everywhere), with the exception of Class 4. The overall accuracy is 92%. These first results demonstrate the possibility to classify different movement disorders with accurate performance using a k-NN network for classification and using one only IMU platform for data acquisition.

4.3 Healthy people or people with Parkinson's disease?

In the previous section, it was shown how given an IMU sensor, features calculated from the raw data, an initial classification of pathological movements can be obtained using machine learning algorithms. The inertial data acquired during these tests were emulated, i.e. collected under controlled conditions and in the laboratory. It is still important to verify that the analysis process adopted is also applied under real-life conditions. To do this, a second step was to analyse an initial dataset available from the web. The idea is to extract information characterising Parkinson's disease and verify that the hypotheses assumed so far correlate with the real data.

4.3.1 PD-BioStampRC21 Dataset

The database[63] examined in this study is constructed from acceleration data acquired through an IMU device, the MC 10 BioStamp RCsensor. In particular, five sensors were placed on each patient - four on each limb and the last on the chest - collecting acceleration data for two consecutive days. Thirty-four subjects, seventeen healthy and seventeen with PD, ranging in age from 37 to 84 years, participated in the data collection. The participants were also examined by a doctor using the UPDRS scale to assess the severity of the disease. The neurologists performed the standardised exercises from UPDRS 3.17. As mentioned above, PD resting tremor occurs at a frequency between 3 and 6 Hz. In the dataset, tests are selected to evaluate the tremor and then a frequency analysis of the accelerometer data is performed. As can be seen in the Fig. 4.9, in the case of tremor at rest, the significant harmonic tones are in the range of [4-9] Hz. In particular, this test was performed under OFF conditions, i.e. when there is no effect of the medicine.

If the FFT is compared in the ON condition (Fig. 4.10), with the same test, it is observed that the frequencies always fall in the same range, but with a smaller amplitude. This shows how the medication attenuates motor symptoms.

The control group performed the same tests as the pathological group. The harmonic content of the test performed by a participant in the control group, as can be seen in Fig. 4.11, differs from the two examples shown above. Particularly, in the [3-9]Hz range, no significant harmonic tones are present. This difference was observed in all control participants and highlights how differences between the two groups can be found from the accelerometer data. It is also shown that tremor is a movement disorder that has an identified frequency characteristic.

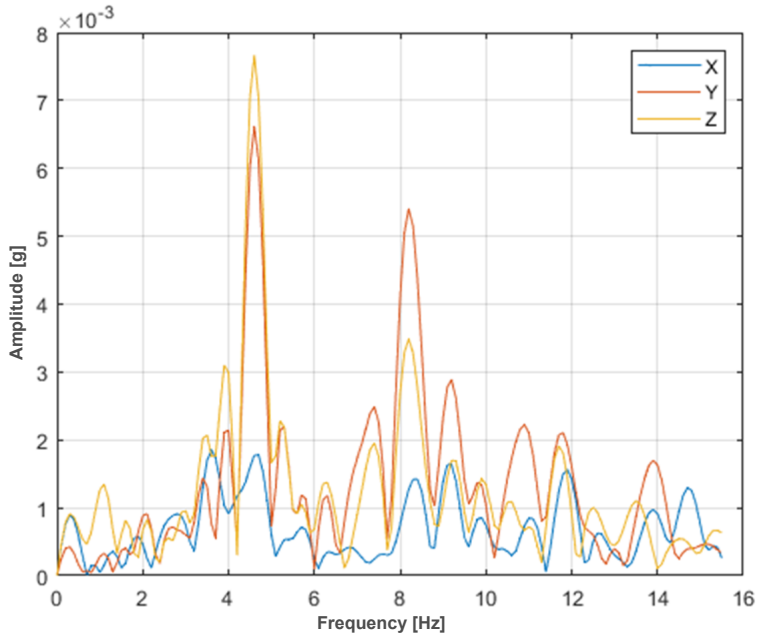

Figure 4.9: Frequency spectrum of the UPDRS 3.17 test for subject 12 with OFF medication

4.3.2 Classification Results

The next step was to take the dataset, extract from the data the 11 characteristics defined and validated in Chapter 3, and then train machine learning algorithms to distinguish control participants from Parkinsonian participants. All features were calculated over a 2-second window, with a 1-second overlap between consecutive windows. Among all available Machine Learning algorithms two of them have been chosen after thorough documentation: the Fine Tree (FT) and the Narrow Neural Network (NNN). The aim was to train the two networks to recognise and distinguish PD patients from healthy ones. Data were randomly extracted from all the acceleration data files of each patient, with the only limitation being that 50% of the data were taken from PD patients and the remaining 50% from healthy patients

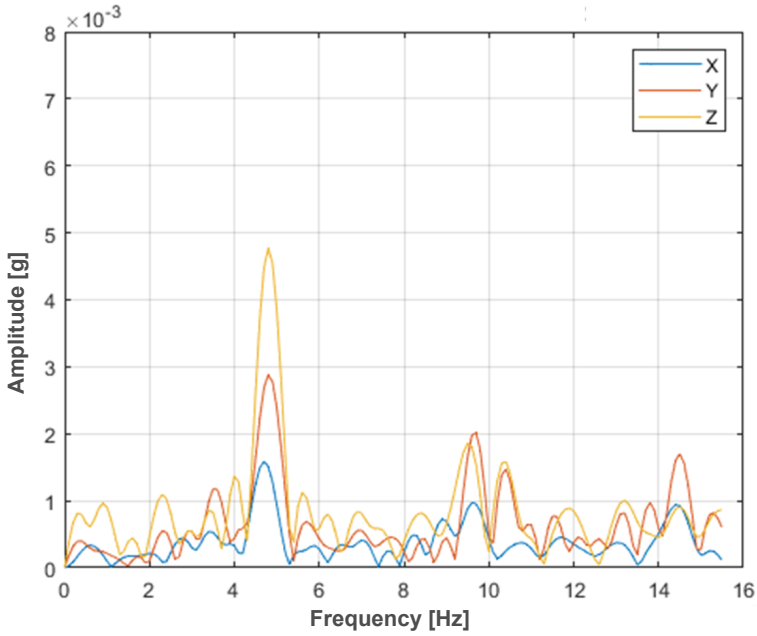

Figure 4.10: Frequency spectrum of the UPDRS 3.17 test for subject 12 with ON medication

to ensure uniformity. The training phase was performed on 16000 samples randomly selected from the 83203 total data extracted previously, while the testing phase was performed on 5000 data randomly selected from the 16761 overall data. Two classes were considered: 0 for healthy subjects and 1 for PD patients.

Comparison between Narrow Neural Network and Fine tree model

After training the model, a test phase was implemented. The confusion matrix in Fig. 4.12 and in Fig. 4.13 shows the samples correctly classified by the algorithm on the main diagonal, while the performance coefficients are shown in table 4.4.

For the NNN model, a test accuracy of 68% was obtained; for the control

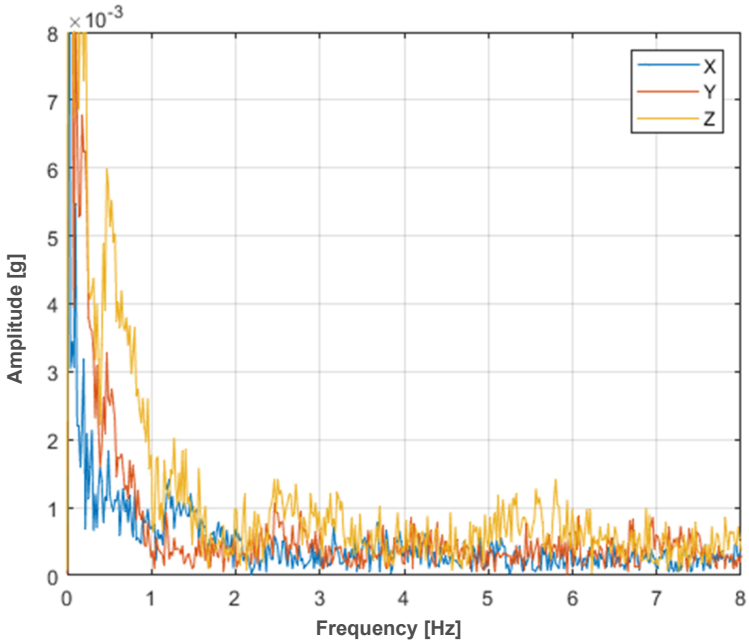

Figure 4.11: Frequency spectrum of a healthy participant

group, a Recall value of 77.5% was obtained, compared to 59.29% in the case of the PD group. In the PD group, the highest accuracy is obtained in the case of the precision parameter, with a value of 72.10%.

The Fine Tree model provides a 13% improvement in overall accuracy. From the confusion matrix in Fig. 4.13 , it can be seen that class 1 was always classified accordingly, while class 0 was confused with class 1 in 28% of the cases. By assessing the performance parameters, it can be seen that for the control group, values above 70% were obtained, while in the case of the PD group, the values obtained were above 60%.

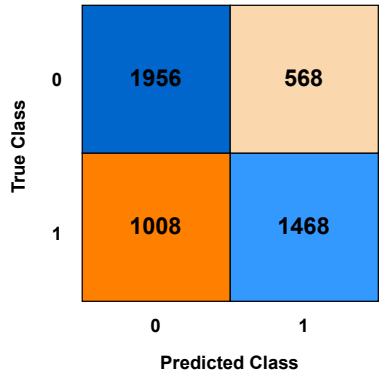

Figure 4.12: Narrow Neural Network Confusion Matrix for the test phase

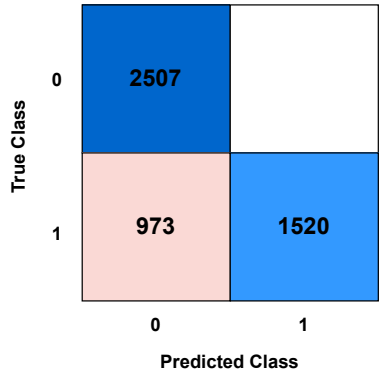

Figure 4.13: Fine Tree Confusion Matrix for the test phase

4.4 Motor State Remote Monitoring in Parkinson's Disease

The results discussed in the previous sections show how identified technologies and algorithms when well combined can provide information on the disease. In particular, by calculating specific features on inertial data, it is possible both to identify different motor symptoms and to distinguish tests performed by PD patients from healthy ones. Building on these ex-

Table 4.5: Performance parameters calculated for NNN and FT phase test

	Narrow Neural Network			Fine Tree		
Class	**Precision**	**Recall**	**F1-Score**	**Precision**	**Recall**	**F1-Score**
0	65.99%	77.50%	71.28%	72.04%	100%	83.75%
1	72.10%	59.29%	65.07%	100%	60.97%	75.75%
Accuracy	68.48%			80.54%		

perimental results, we move on to consider the possibility of using wearable technologies to monitor patients in an everyday environment and subsequently process the data to identify any motor abnormalities. In the case of people with Parkinson's disease, continuous monitoring can help doctors to control the evolution of the disease and to check adherence to pharmacological treatments. In this section, the challenge is to combine wearable sensors and machine learning-based algorithms to classify motor states using unsupervised data collected during everyday life.

4.4.1 Motor Fluctuation and standardised diagnosis

PD diagnosis typically rely on the appearance of motor symptoms [64], including tremor, bradykinesia, postural instability, freezing of gait, and rigidity. Manifestation of motor symptoms is highly variable among people with PD, they can fluctuate during the day (especially in later disease) and, in some cases, they deeply impact people with PD's quality of life and require complex clinical management. Dopaminergic medications such as Levodopa are most commonly used to manage motor symptoms [65]. Levodopa improves motor symptoms and function [66, 67], thus enhancing quality of life [68]. The management of the medication regime (e.g., frequency and dose) is linked to the disease progression, and prolonged use of levodopa can lead to side effects, particularly dyskinesias and motor fluctuations [66]. For participants under dopaminergic treatments, two distinct phases (motor states) can alternate during daily life: ON and OFF periods. The ON phase is characterized by an improvement in motor symptoms fol-

lowing medication intake. As the medication effects wears off, people with PD can experience an OFF period, when they experience a general worsening of symptoms [64]. Good adherence to dosage and timing of medication regimens reduces motor fluctuations between ON and OFF periods, limits 'OFF' periods, and helps managing motor symptoms. Studies have proven that adherence is often poor and in some cases under 65% [69]. Changes or adaptations of the medication regimes usually follow infrequent face-to-face clinical assessments, which lack important insights into the effect that medication has on people with PD's everyday life. Furthermore, the assessment of dyskinesia and OFF state is done through the evaluation of diaries, which are often laborious and inherently flawed. In this context, real-world remote monitoring with wearable technology (e.g., body-worn devices) could be an effective solution to have an objective insight of people with PD's motor state and their response to medication over the course of a day. The quantitative evaluation of symptoms and response to medication over a prolonged period of time could help clinicians to deliver an optimsed and customised medication regime, supported by objective data analyses and validated algorithms. To achieve this goal, it is useful to exploit Wearable Technology (WT) for example body-worn devices that allow objective quantification of mobility [70] [71] and motor symptoms in people with PD [72, 73], [74].

Wearable devices have been used for monitoring and evaluation of Parkinson's mobility and motor symptoms [35, 75–78].

Nevertheless, two main limitations can be found in the current body of work: i) participants are often monitored in a controlled environment or with the supervision of an observer and under controlled ON vs OFF state; ii) often the high accuracy and methods developed to identify motor states in controlled scenarios do not guarantee the reliability and robustness of the proposed techniques when applied to real- world environments. Conversely, limitation i) warrants the availability of controlled ground truth values of motor states, as participants are tested in controlled environments and under controlled conditions/protocols. Indeed, if it is desirable that people

with PD are monitored in real-world environments, to date, the diary is the only validated tool that can provide useful information on the participant's self-assessed motor state in unsupervised environments [79]. Although the diary is a subjective assessment tool and not always accurate, (e.g., dyskinesia may be confused with tremor [80]), it represents a reference system for the development of automated motor state recognition techniques. In this context, the idea is to train machine learning (ML) algorithms to recognize 'ON'-'OFF' and 'DYSKINESIA' motor states using IMU data by first selecting appropriate features and using participant diaries as labels for the motor states.

4.4.2 Participants and Measurement Protocol

People with PD were recruited as part of the Medical Research Council (MRC) Confidence in Concept (CiC) funded study "Translating digital healthcare to enhance clinical management: evaluating the effect of medication on mobility in people with Parkinson's Disease" (ISRCTN Number: 13156149, https://www.isrctn.com/ISRCTN13156149). This study is also a sub-study of the Mobilise-D – Clinical Validation Study (REC reference: 20/PR/0792) [81]. A convenience sample of 30 people was defined based on the Consensus-based Standards for the selection of health Measurement Instruments [82]. Participants' clinical and demographic characteristics are presented in Tab. 4.6.

Ethical approval was obtained from the London - Westminster Research Ethics Committee (REC reference: 21/PR/0469) and the study was carried out in accordance with the Declaration of Helsinki [83]. All participants were aged 18 years or older, had clinical diagnosis of PD according to the recent criteria of the Movement Disorder Society [84], were in Hoehn and Yahr stage 1 to 3, on stable Parkinson's disease medication, and were able to walk 4 meters independently. Participants were initially screened to determine eligibility prior to being enrolled in the study [85–91]. At the end of the visit,

Table 4.6: Demographic and clinical characteristics of participants recruited for the study

Characteristics	Mean ± Std.Dev	Median (Min-Max)
Males-Females n= 22-8		
Age (years)	63±9	
BMI (kg/m^2)	26.2±4.2	
Disease duration (years)		5 (1-17)
Hoehn and Yahr stage n (%)	I: 1 (3%) II: 29 (97%)	
MDS-UPDRS Part III (0-132)		30 (7-43)

for the 7-day remote monitoring period, they were equipped with: an IMU device (Axivity AX6, dimensions 23 × 32.5 × 8.9 mm, weight 11 g, sampling frequency 100 Hz, accelerometer and gyroscope ranges of ± 8 g and ± 2000 $^o/s$, respectively); a smartphone that collected contextual information; and a smartwatch, that, via a customized Smartphone App, reminded them of the medication intake times and allowed them to confirm the medication intake. Finally, a paper-based diary was provided to annotate motor states (with a granularity of 30 minutes), particularly OFF (filling the time slot with the character "O") and dyskinesia (filling it with the character "D"). Each diary included only 16 hours a day (from 6 AM to 10 PM). Fig. 4.14 shows an example of a completed diary. The monitoring lasted one week.

4.4.3 Data Processing

Among the 30 participants involved in the study, 26 were selected, and 4 were excluded due to data unavailability. Data were continuously logged for 7 days and then downloaded to a computer. A MATLAB®-validated-algorithm [73, 93] was applied to accelerometry raw data to identify walking bouts (i.e. a walking bout is characterised by a minimum of three steps) and for each walking bout other outcomes such as gait speed and step count.

The purpose of this study was to train a ML algorithm to identify 'ON',

CiC- Effect of medication on mobility in people with PD

Subject Initial _____ Subject ID _____

DAY/TIME	6:00 7:00		7:00 8:00		8:00 9:00		9:00 10:00		10:00 11:00		11:00 12:00		12:00 13:00		13:00 14:00		14:00 15:00		15:00 16:00		16:00 17:00		17:00 18:00		18:00 19:00		19:00 20:00		21:00 22:00	
Monday	O	O															O	O	O	O								D		
Tuesday			O	O																										
Wednesday																											D	D		
Thursday											O	O																		
Friday		O	O	O							O	O											D	D						
Saturday		O	O	O																										
Sunday													O	O	O	O							O	O			O	O		

Figure 4.14: Diary example used by participants during the experimental campaign. 'O' identifies the OFF state while 'D' is the Dyskinesia state. Each square is considered as half an hour. [92]

'OFF', and 'DYSKINESIA' states using raw inertial data (accelerometry and gyroscope data) and selected feature; the participants' diaries were used as reference data for the motor state. Gait analysis outcomes and medication intake times were used as ancillary data to better interpret the obtained results. The block diagram in Fig. 4.15 describes the procedure adopted in the analysis. After the recording phase, the raw data from the accelerometer and gyroscope (both triaxial) were considered.

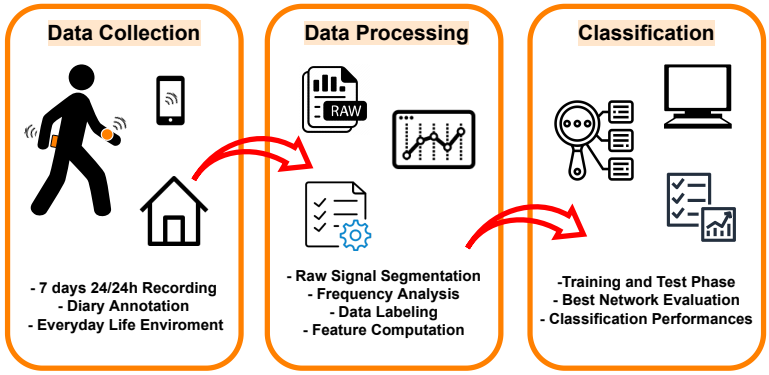

Figure 4.15: Flow chart describing the main process of experimentation. [92]

Fig.4.16 shows an example of accelerometer data acquired during a par-

ticipant's normal daily activity over 24 hours. The medication intake time is highlighted in each axis with different colours.

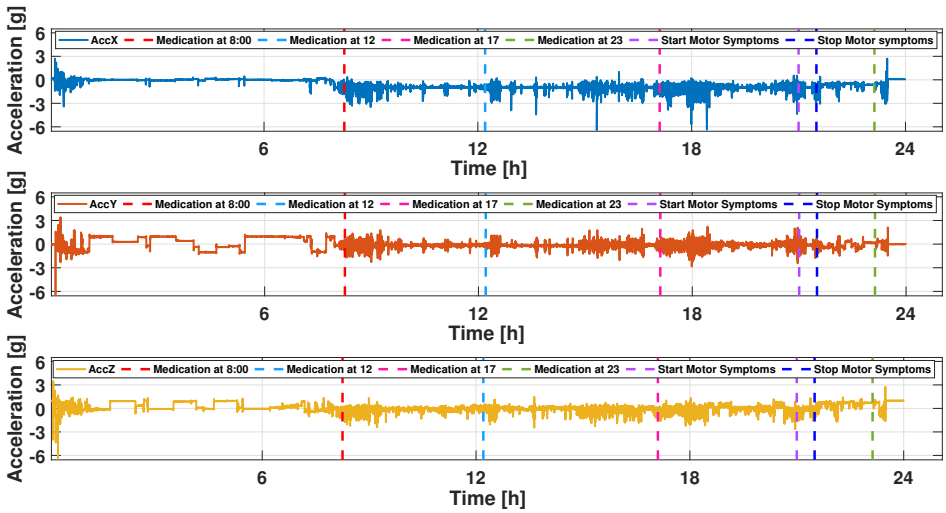

Figure 4.16: Raw acceleration data for each axis during the one-day recording. Vertical lines indicate the medication intake time. [92]

The objective of this procedure was to check whether the harmonic content of interest was also present in the intervals in which the participant declared to be in an 'OFF'/'DYSKINESIA' state.

In Fig. 4.17, the graph on the left shows 5 minutes of an accelerometer trace of a participant who reported being in the OFF state. From the gait analysis data, it can be deduced that the person was not walking at that specific time.

Next, the Fast Fourier Transform (FFT) of the signal was performed (Fig. 4.17, graphs on the right), and in this example, it can be seen that two tones, in particular, emerged along the z-axis: one at 2.5 Hz and one at 5 Hz. The same procedure was performed for each participant, for each of the recorded days, and it was observed that these two tones occurred in those intervals labeled as OFF state, in the participants' diaries.

Based on these considerations and the knowledge that some motor symp-

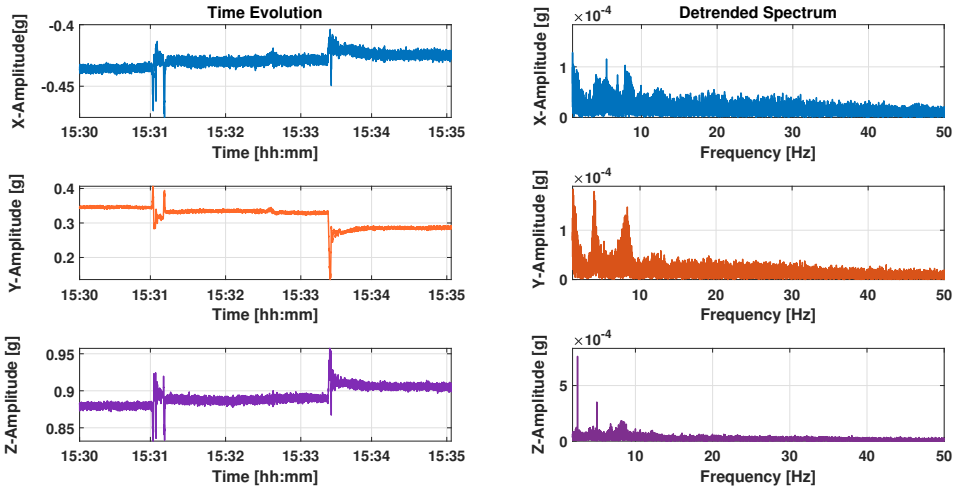

Figure 4.17: Time series of acceleration (left) and detrend spectrum (right) considered over a 5-minute observation window across 3 dimensions (x,y,z).

toms such as tremors can be associated with a characteristic frequency range (e.g. Rest tremor can be in the range of 4-6 Hz) [94], we considered the frequency information present at 2.5 Hz and 5 Hz. These frequencies were chosen as they are associated with motor symptoms (such as tremors) and to exclude frequencies associated with walking (2 Hz) [95]. For each participant, the entire signal was divided into 10-second windows and filtered with a third-order Savitzky-Golay with a frame length of 51 samples, and for each of these, the FFT was calculated by selecting and saving the harmonic content only in the frequencies of interest. Subsequently, the two harmonic contents were summed up point by point (an example is provided in Fig. 4.18) and labelled using the diary annotations.

4.4.4 Data Analysis

The implementation of ML models for the classification of 'ON', 'OFF', and 'DYSKINESIA' was carried out in MATLAB^{TM} R2022a (Mathworks, Natick, MA) to identify possible features that can objectively describe motor

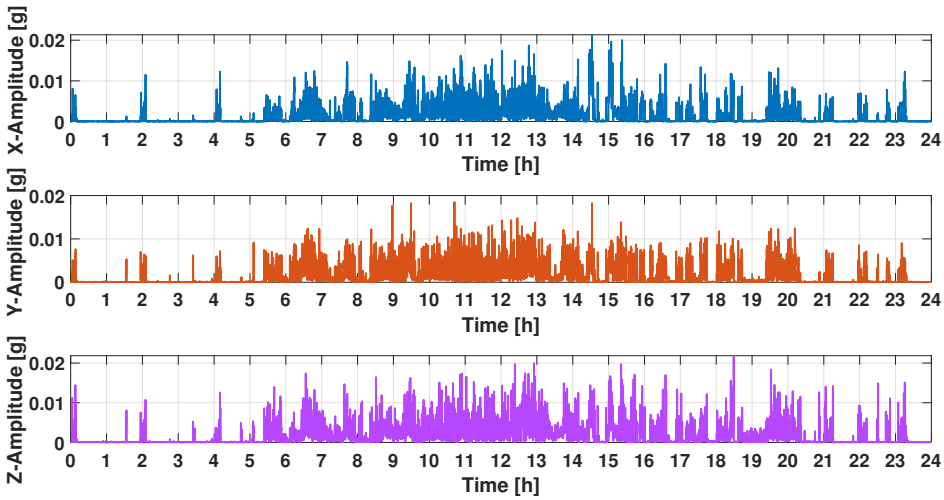

Figure 4.18: Time evolution of amplitudes related to the frequencies of interest (2.5 Hz and 5 Hz)

symptoms. The first step is to define the classes, in particular:

- ON state identified as Class 0;
- OFF state identified as Class 1;
- DYSKINESIA state identified as Class 2.

After processing and labelling the data, feature extraction was performed. 6 features already adopted in the literature to identify and distinguish pathological movements voluntary movements, and OFF/ON state in inertial data were considered [80], [39]:

- Average, i.e. the mean value of the signal, previously computed as the sum of each-axis component;
- Squared sum on time domain signals containing only 2.5 and 5 Hz frequency components under 25th percentile;

- Squared sum on time domain signals containing only 2.5 and 5 Hz frequency components under 75th percentile;
- Maximum of the signal spectrum;
- The average of the difference between the maximum and minimum peaks of the time domain signals containing only 2.5 and 5 Hz frequency components;
- Signal Energy.

The features above were computed for both accelerometer and gyroscope data, extrapolating only 2.5 Hz and 5 Hz components, over 5-minute segments, assigning the same label to all computations belonging to the same 30-minute interval, which is the resolution provided by participants' diaries. Before moving to the training phase of the classification, the data were normalized employing the Z-score method [96]. However, 70% of the dataset was used for the training phase, where classes were represented in a balanced way and 30% for the testing phase.

Results

The ML models implementation was carried out using MATLAB®. Machine Learning Tool was adopted to select the best ML models for the processed data. In detail, a first test was performed on the three-class problem (0,1,2) and a second test was executed to discern binary output (classes 0,1), where class 1 includes all samples previously belonging to classes 1 and 2. The most accurate networks in the training and test phases were: i) a kNN network for identifying the three classes; ii) a Fine Tree (FT) tool to classify only the ON-OFF classes . In case (i) the kNN network was trained to distinguish the three classes (ON, OFF and DYSKINESIA) and the overall test accuracy was 83.63%. The test phase confusion matrix is shown in 4.19; the values predicted correctly by the network are shown on

the main diagonal, and it can be seen that class 0 was predicted correctly with an accuracy of 96.80%, class 1 with 74.31%, and class 2 with 80.90%.

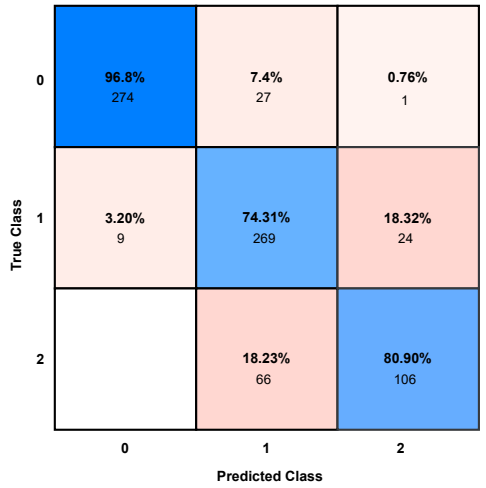

Figure 4.19: Confusion Matrix of test phase when 3 classes are considered.

Tab. 4.7 shows the classification performance expressed by four indices: Precision, Recall, F1-score, and Specificity. These indexes were calculated for each class: particularly relevant is the specificity that gets values higher than 0.8 for all classes. As evident also from the confusion matrix in Fig6, the classifier mis-classified class 1 for class 2 and vice versa. This led the authors to consider classification step (ii) which involved only the recognition of two classes. Class 2 was incorporated into class 1 and the FT tool obtained a test accuracy of 95%.

Table 4.7: Classification Performance Results in Test Phase with 3 classes

	ON [0]	**OFF [1]**	**DYSK. [2]**
Precision	0.988	0.743	0.809
Recall	0.907	0.891	0.616
F1_Score	0.937	0.810	0.700
Specificity	0.981	0.804	0.959

Fig. 4.20 shows the confusion matrix and on the main diagonal, it can be seen that the correct predictions are above 94%. The performance indices show a general improvement for class 1, in particular, as it can be seen in Tab. 4.8, the Precision index goes from 74% in the i) case to 96% in the ii). For class 0 all indices are greater than 94%.

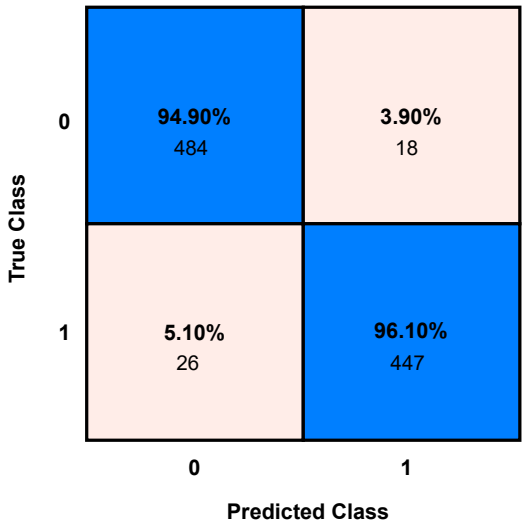

Figure 4.20: Confusion Matrix of test phase when 2 classes are considered

Table 4.8: Classification Performance Results in Test Phase with 2 classes

	ON [0]	**OFF [1]**
Precision	0.949	0.961
Recall	0.964	0.945
F1_Score	0.957	0.953
Specificity	0.945	0.964

Discussion

The goal of this study was to identify 'ON', 'OFF' and 'DYSKINESIA' states from a single IMU's data collected in people with PD during everyday life, in real-world environment. The identification of these states could help clinicians to check the effectiveness of dopaminergic treatment and to assess how the disease is progressing. In this work, the aim was to find associations between inertial data and labels obtained from the diaries that participants completed during the week of recording. Several studies have discussed about the 'ON', 'OFF', and 'DYSKINESIA' states classification [35],[80],[36]. Specifically, in [35],[80], the authors goal was to identify only the 'ON' and 'OFF' classes, while in [36] the identification of the 'DYSKINESIA' class is also included. In these studies, classification was performed from inertial data from multiple sensors placed on the participant's body and labels were assigned by an external observer under supervised conditions. In this case study, we aimed to identify the three motor states from a single inertial sensor, so as to reduce the number of wearable devices and consequently participants' burden. A limitation of this study is represented by the use of a diary as a self-assessment tool. This instrument involves a subjective component that must be taken into account. To date, however, it represents a validated method to be used to get daily reports on the participant's status [79]. The preliminary results obtained from the combination of data from a single sensor and diaries are encouraging: in the case of the three-class classification, an overall test accuracy of 84% was achieved while in the two-class case, the accuracy value reached 95%. These results mark a good starting point for the development of automated measurement systems capable of analyzing data acquired from wearable technology in the real world.

4.5 Final Observation

This chapter aimed to verify the use of inertial sensors and data processing techniques applied to a medical context. In the first analysis, classification algorithms were trained to recognise simulated pathological movements. The accuracy results obtained show that the features assumed in the simulation phase also perform well in the application case. Laboratory experimentation was followed by verifying the characteristics of real acquired data. In particular, the dataset is characterised by a group of people with PD and a control group of healthy subjects. The study showed how trained machine learning algorithms can distinguish between the two groups with good accuracy. This shows that the features hypothesised in Chapter 3 are generalisable and can distinguish tests performed by PD patients from healthy ones. In the last section, building on the previous encouraging results, an experimental campaign characterised by 24 PD patients monitored remotely by an inertial sensor is described and analysed. A single sensor placed on the lower back was used for 7 days 24 hours a day. The aim was to analyse the accelerometer time series and combine it with information from the diaries filled in by the patients to automatically identify motor states (ON-OFF-DYSKINESIA). The information and results obtained can be a starting point for developing an automatic measurement system that can acquire and process data in real-time and remotely. A tool that can provide objective disease results, helping the doctors in increasingly accurate and timely diagnoses.

Chapter 5

Sport Field: IMU device to objectively evaluate coordinative abilities and reaction time

An automatic measurement system characterised by wearable inertial systems and data analysis algorithms described in the previous chapters can also find wide application in the field of sport. In particular, inertial sensors can be valuable measurement tools to be used to assess coordination abilities in healthy people.

5.1 The research motivation

Monitoring coordinative abilities in sports applications is often carried out by trainers who adopt subjective protocols and evaluations not supported by repeatable and reproducible measurement setups. This often leads to unreliable evaluations that do not allow us to quantify the positive or negative

effect of some training in a simple way. The measurement of coordinate and conditional capacities during physical exercise, such as the reaction time to an external stimulus, can provide essential information to enhance cognitive and physical skills on performance. In this scenario, the rapid spreading of wearable devices able to capture human movements and provide data to the users could be a useful instrument to face the problem of simplifying the development of automated, repeatable, and reproducible measurement procedures easily adopted by a community of athletes or coaches. The aim of this chapter is to demonstrate how algorithms and devices used in medical applications can also be easily adapted to sports contexts. In this regard, the following aspects will be addressed: i) analysis of standard methods used for motion assessment during sports training ii) validation of a measurement set-up characterised by IMU for the objective measurement of reaction time and coordination; iii) development of an automatic measurement protocol and extraction of useful features to characterise and extract information in training phases; (iv) assessment of coordination abilities in different groups of athletes differentiated by age and gender.

5.2 Standardised method to evaluate coordinative abilities

Coordinative abilities are neuro-motor characteristics that distinguish our movements [97], which influence the learning and refinement of new motor acts and their stability over time. Coordination allows people to perform a movement, or group of movements, with better quality and effect [98]. Furthermore, these abilities promote the efficient execution of motor actions under a variety of conditions, enhance the restructuring of movements in high-performance training phases, improve basic and applied motor abilities, and aid the use of conditional abilities [99]. Indeed, they are the basis for learning and improvement of technical abilities and are in close coop-

eration with conditional abilities [100]. Body movement is determined by the individual's ability to effectively use the surrounding environment information [101] and coordinative training interventions can be fundamental in enhancing also cognitive abilities, on which functional motions deeply depend [100]. The most common assessment of neurological efficiency is reaction time [102, 103]. Reaction time is the period between the onset of stimuli and the initiation of reactions to them. This factor is a valuable indication for investigating central nervous system ability and motor function [104]. Recent work states that maintaining a good state of reaction time training can help us to improve our ability to concentrate and overall performance [105]. Body training is a fundamental practice, but training coordinative capabilities are equally important, and rarely it is considered a specific training program. Authors in [106], reported that subjects with better visual information acquisition abilities perform better. For instance, an athlete with a trained visual system performs better in comparison with an athlete of similar characteristics, but with a less performing visual system. To evaluate reaction time, a possible methodology concerns oculo-manual examinations, such as the Ruler Test (RT) and Tapping Test (TT). These tests are often used as an indicator for visual control, hand-eye coordination, and response time [102, 107]. To date, the handling of these tests is generally carried out by an operator. In recent years, technological devices have been implemented to evaluate body or anatomic section movements under different stimuli and motor tasks and their related reaction time [108], [109]. Gesture recognition devices that detect limb motions in space and time can provide essential information about patients' coordinative abilities, particularly in the pathological field as a valuable tool for diagnosis and disease monitoring [110].

5.3 Experimental validation of wearable technology in sports applications

To introduce inertial sensors in coordination tests, it is necessary to implement a validation process that compares the proposed new measurement methods with standard ones.

5.3.1 Participants and Test Procedure

Twenty voluntary students, 11 males and 9 females, from the University of Cassino and Southern Lazio, were enrolled and selected in the study during an internship activity. The study was limited to individuals who self-identified their dominant hand as preferred for writing, performing sports activities, using a tool or leading out in movement. The participants were divided into a group of 10 for RT, 6 male and 4 female (Mean Age 22.6, ranged from 20 to 26) and a group of 10 for TT 5 male and 5 female (Mean Age 23.3, ranged from 22 to 24). After being adequately informed about the prerequisites for participation before testing, all students underwent two testing sessions on two non-consecutive days, at the same time of day, in the following order: ruler test, tapping test. Participants were instructed to avoid eating large meals and consuming caffeinated beverages for two hours before testing (formerly coffee, cola or tea) and to avoid smoking and drinking alcoholic drinks for at least 24 hours before the exam. Subjects had to be fully hydrated (due to summer temperatures) and were asked to avoid intense exertion or physical activity for 24 hours before testing. Dangling jewellery, watches, bracelets or earrings had to be removed as they could impede instrumentation. Subjects with injuries or diseases or who were not in good health were excluded from the study. All students were familiarized with the testing procedures one hour prior to the tests. This project was approved by the Institutional Review Board of the University of Cassino and Southern Lazio (No. 11253.2021.05.12). Before participating

in the study, subjects have been informed in detail about the protocol. Moreover, informed consent and authorization about benefits and risks have been obtained in accordance with the Declaration of Helsinki for Human Research of 1964. Tests were conducted using the IMU sensor validated in Chapter 3. For each test subjects repeated the trials 20 times, with a time interval between each trial for data storage and parameter adjustment (30 s). During the break, the user was instructed to assume a resting position. Protocols from two previous studies were referenced for both tests [111], [112], and only the dominant limb was evaluated.

Ruler test

Participants were asked to sit at the edge of a table, elbow on the surface, and wrist extended over the side. The sensor was attached to one of the ruler's ends. The observer held the ruler in the air between the participant's thumb and fingers without touching it, aligning the zero point with the participant's fingertips. When a participant was ready, the observer dropped the ruler without notice, and the subject should catch it as soon as he saw it fall. The distance travelled by the ruler before catching will be measured in centimetres. The data were used to calculate the reaction times by applying the standard formula described by eq. 5.1 [113].

$$t = \sqrt{\frac{2d}{g}} \tag{5.1}$$

where d is the distance and g is the gravity acceleration.

Tapping Test

During the tests, the subject's hand rested flat on a desk surface, with the fingers extended and the index finger on the counting device. The subject's elbow was placed on the desk with a 90-degree extension. The sensor was placed on the second middle phalanx of the dominant hand,

and participants were instructed to tap as many times as possible in a 10-second timeframe, flexing and extending the metacarpophalangeal joint of the tested index finger. Sensor acquisition started as the subject had performed the first movement of the index finger and ends when the 10 seconds expired. The recovery phase between a trial and subsequent was set to 30 s (3 times with respect to trial time), to complete spent energy restoration (anaerobic metabolism), permitting to perform all 10 trials in optimal physical condition. The data acquired by the sensor were compared to those collected by the observer's counting and a dedicated application (CNS Tap).

5.3.2 Measurement set-up

An experimental protocol for testing was defined and, as can be seen in Fig. 5.1: two different setups were implemented. An inertial measurement unit (IMU) was used to make the objective measurements during the RT and the TT. The employed sensor acquisition parameters were: a sampling frequency of 100 Hz, an accelerometer range of $\pm 4g$. In the first test (Fig. 5.1 a), the sensor was anchored to the subject's index finger and in the second test (Fig. 5.1 b) the device was placed on the ruler; in both cases, the inertial data was sent to the PC via Bluetooth. The data collected by the device were compared with those conventionally evaluated by the operator.

The data collected by the device were analyzed by the implementation of dedicated algorithms able to: 1) calculate the subject's reaction time considering data from ruler tests; 2) count tapping events in a specific interval using tapping tests data. Fig. 5.2 displays the algorithm block diagram that describes the procedure used to calculate features of interest. Fig. 5.3 shows the result obtained during a ruler test, in particular the first line shows the x-axis acceleration data, while in the second line we can observe the time interval spent by the subject to take the ruler. In this test, the computed reaction time is 0.23 s. In Fig. 5.4, acceleration data during the tapping test

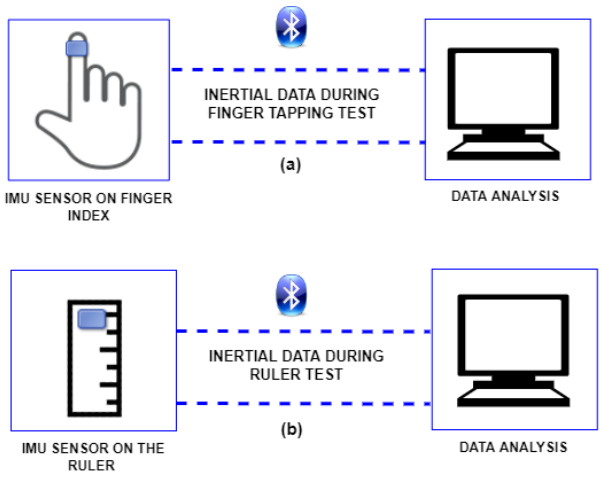

Figure 5.1: Measurement set-up to realise tapping (a) and ruler (b) tests. [20]

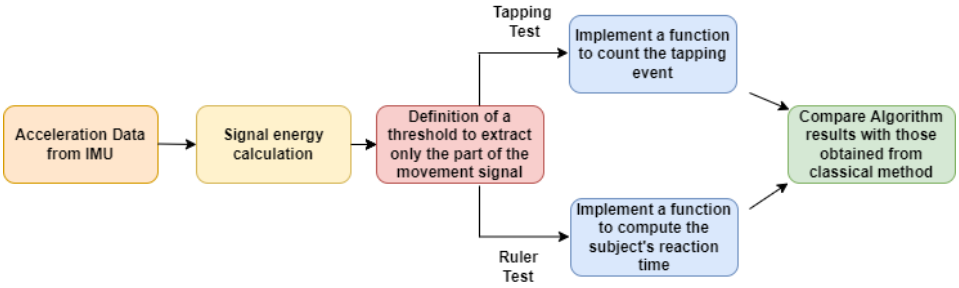

Figure 5.2: Block diagram describes the logical procedure and the main characteristics of the algorithm.[20]

are shown and it could be seen how the algorithm computed and highlighted about six taps per second (each red circle on the signal picture (Fig. 5.4 is a tapping detection). The signal peaks represented the instant when the subject index finger pressed on the thumb. In addition, in the case of the RT, the x-axis only has been considered, since the ruler has been aligned with the IMU x-direction. For TT, acceleration along z-axis has been considered because the main tapping movement was realised in such a direction.

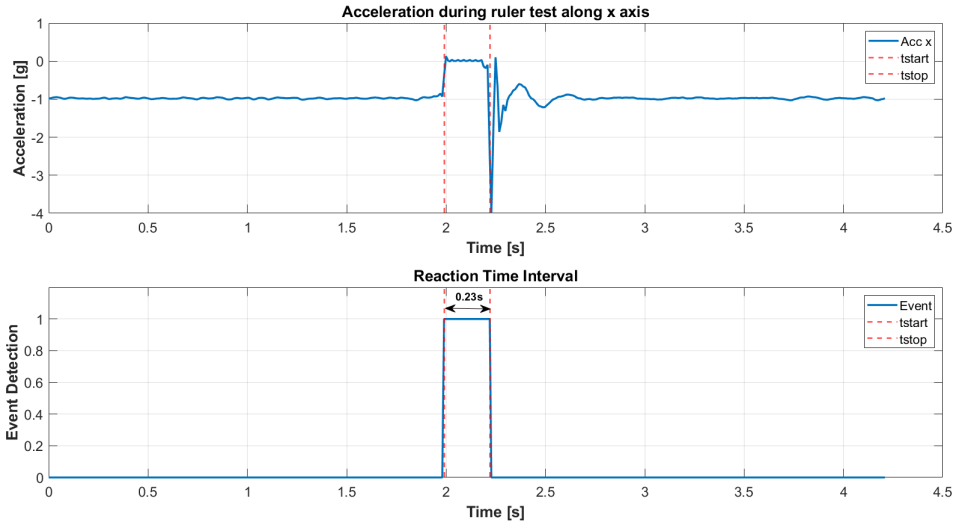

Figure 5.3: Ruler test result: the first row shows the acceleration data along x axis, in the second row is displayed subject reaction time.[20]

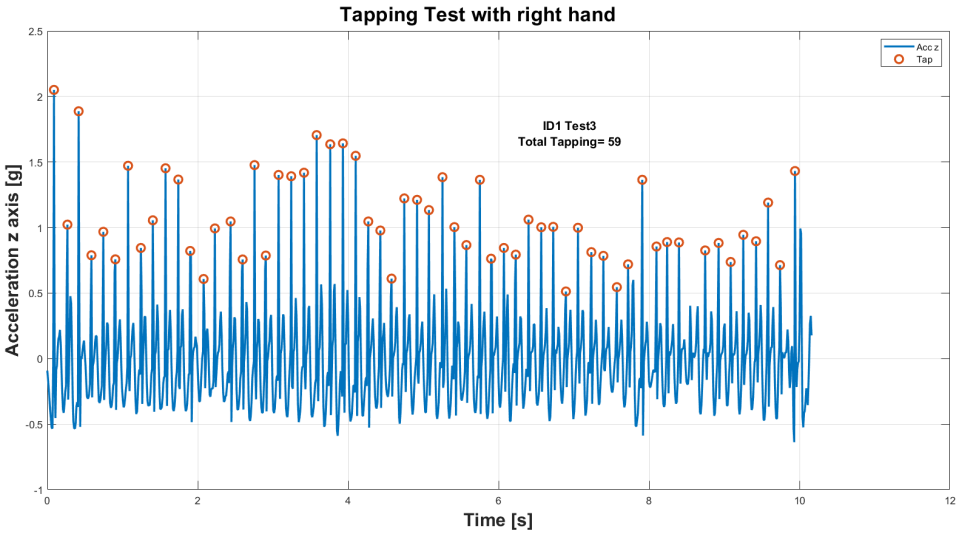

Figure 5.4: Acceleration data along z axis during tapping test: the tapping instants are highlighted.[20]

5.3.3 Results

After the processing data, a statistical analysis was carried out. Table 5.1 presents a summary of the subjects' anthropometric measurements, data are expressed as mean value and relative standard deviation. A descriptive analysis was conducted to verify the data distribution. A preliminary analysis of the results of both tests was carried out with the Shapiro–Wilk normalization test on different sets of data. In the first set, all collected data were analysed together; in the second one, the results were divided by gender. In both cases, and for both tests, the results were not normally distributed. Then, a nonparametric Repeated Measures ANOVA analysis was carried out.

Table 5.1: Mean and standard deviation of both genders anthropometric measurements

	Age (years)	**Height (m)**	**Weight (kg)**	**BMI kg/mˆ2**
Male	22.8 ± 1.2	1.76 ± 0.10	74 ± 12	24.0 ± 1.6
Female	23.1 ± 2.0	1.600 ± 0.036	54.9 ± 7.0	21.5 ± 2.3

In Table 5.2 RT data, measured by mean of two measurements methods (Observer and IMU sensor), are shown. Data are expressed as mean value and relative standard deviation. As highlighted in Table 5.2, a significant difference was found between the two types of measurement, although the IMU sensor provided lower mean reaction time values than the observer measurements. In particular, the percentage difference between observer and IMU measurements less than 5% (4.7%) was observed.

The mean values and standard deviations of the TT results are shown in Table 5.3. In the TT case, the results for the three different measurement methods (Observer, App, IMU sensor) were not statistically different and were comparable. The difference between each test was less than 3% (ranging from −2.99% to 3.51%).

Table 5.2: Mean and standard deviation of RT reaction time expressed in seconds for different measurement methods

	Observer (s)	IMU sensor (s)
All	0.170 ± 0.029	0.160 ± 0.031
Male	0.170 ± 0.029	0.160 ± 0.032
Female	0.170 ± 0.028	0.160 ± 0.031

Table 5.3: Mean and standard deviation of TT number of taps in 10 s for different measurement methods

	Observer (tap/10s)	App (tap/10s)	IMU sensor (taps/10s)
All	61.0 ± 7.0	61.4 ± 6.5	62.3 ± 5.9
Male	53.0 ± 8.2	61.8 ± 6.7	61.4 ± 7.7
Female	59.1 ± 4.9	61.1 ± 6.2	60.6 ± 2.1

Discussion

Participants were all young subjects and were homogeneous in gender, age, and BMI. In fact, data analysis showed that the population was normal weight with a BMI value between 18 and 25 kg/m^2. The comparison of the two approaches employed in RT showed statistically different results: in detail, the IMU sensor reported lower response time values than the observer measurements. Simulating voluntarily entered errors, movements ranging from 0.1 cm to 1 cm cause reaction times that can differ from 0.4 ms to 4.6 ms, approaching our percentage difference of 4.7%. Measurement becomes significantly more objective using IMU, in order to remove the observer's error. In TT, differences between the data collected by the three distinct measuring methods were negligible, so the test can be performed by all three methods. The IMU sensor allows a quantification of the range of motion, which is a useful indicator of neuromuscular fatigue in terms of coordination ability, as evidenced by the graph 5.5, the number of taps has a decreasing trend between the first and last repetition for each subject. This physiological decline could be linked to exhaustion which may cause a change

in the acceleration between the first and last trial. In this case, the IMU might be used to normalize the amplitude and utilize it as the coefficient of a linear line crossing between the first and final values, which will have a decreased amplitude. The absolute value of the resulting equation's angular coefficient might be referred to as the coefficient of fatigue. As can be documented in Fig. 5.5, the coefficient of the equation interpolates in all the average peak values of the 20 performed trials, and it is shown that the decrease is minimal. This is evidence that the subject was able to perform each trial at maximum energy efficiency. Thus, it can be said that the 30 s of rest between trials was sufficient for a full recovery. The IMU sensor can be used as a tool to identify the fatigue index represented by the coefficient in the equation if the times imposed in the test are different. That is, test execution times higher than 10 s and recovery time less than or equal to 30 s. In this way, neuromuscular efficiency can be represented by the fatigue index. Furthermore, it could be a representative indicator of neuromuscular efficiency or a useful parameter in medical rehabilitation for evaluating the type of rehabilitation and type of performance (e.g., dexterity sports). It is recommended that the recovery time be higher than three times the exercise time.

5.4 Development of automatic measurement protocol

In this section, an automatic measurement protocol for the assessment of coordination abilities based on the use of IMUs integrated into wearable devices is proposed. A novel protocol based on the ruler and tapping tests and a set of objective key performance indicators, derived from IMU measurements, to assess the test outcome. In detail, the protocol is based on the sequence 1) ruler test; 2) tapping test; 3) ruler test. Starting from such considerations, the present section is mainly devoted to i) proposing

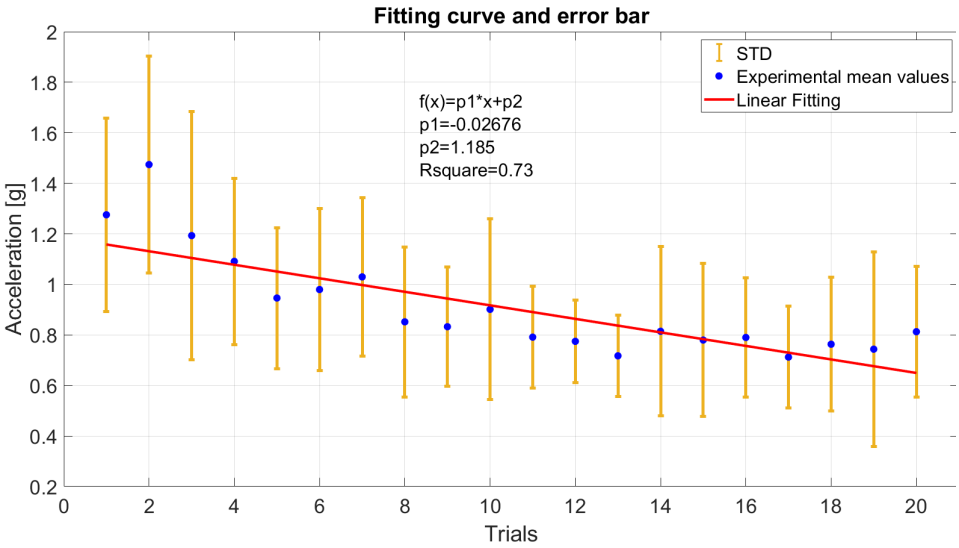

Figure 5.5: Fitting curve calculated from the mean amplitude of the peaks obtained during the tapping trials by each subject

a measurement protocol to have both training and evaluation purposes for sports people, capable of producing a detailed and easy-to-read report on their physical status; ii) creating an automated measurement set-up, which is able to capture movements through the use of an Inertial Measurement Unit (IMU) and process the acquired data in real-time to estimate several quantities of interest.

5.4.1 The measurement protocol

In this study, eighteen voluntary students from the University of Cassino and Southern Lazio are involved. In particular, 9 males and 9 females took the test during an internship activity in the framework of the Motor Science Course. For each subject, anthropometric data that are age, length of the index finger used for the tapping test, weight, and height are collected. More in detail, height and weight are combined in a synthetic parameter that is the Body Mass Weight (BMI). Fig. 5.6 describes anthropometric

information for each subject, while in Tab. 5.4, the mean and standard deviation of the main information of the group are reported. For a complete overview, information on sports and personal activities has been requested and summarized in Tab. 5.5. Participants are informed about the structure of the protocol and the execution of the tests. In detail, they are asked to perform a test containing three different exercises in the following order: ruler test; tapping test; ruler test. The first exercise with the ruler shows the reaction time at rest, then they are asked to perform the tapping test in an energy-exhausting fashion, and, finally, the ruler test is repeated again to highlight any possible change in the reaction time after the tapping test task. To record the inertial data of the different tests, the sensor is fixed by the operator on the ruler for the RT and the index finger of the dominant hand for the TT; Fig. 5.7 shows the position and orientation of the sensor in the three different phases described above. Data acquisition starts at the beginning of the test and stops after the last ruler test. At the end of each test, the data are saved in the cloud via the proprietary app. This project was approved by the Institutional Review Board of the University of Cassino and Southern Lazio (No. 24777.2022.12.12). Before participating in the study, subjects have been informed in detail about the protocol. Moreover, informed consent and authorization about benefits and risks have been obtained in accordance with the Declaration of Helsinki for Human Research of 1964.

Table 5.4: Mean and standard deviation of the anthropometric data of all subjects

Information	**Mean** (μ)	**Std. Dev.** (σ)
BMI $[kg/m^2]$	23.31	3.63
Finger Length $[cm]$	8.69	0.89
Age $[y]$	25.33	3.71

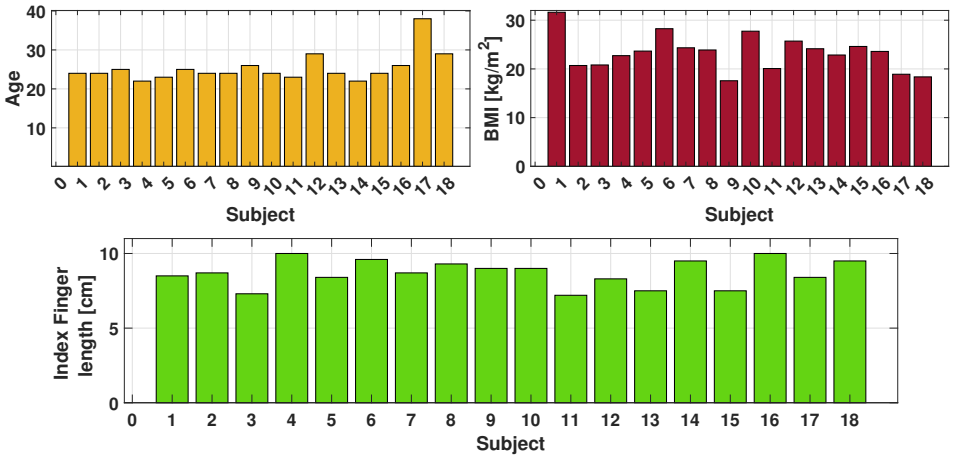

Figure 5.6: Anthropometric data evaluated for each subject

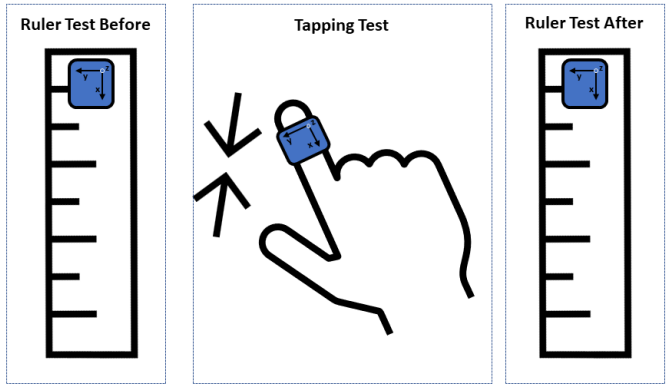

Figure 5.7: Measurement protocol: the IMU sensor orientation and positioning during the three exercises

5.4.2 The developed set-up

To perform objective measurements MMR IMU sensor has been adopted both for ruler and tapping tests, according to the measurement protocol explained before. Pictures of the set-up arranged for each test can be seen in Fig. 5.9. In detail, in Fig. 5.9a, two people are involved to perform the

Table 5.5: Sports and activities done in free time by each subject

Activity	Subject IDs
None	ID1; ID17
Play Guitar	ID2;ID10;ID16
Gym	ID3; ID4; ID7;ID10;ID14
Videogames	ID4;ID5;ID6;ID8;ID16
Basket	ID5
Padel	ID6;ID8;ID13
Tennis	ID8
Dance	ID9;ID14;ID15
Body Building	ID10
Taekwondo	ID11
Weightlifting	ID12;ID13
Swimming	ID14
Athletics	ID14
Football	ID16
Fitness	ID18

ruler test. The first one keeps the ruler and, at a random instant, leaves it falling, while the second person should catch it in the fastest possible time as soon as the ruler is left in falling mode. Fig. 5.9b reports another voluntary person performing the tapping test. In this case, the only constraint is represented by the tapping amplitude that must be as close as possible to the one indicated in the handcrafted background panel, equal to 4 cm.

The operations of setting sensor parameters and uploading data are carried out via Metabase's proprietary application [114], and the MMR communication technology is based on the Bluetooth Low Energy 4.0 Smart® module.

Acceleration data are acquired via the MMR by setting a sampling rate of 100 Hz and a range of $\pm 8g$, where g is the gravity acceleration constant, equal to 9.81 m/s^2. The overall test duration is not fixed because it depends on the subject's endurance time during the TT. Once the data has been

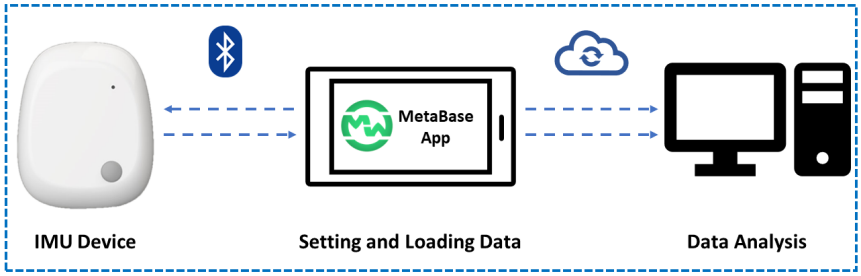

Figure 5.8: The implemented setup is characterized by sensor, devices, and technology used in the acquisition data process

acquired, it is stored in a cloud and then downloaded to a PC for analysis. It is worth noting that the setup is composed of three elements: the IMU sensor, a gateway device, and a PC. In order to minimize the hardware impact, the setup could also be composed of the sensor and the PC only. Nevertheless, for flexibility reasons and to fast execute the tests, a tablet has been used as a gateway in order to exploit Bluetooth low-distance ranges, without the need to have the processing unit close to the test location.

5.4.3 Automated Measurement Algorithm

To analyze the data set, an algorithm (see Fig. 5.11), that receives the raw accelerometer data of the single test as input and computes the corresponding time intervals of RT and TT activities is implemented.

Table 5.6: Validation of proposed algorithm with respect to golden standard methods

RULER TEST	**Mean Value**	**Std.Dev.**	**Overlapped pdf Area**
Manual Inspection	0.170	0.029	0.87
Our Algorithm	0.160	0.031	
TAPPING TEST (10 s)	**Mean Value**	**Std.Dev.**	**Overlapped pdf Area**
Application	61.4	6.5	0.93
Our Algorithm	62.3	5.9	

(a) Ruler Test set-up

(b) Tapping Test set-up

Figure 5.9: Pictures of the set-up mounted for executing ruler and tapping tests

The algorithm acquires all raw acceleration data along three axes and separates those belonging to Ruler Tests from data deriving from the execution of the Tapping Test.

An example of accelerometer data recorded during a test is shown in Fig. 5.10. In detail, the shown data consist of a demo test, lasting 8 s, where the sequence RT-TT-RT is reported. A small amount of data between RT and TT is discarded since it refers to the sensor position change from the ruler to the subject's index finger.

The main operations of the developed algorithms concern the estimation of reaction time from the ruler test data, by analyzing the accelerometer data along the x-axis (Fig. 5.11a) and the computation of the number of taps by considering the accelerometer data along the z-axis (Fig. 5.11b). The

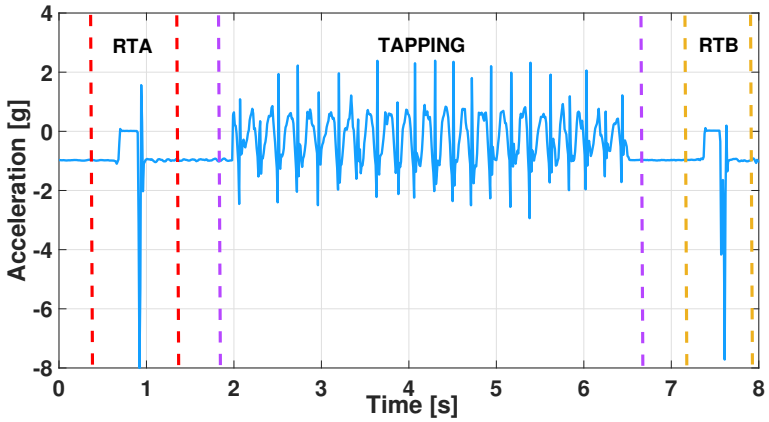

Figure 5.10: Example of the accelerometric data along the x-axis recorded during a complete test[115]

axis selection is made by considering the sensor orientation and the main direction of motion, i.e. the one in which a greater excursion of acceleration is observed.

Going into deep with the developed algorithm, the main sections are explained in the following. For the RT algorithm, the Matlab^{TM} routine *findchangepts* [116] is used to detect the acceleration abrupt change during the falling ruler, while for the tap number detection, the *findpeaks* [117] routine is chosen. The adopted algorithm has been already validated in our previous work [20], at least as concerns the estimation of reaction time and number of taps. Furthermore, in [20], results derived from the IMU sensor were also compared with standard visual inspection and with those provided by a Tablet app that used its display as a touch sensor. Particularly, Tab IV in [20] shows the obtained results that confirm full compatibility with a confidence level of 95%.

Briefly, the characterization results are reported in Fig. 5.12, in terms of Gaussian probability density functions (pdf), obtained thanks to the Central Limit Theorem (n = 400) where a high-level of overlapping is visible, and in Tab. 5.6, in terms of Mean Value and Standard Deviation (Std.Dev.). Such

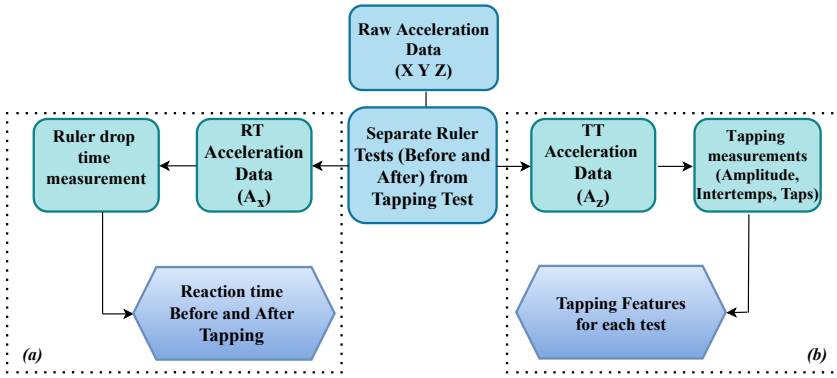

Figure 5.11: Automated measurement algorithm diagram: in part (a) the procedure to compute reaction time, while in part (b) the process used to obtain the number of tapping are reported [115]

an overlapping has been quantified in terms of common area in Tab. 5.6 as "Overlapped pdf Area" column values [20]. The obtained high level of agreement allows using the automated algorithm instead of manual inspection and, therefore, by adopting an objective procedure, and increasing the overall reliability of the obtained results, especially in terms of processing speed and avoidance of systematic errors, that could occur when human operators are involved. Clearly, the comparison has been carried out in a very controlled environment, where all possible systematic errors by the operators have been fixed.

In its full version, the algorithm performs a deeper analysis with particular reference to TT.
In detail, the accelerometer data are used to:

- count the total number of taps of the executed test and grouping them in variable time observation windows;
- compute the intertemps, i.e. the time distance between each couple of consecutive taps to highlight possible fatigue phenomena that could arise in the subject;

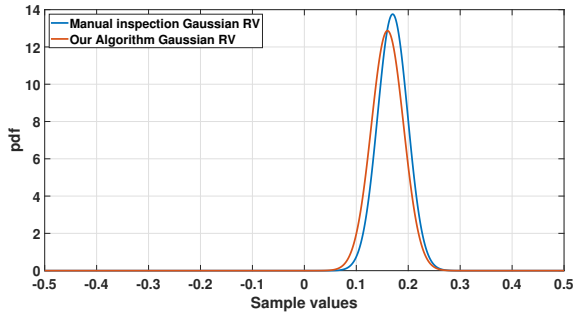

(a) Ruler Test distributions

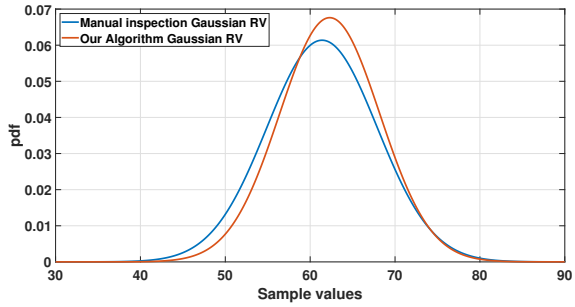

(b) Tapping Test distributions

Figure 5.12: Distribution of Ruler and Tapping Values for Validation Purpose

- estimate the frequency behavior in total size (whole test duration), batch size (for specific observation window) of the accelerometer data.
- compute the acceleration excursions: the amplitude of the acceleration data is calculated and monitored during the whole test execution time.

5.4.4 Obtained results

In this subsection, detailed results obtained through the implemented algorithm are shown for the ruler and tapping tests. Particularly, from the ruler test, pieces of evidence about reaction time subject by subject and comparison between obtained times before and after exhausting tapping task are

provided. As the tapping test regards, several processing aspects are considered, and, particularly, results are grouped as follows: 1) Tap counting and grouping; 2) Intertemp evaluation; 3) Frequency behaviour observation; 4) Acceleration Amplitude Excursions. The provided results can easily be accessed by a user through a simple selection in the developed algorithm interface. Particularly, they can be evaluated by a medical doctor to achieve a personalized report about the subject's health status and coordinative capabilities.

Reaction Time Evaluation

The proposed test has been used to evaluate the reaction time in a group of healthy subjects. In particular, RT is used to evaluate and compare the reaction time before (RTB) and after (RTA) the tapping test. A bar diagram in Fig. 5.13 shows the obtained results.

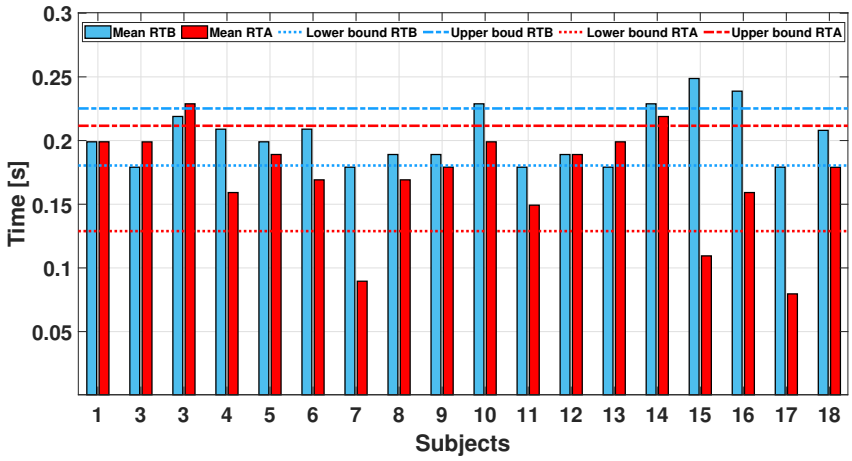

Figure 5.13: Bar Diagram of reaction times before and after tapping test evaluated for each subject

The horizontal lines indicate RTB and RTA bounds for all subjects. A bound is defined as the following interval:

[Lower Bound, Upper Bound] = $[\mu - \sigma, \mu + \sigma]$, where μ and σ are the average and the standard deviation values computed on the whole subject sample. The red lines define the RTA bound while light blue lines include the RTB bound. All participants' reaction times fall into the bound in the case of RTB, i.e. before carrying out the tapping test. On the contrary, the RTA, i.e. the reaction time evaluated after the tapping test, has subject-based specific behavior, not always adhering to the computed bound.

To better analyze the results, the subjects are divided into two groups: subjects with RTA $\leq$ RTB and subjects with
RTA $>$ RTB. In Fig. 5.14 (a), it can be seen that 15 out of 18 subjects do not increase their reaction time, while the remaining 3 have a slight worsening of it after the tapping exercise, as can be seen in Fig. 5.14 (b). All summary values of mean and standard deviation calculated for the three groups identified for the reaction time tests are given in Tab. 5.7. Due to the inherent nature of the procedure, a single value of RTA and RTB is available for each subject. Therefore, a detailed analysis of the single-subject effect cannot be performed. Anyway, it is possible to consider the whole group as a representative sample of a population, being identified by young and healthy people. In this approach, results provide an average decrease in the reaction time after the TT, although the range intervals are partially overlapped. The idea to repeat the process multiple times on the same subject has an important drawback: it is not possible to ensure the same measurement conditions needed to evaluate features such as repeatability and type-A uncertainty contributions. Moreover, to assess the statistical significance of results, three statistical analyses, such as the Friedman test [118] and the Durbin-Conover test (pairwise comparisons)[119], and also the Paired Samples T-Test [120] have been carried out. For each of them, the obtained P-values were evaluated and compared with the typical reference level of 0.05. As for the Friedman test, a P-value equal to 0.018 was obtained. As for the Durbin-Conover test (pairwise comparisons), the P-value was equal to 0.014. As for the Paired Samples T-Test, considering the Hypothesis

that the measures (RTA and RTB) have a non-null difference mean value, a P-value of 0.006 resulted. Therefore, with a confidence level higher than 95%, it is possible to state that there is a statistically significant meaning between reaction times before and after the tapping test.

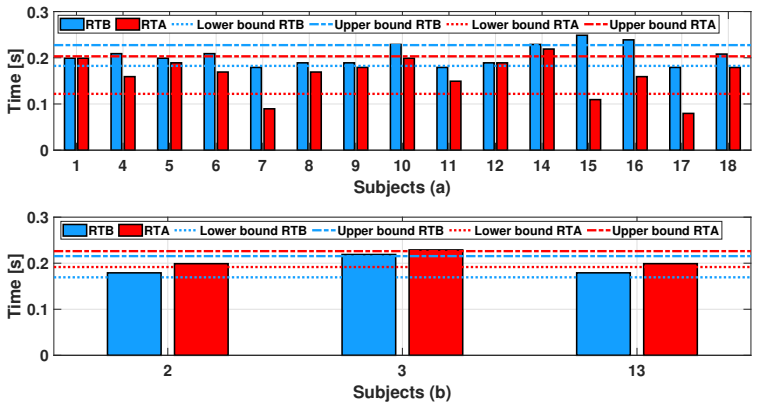

Figure 5.14: Bar chart of reaction times before and after the tapping test for subjects with improved (a) and worsening (b) RTA

Table 5.7: Mean and standard deviation of reaction times calculated for each subgroup

	RTB Mean (μ) [s]	**RTB Std.Dev.** (σ) [s]	**RTA Mean** (μ) [s]	**RTA Std.Dev.**(σ) [s]
All Subjects	0.200	0.022	0.178	0.033
Subjects with RTA<RTB	0.204	0.023	0.169	0.031
Subjects with RTA>RTB	0.192	0.023	0.209	0.017

Tapping Test Results

The tapping exercise is performed between the two ruler tests and the subject performs it until he/she is exhausted. From the raw data of this test, thanks to the validated algorithm, several aggregated and individual fea-

tures, which provide more detail of the subject's performance, can be extracted.

Tap counting and grouping

To evaluate the performance of the tapping test, the first observation concerns the number of taps performed during the whole test. As can be seen in Fig. 5.15 the upper graph shows the total taps obtained for each subject, and the other plot shows the total time taken to perform the test.

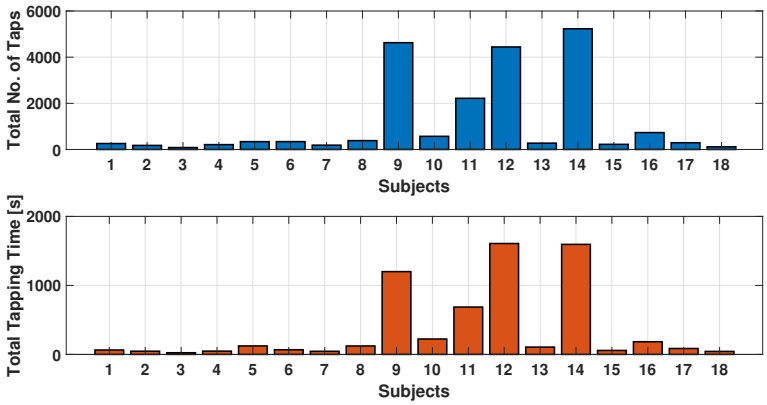

Figure 5.15: Bar diagrams: the first row shows the Number of Tapping for each subject; the second row displays the total tapping test time for each subject

From the results, it can be seen that 4 out of 18 participants showed a higher degree of resistance during the exercise, managing to perform the test for more than 20 minutes and scoring more than 4000 taps. On the other hand, 7 subjects were able to perform the exercise for more than one minute, while the remaining 7 performed the test for less than one minute. The variability of the time taken to perform the tapping test until exhaustion strongly depends on the physiological characteristics of each subject.

Fig.5.16 shows the error bar in the TT. In the first subplot, it can be seen the mean value and the standard deviation of the number of taps computed

every 5 seconds for each participant. It can be observed a non-uniform behavior among participants: specifically, their variability is quantified by the standard deviation reported as a vertical bar in the plot. To better illustrate this phenomenon, two limit cases have been considered: ID 5 and ID 12. The TT evolution of the specified participants has been computed by spectrogram function and reported in the second and third subplots, respectively. To make a uniform comparison, only the first 120 s of tests have been reported for both IDs, as well as the spectrogram settings have been taken in coherence with the error bar computation settings (5-second-window, no overlap). The yellow lines in the spectrograms indicate the frequencies containing the highest power density. As ID 5 concerns, their high standard deviation value results in a highly variable main frequency behavior (i.e. the yellow line often changes its frequency position). On the contrary, observing ID 12's test trend, a main frequency equal to 3 Hz is constantly kept along the test's duration, justifying the lower standard deviation value.

Intertemp Evaluation

A further processing stage consisted of the assessment of the intertemps, i.e. the time distance between two consecutive taps. In detail, the intertemp time distribution for each subject during the whole test is shown in Fig 5.17. Subjects who performed a long test (IDs: 9, 11, 12, and 14) obtained most intertemps in [0.3, 0.4] s range, while for subjects performing a shorter tapping test, the overall intertemp distribution generally moves downward, proving a faster way to tap, which leads to a shorter endurance time. (Fig. 5.18).

To obtain quantitative overall information about their distribution, the mean and standard deviation have been calculated for each subject. Obtained results are presented in the form of error bars superimposed on the mean values and they are shown in Fig. 5.18.

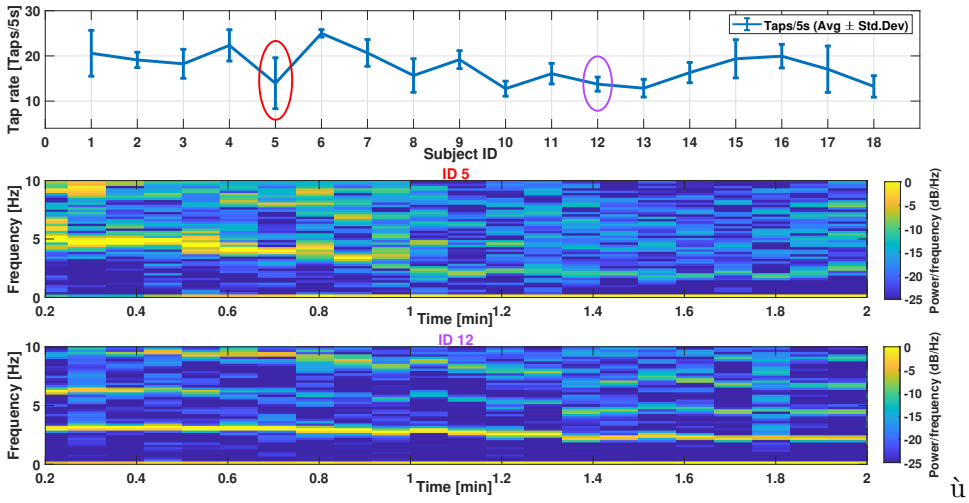

Figure 5.16: Error bar in Tapping Tests: evaluation of mean value (Avg) and standard deviation (Std.Dev) for all involved participants. Spectrograms related to IDs 5 and 12, concerning the first 2 minutes of activities, are reported in subplots

The results clearly state that the mean values are only an approximation of the real behavior, since the standard deviation values are generally very high, especially for subjects performing a short tapping test, while they got a more stable behavior for subjects having a long-lasting test, as 9, 12 and 14.

To find a possible linear relation between intertemps and test duration, a fitting procedure has been carried out. Results are presented in a graphic mode for Subject 18 (see Fig. 5.19) and in terms of the mean and standard deviation of the obtained angular coefficients in tabular form (see Tab. 5.8). In detail, table contents are expressed using ms/s measurement unit, just to obtain higher values easier to be reported and commented. By analyzing such results, it is evident that the majority of subjects show an increase in tap intertemps, which could be seen as a fatigue effect due to prolonged exercise.

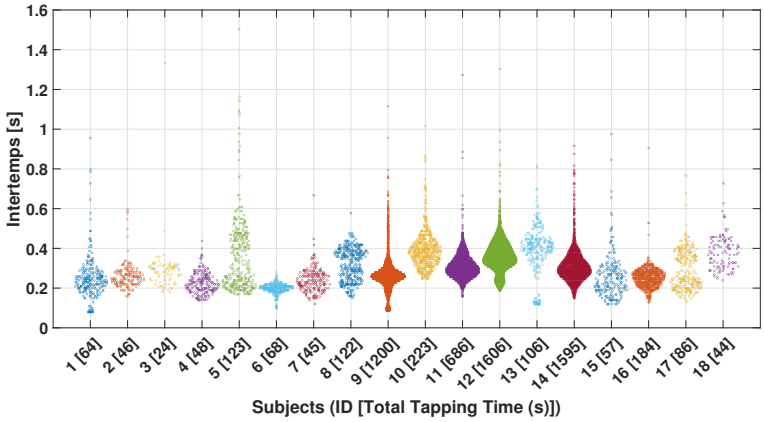

Figure 5.17: Intertemps distribution for each subject during the whole tapping test

In more detail, the obtained results show two different behaviors: i) subjects increasing the time between consecutive taps; ii) subjects keeping a nearly constant rhythm during the test (the decrease rate is almost null). The subjects with an increase in the number of taps were 13, while the remaining 5 were those who showed no substantial change.

Frequency behavior observation

Another way to analyze the timing during the tapping exercise is the observation of the frequency behavior. Particularly, we have at least two ways to

Table 5.8: Mean and standard deviation of angular coefficients calculated for all subjects and their different behaviors - intertemp case

	Mean (μ) **[ms/s]**	**Std.Dev.** (σ) **[ms/s]**
All Subjects	1.70	1.75
Subjects with increasing intertemps	2.38	1.60
Subjects with decreasing intertemps	−0.07	0.06

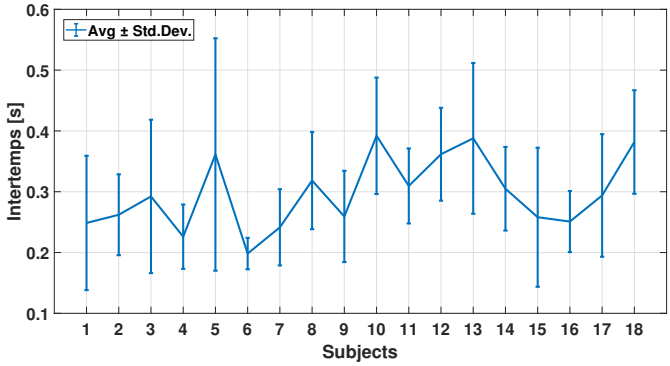

Figure 5.18: Mean (Avg) and Standard deviation (Std.Dev) of intertemps computed for each subject during the tapping test

analyze frequency data: i) perform a Fast Fourier Transform (FFT) on the whole time sequence data or ii) consider a specific time frame to observe and use it as input for the frequency transformation.

A snapshot of the frequency analysis performed by the algorithm is depicted in Fig. 5.20. The considered processing ways can be seen in the second and third subplots of the cited figure. It is important to note that the frequency spectra are obtained after a detrend operation, in order to remove the DC component and be able to discriminate frequency components higher than 0 Hz. Although the results are plotted only for Subject ID 1, similar considerations can be drawn for the whole population sample. In detail, the spectrum considering the entire tapping test time series shows a predominant frequency tone at around 4 Hz, with smaller amplitudes in the surrounding frequency interval. On the contrary, when only a batch is considered (the last 24-second case is reported in Fig. 5.20) a general decrease of the predominant tone frequency location is observed, probably due to a progressive slowing of the tapping rate, still imputable to the fatigue effect the subject experiences.

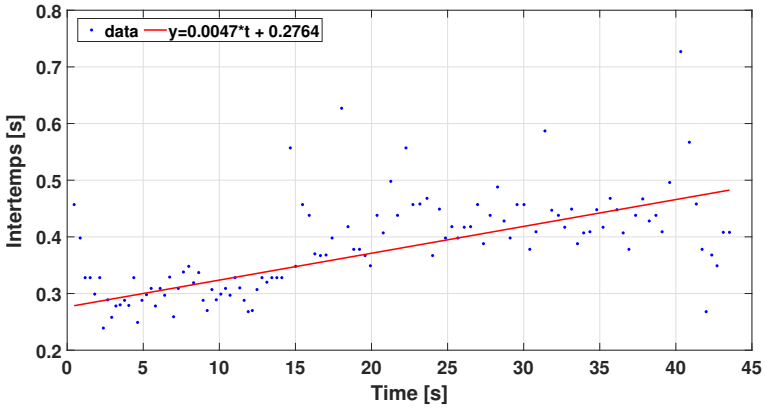

Figure 5.19: Example of linear fitting for intertemps versus task execution time - Subject ID: 18

Acceleration Amplitude Excursions

The last proposed processing stage regarding the tapping test is the analysis of the amplitude of the acceleration signals. Indeed, although the subjects were required to get a fixed-angle excursion during the test, the way they got it was not uniform and generalizable. For this reason, after analyzing the time and frequency behaviors, we put our attention also to amplitude values. Symmetrically, we performed the same processing stages as the intertemp case, so it is possible to note their distributions (see Fig. 5.21) and the linear fitting versus time. In Tab. 5.9, information about the angular coefficients of the fitted lines is reported.

To get the same information level, we should consider that the fatigue effect in this case should correspond to a decrease in the amplitude values and, consequently, to a negative angular coefficient in the fitting process. That is the case of 14 subjects over 18. It is important to highlight that most subjects exhibit a reduction of the reaction time together with an increase of the intertemp trend and a decrease of the amplitude behavior versus time. This could be a joint phenomenon to be considered as a whole

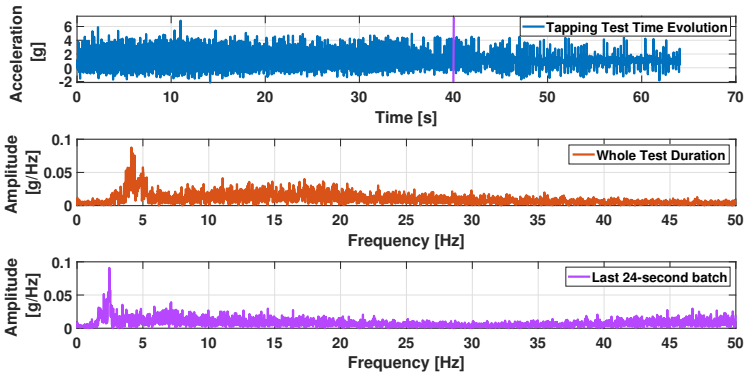

Figure 5.20: Time and frequency behavior observation - Subject ID: 1. Particularly, the frequency spectrum is reported for the whole test duration and considering only the last 24-second interval (batch mode)

Table 5.9: Mean and standard deviation of angular coefficients calculated for all subjects and their different behaviors - amplitude excursion case

	Mean (μ) [$\mathbf{mm/s^3}$]	**Std.Dev.** (σ) [$\mathbf{mm/s^3}$]
All Subjects	-64	73
Subjects with increasing amplitudes	11	10
Subjects with decreasing amplitudes	-86	69

for a medical doctor to assess a subject's performance level.

5.4.5 Results Discussion

In several cases, the literature demonstrates that reaction time might provide an indicator of the central nervous system's ability to receive and synchronize movement conveyed by the peripheral nervous system [121]. This cognitive-motor relationship is essential for several areas of everyday life. In this investigation, we utilized the TT to determine the fatigue index resulting from repeated movements, of eighteen young and healthy subjects. The

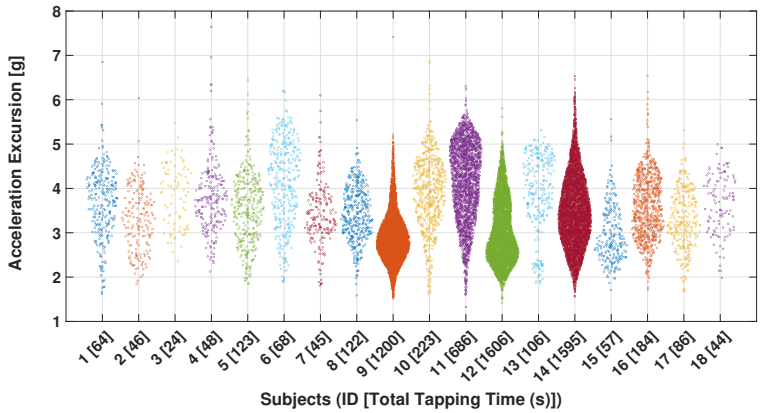

Figure 5.21: Acceleration amplitude distribution for each subject during the whole tapping test

participants were required to complete the test in an exhaustion modality. Indeed, subjects were instructed to execute the tapping task at the highest pace they could sustain. In addition, we determined that each tap must accomplish a minimum excursion of four centimeters. To ensure that the imposed amplitude was maintained consistently, the minimum amplitude to be maintained was indicated through a red line. A purpose-built box was made to conduct the tests. Furthermore, utilizing RT allowed for the completion of further evaluations in order to have a better understanding of the effects that repetitive motion has on the anatomic body districts and motor tasks. As a matter of protocol, subjects performed an RT before (RTB) and after (RTA) the TT.

The measurements and results obtained during the TT could lead to the definition of a fatigue coefficient. In particular, the increasing intertemps and decreasing amplitude, discussed in the previous section, can be an indication of fatigue occurring during a repetitive exercise performed at maximum speed.

However, when the TT is done at a maximal pace, the frequency lowers in a matter of seconds, indicating the onset of muscular exhaustion. Fa-

tigue could be task-dependent, as are the factors that lead to decreased motor performance during quick and repeated activities [122]. Even though the length of effort is equal, it is feasible to hypothesize that the physiological processes behind fatigue induced by rapid and repeated finger tapping differ from those behind fatigue induced by an isometric contraction [123]. On the other hand, some subjects maintained a fairly constant rhythm while performing the test: in the case of isometric muscular contractions, these processes have been widely explored; they involve changes in excitability in both the spinal cord and M1 networks [124]. During rhythmic motions performed at maximal speed, peripheral exhaustion in muscle fibers and neuromuscular synapses reduces the effectiveness of muscle contractions [125]. Nonetheless, alterations in the excitability of spinal and supraspinal regions also define fatigue in these motions [126]. At the cerebral level, the excitability of the inhibitory interneurons of the M1 rises as maximal movement speed declines [127]. Fatigue during the tapping test does not affect central muscular drive or force loss, and some evidence suggests it may involve motor rhythm creation [128]. In addition, exhaustion during an activity such as tapping may alter the activation-time sequence of agonist and antagonist muscles, with co-activation increasing as fatigue grows. This indicates that the muscles involved in moving the index finger are activated simultaneously, reducing their pace of execution [129].

Based on our results, it is reasonable to hypothesize that skeletal muscle fiber activation may be responsible for changes in reaction time. The chemical energy supplied by metabolic processes is converted into mechanical energy by the muscle fibers, which, working on the bone levels, culminate in movement. When the load is minimal, type I fibers are the most active, but type II fibers become more operative as the demand for force increases [130]. Muscle fibers expand when stimulated and contract when inactive [130]. This is because exercise causes an increase in myofibrils, which increases the size of muscle cells overall [131]. The central nervous system recruits motor units based on the size of the fibers, beginning with

smaller and less powerful excitable fibers compared to bigger and more powerful fibers since the size of the fibers affects their potential to generate force. Phasic motor units, instead, include mayor-size motor neurons, have a higher interval discharge frequency, and have a much greater electrical pulse intensity. They are mostly located in the limb muscles [132]. Indeed, activities requiring dexterity, such as TT, engage the interosseous and lumbrical muscles of the hand via myoelectric stimulation induced by repetitive movement. The lumbar interosseous joint is the primary unit involved in TT movement. The interosseous muscles are palmar muscles and muscle occupies the space between the metacarpal bones. The lumbar muscles flex the metacarpophalangeal joints and extend the interphalangeal joints of the final four fingers of the hand [133].

In terms of RT reaction times, about 16% improvement in post-tapping was observed in 14 subjects, while about 9% worsening in RTA was observed in the remaining four subjects. The concept of viscoelasticity could provide an explanation for these findings. Viscoelasticity is the property of a substance to show both elastic and viscous behavior. Viscosity is directly related to temperature in an inverse relationship. That is, when temperature increases, viscosity decreases [134]. In muscles, a similar phenomenon occurs. The viscosity and hence the passive tension of the whole muscle structure are decreased by heating the muscle. As the muscle's elasticity decreases, its tendency to stretch increases [135]. TT acted as a stimulator or warm-up, increasing heart rate and, subsequently, blood and oxygen flow to the working muscle groups, warm-up also decreasing in energy rates activation of metabolic chemical reactions, in muscle blood flow and in muscle viscosity [136]. The TT test may promote the viscoelastic properties of the musculotendinous skeletal system. Temperature increase generates an enhancement in viscoelastic functions of the muscle, which allows for faster, more fluid movements with the recruitment of a greater number of muscle fibers deputed to work [137]. Thus, it is conceivable to assert that the viscoelasticity of the system is the primary contributor to the result-

ing enhancement in RTA. In conclusion, viscoelasticity decreases in heated muscle, resulting in increased flexibility and decreased rigidity, facilitating movements that require rapidity, as in the case of the two tests considered, for the assessment of reaction time.

5.5 Coordination ability assessment in age and gender differentiated groups of athletes

In this section, it was presented an experimental campaign to collect normative data for a sensor-assisted tapping test to evaluate its performance against a standardized method. The study was conducted on 53 students aged 21-30 years. Tapping motion was measured with an IMU sensor placed on the left and right index fingers during five 10-second trials. Differences were found between the genders, dominant and non-dominant hands, number of taps, amplitude range, and intertemps. With the sensor, efficient and accurate assessment of tapping speed and movement kinetics was possible, making it useful for scientific and clinical investigations of motor function.

5.5.1 Study Protocol

Fifty-three voluntary students from the University of Cassino and Southern Lazio were enrolled in this study. In particular, 28 men and 25 women took the test during an internship activity in the framework of the Motor Science Course. The procedure for carrying out the tests was based on the traditional method of execution that corresponds to the Halstead-Reitan Battery [138]. The TT is one of the tests included in this battery: standard versions required participants to push a button with their index finger as rapidly as possible for 10 seconds while a counter recording the number of presses. Each test was performed five times and then the mean number of taps performed by each subject was evaluated. The participants were divided by gender and age group. In our work, we used the same procedure

for performing the original test [138] but with an automated system that reduces operator-induced error. Compared with the work of Ruffi et al. [139], it was provided much more detailed in this case study, such as intertemps and amplitudes, that allow for a better analysis of the subjects considered, even though only two courts were considered. The experimental protocol presented in this paper, on the other hand, takes into consideration two of the four cohorts reported in the work [139], specifically 4 groups were identified:

- Men aged 16-24 years (Group 1);
- Men aged 25-30 years (Group 2);
- Women aged 16-24 years (Group 3);
- Women aged 25-30 years (Group 4);

All results for both the dominant and non-dominant hand were assessed. Participants were asked to perform the test for 10 seconds and to repeat it five times. In contrast to the experiment mentioned above, data are acquired through the use of a wearable inertial platform fixed on the subject's index finger. Over one month, participants were gathered in groups of 10 to perform measurement tasks. In particular, two measurement sessions were carried out: the first in which the exercise was performed with the right limb, and the second with the left. The test day was divided into sessions of five non-consecutive tests, with ten-minute breaks between each test to avoid fatigue. Each participant had to complete the five tests scheduled for that day. Subjects were asked to abstain from caffeine-containing substances and exercise the previous day. Moreover, participants were informed of the protocol's design and the testing procedures. This work was approved by the Institutional Review Board of the University of Cassino and Southern Lazio (No. 24777.2022.12.12). Informed consent and authorization about benefits and risks have been obtained in accordance with the Declaration of Helsinki for Human Research of 1964.

5.5.2 Experimental Characterisation

The inertial platform MetaMotionR (MMR) was used in this study. An experimental characterization was necessary to define the sensor position that would have the minimum possible influence on the measurement results. Specifically, 10 students were identified and asked to perform two different tests, each repeated five times consecutively. In particular, there are two different configurations (Fig. 5.22):

- Position A: the sensor is placed at a fixed distance from the metacarpal joint of the index finger, specifically 2 cm away;
- Position B: the sensor is placed on the distal phalanx of the index finger, regardless of the distance from the joint.

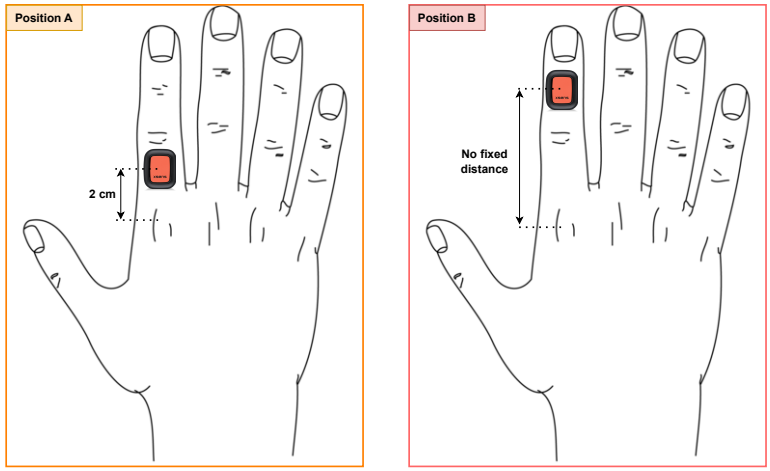

Figure 5.22: Experimental characterisation: in position A, the sensor is placed at a fixed distance from the metacarpal joint; in position B, the sensor is placed on the distal phalanx.

In both cases, participants are asked to perform the taps with the dominant hand's index finger as quickly as possible. To check which one was

suitable for the chosen protocol, the coefficient of variation (Cv) was computed and it was described in Eq. 5.2.

$$Cv = \frac{std(NTap)}{mean(NTap)} * 100 \tag{5.2}$$

where $NTap$ is the number of performed taps. Its meaning is to evaluate the weight of the standard deviation value with respect to the mean value. In detail, the lower the value, the better the measurement repeatability, and the better the adopted configuration.

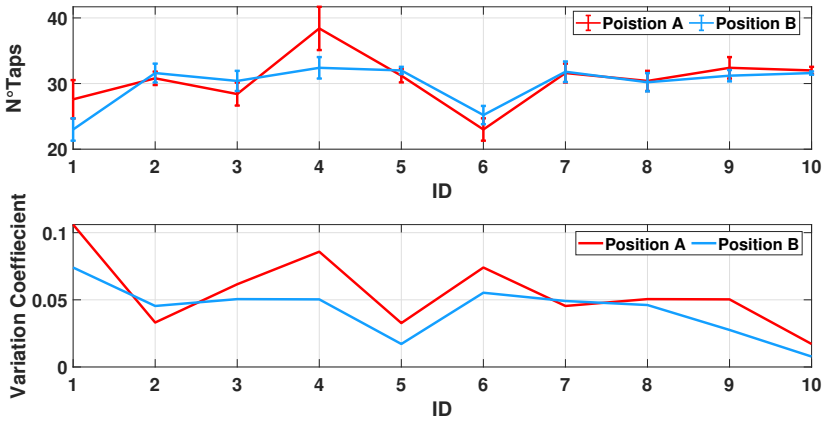

Figure 5.23: The top figure compares the average number of taps obtained by all subjects in the two different study positions. The second graph shows the comparison between the coefficient of variation calculated in the two different configurations A and B.

As it can be seen in Fig. 5.23 and Table 5.10 in the case of position B, less variability of the Cv is observed for all participants as the number of taps increases. This result shows that the sensor placed on the distal phalanx influences the measurement process less than in case A. For the above-described reasons, the sensor was placed in configuration B for the measurement protocol.

Table 5.10: Coefficient of variation computed in the two different configurations.

	POSITION A Cv [%]	**POSITION B** Cv [%]
ID 1	10.6	7.40
ID 2	3.31	4.54
ID 3	6.16	5.05
ID 4	8.58	5.03
ID 5	3.27	1.71
ID 6	7.40	5.53
ID 7	4.54	4.91
ID 8	5.05	4.61
ID 9	5.03	2.76
ID 10	1.71	0.78

5.5.3 Measurement Set-up

As can be seen in Fig. 5.24, the sensor was anchored to the subject's index finger; before the start of the session, the subject was asked to keep the hand resting on the plane and during the test to perform as many taps as possible at maximum speed, trying to maintain a fixed amplitude of 4 cm. The test was timed using a conventional smartphone stopwatch.

Figure 5.24: Tapping Test Set-Up

In this first experiment, both the accelerometer and the gyroscope are used; a sampling frequency of 100Hz is set and for the accelerometer, a range of $\pm 8g$ is selected, while for the gyroscope a range of $\pm 1000\ ^{o}/s$ is selected.

5.5.4 Data Processing and Analysis

The inertial data acquired during the tests were analysed using an algorithm implemented in MATLAB^{TM} R2022a (Mathworks, Natick, MA). In particular, Fig. 5.25 shows the logical process used by the algorithm to extract specific characteristics from the raw data.

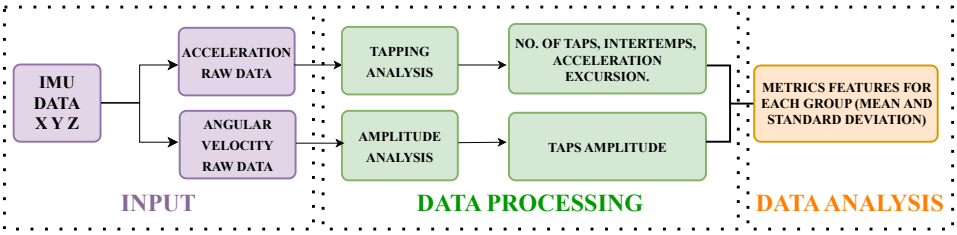

Figure 5.25: A block-diagram description of the proposed processing stage[140]

In the first step, the algorithm receives raw acceleration and angular velocity data as input (Fig.5.26).

With regard to the acceleration data, the following information was obtained by using the Matlab^{TM} *findpeaks* [116] routine:

- The number of total taps during a single test (calculated as the number of positive peaks found in each trial Fig. 5.27);
- The acceleration excursion obtained for each individual tap (calculated as the amplitude of the positive peak);
- The intertemps (calculated as the time distance between one tap and the following one);

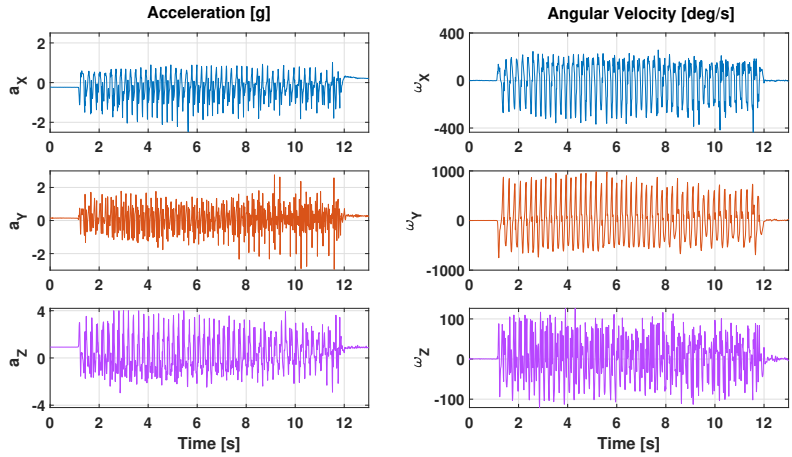

Figure 5.26: Raw data acquired during a test: the figure on the right shows the data acquired using the accelerometer while the figure on the left shows the data acquired using the gyroscope[140]

From the angular velocity data, we want to calculate the taps amplitude, defined as the maximum opening of the index finger obtained during the movement. To obtain the amplitude in degrees from the angular velocity, the following steps were performed:

- Resampling of the signal (With a new frequency equal to 1000 Hz);
- Search for the zero crossing points of the function under examination, to identify the intervals of interest;
- Numerical integration of the signal between the selected intervals.

Fig.5.28 shows the Fast Fourier Transform (FFT) of the accelerometer traces of 4 subjects taken from the 4 groups respectively. Initial analysis shows that there is a difference in tap frequency between the subjects.

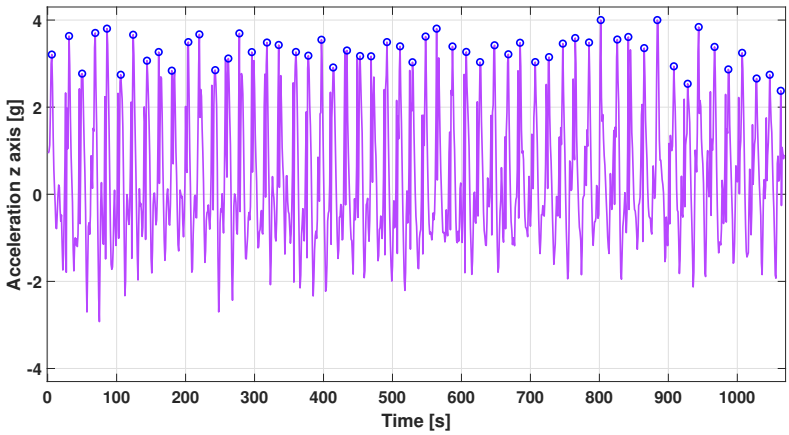

Figure 5.27: Identification of the tapping number on the acceleration along the z-direction. [140]

5.5.5 Obtained Results

After processing the data and deriving the characteristics of interest for each group, the mean and standard deviation were calculated and the results are shown in the following Tables, 5.12, 5.13, 5.15, 5.14. Specifically, Tab. 5.12 shows the mean and standard deviation values calculated on the total number of tapping performed by each group in the case of the Dominant Hand (DH) and Non-Dominant Hand (NDH). It can be observed that for both the women's and men's gender, the number of tapping is greater in the DH than in the NDH case. A descriptive statistical analysis was conducted, which showed that all data were normally distributed. A comparison of the total number of tappings obtained by the two genders shows that men, for both DH and NDH, perform on mean 4 more taps than women.

The Tab. 5.11 shows the results obtained during the experiment presented in the work [138].

The comparison between Tab.5.12 with the reference table5.11 shows that the results obtained in this work differ by 3-4 tapping more than the

Table 5.11: Mean and standard deviation for the Tapping Test: an extract of the reference table [138]

Participants	**n**	**Dominant Hand**		**Nondominant Hand**	
		Mean	**Std.Dev**	**Mean**	**Std.Dev**
Men					
Age 16-24	45	52.9	5.1	48.2	4.4
Age 25-39	45	52.7	6.8	48.7	5.7
Women					
Age 16-24	45	49.5	5.1	45.6	5.1
Age 25-39	45	49.0	4.1	44.6	4.6

Table 5.12: Mean and Standard Deviation for Tapping Test

Participants	**n**	**Dominant Hand**		**Nondominant Hand**	
		Mean	**Std.Dev**	**Mean**	**Std.Dev**
Men					
Age 16-24	21	55.7	4.5	51.8	5.9
Age 25-39	7	56.6	8.4	54.8	4.3
All	28	55.91	5.62	52.58	5.59
Women					
Age 16-24	15	51.9	6.2	49.7	5.7
Age 25-39	10	50.8	3.3	47.3	4.2
All	28	51.51	5.29	48.81	5.18

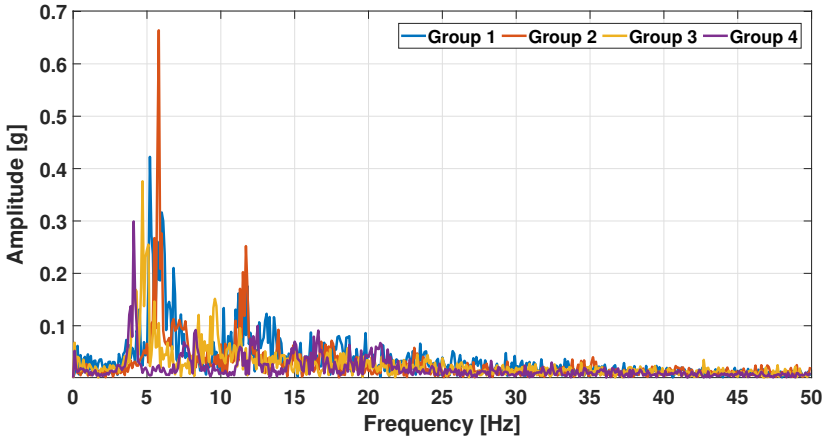

Figure 5.28: An example of acceleration spectra regarding the analyzed groups[140]

results obtained in the past. This disparity may be due to factors that have occurred over the past 30 years. From decade to decade, so many elements could be subject to small evolutionary changes over time, perhaps related to environmental, anthropometric, physiological, or motor habit change factors. Tab. 5.13 shows the mean and standard deviation of the amplitudes obtained during the tap movement. The results show no substantial differences either between DH and NDH or between the two different genders. This is an expected result as a maximum amplitude was set during the execution of the tap test. During the test, the participants had to try to maintain a minimum index finger opening amplitude. By analysing the results, it can be seen that the expected amplitude of about 30° was on average respected.

The results of the mean and standard deviation calculated for the accelerometric excursion and the intertemps, respectively, are shown in Tab. 5.15 and Tab. 5.14. Both cases show how men on mean achieve smaller intertemps and greater accelerometric excursions compared to women.

These trends are highlighted by visualizing what happens on mean on

Table 5.13: Mean and standard deviation of tapping amplitude in radiants

Participants	n	Dominant Hand		Nondominant Hand	
		Mean	Std.Dev	Mean	Std.Dev
Men					
Age 16-24	21	0.55	0.11	0.55	0.10
Age 25-39	7	0.51	0.12	0.51	0.09
All	28	0.54	0.11	0.54	0.10
Women					
Age 16-24	15	0.56	0.09	0.56	0.10
Age 25-39	10	0.55	0,12	0.55	0.12
All	25	0.55	0.10	0.56	0.10

Table 5.14: Mean and Standard Deviation of Acceleration Excursion in g

Participants	n	Dominant Hand		Nondominant Hand	
		Mean	Std.Dev	Mean	Std.Dev
Men					
Age 16-24	21	3.31	0.26	3.26	0.29
Age 25-39	7	3.21	0.18	3.36	0.18
All	28	3.28	0.25	3.28	0.27
Women					
Age 16-24	15	2.93	0.25	2.83	0.30
Age 25-39	10	2.98	0.16	2.98	0.30
All	25	2.95	0.22	2.89	0.28

Table 5.15: Mean and Standard Deviation of Intertemps in seconds

Participants	n	Dominant Hand		Nondominant Hand	
		Mean	Std.Dev	Mean	Std.Dev
Men					
Age 16-24	21	0.19	0.02	0.21	0.02
Age 25-39	7	0.19	0.03	0.20	0.02
All	28	0.19	0.02	0.20	0.02
Women					
Age 16-24	15	0.21	0.03	0.22	0.03
Age 25-39	10	0.21	0.02	0.23	0.02
All	25	0.21	0.02	0.22	0.02

the five trials, in particular in Fig. 5.29 and Fig. 5.30 it is possible to see that on all five trials, both for the dominant and non-dominant hand, men perform the TT faster than women.

Conversely, in Fig.5.31 and Fig.5.32 the comparison is made on the accelerometric excursion: from the graphs it is evident that women in both cases obtain lower acceleration values than men.

5.5.6 Results Discussion

In this investigation, the dexterity-related upper limb features of a sample of college students were assessed. The participants performed a battery of TT according to the standardized procedure, but with the addition of an inertial sensor as an evaluation tool. A result's comparison with the table in [139] showed that, in our version, on mean, the number of taps increased by about 4 for the men and 3 for the women. In the thirty-year-old version proposed by Ruff and Parker, the amplitude of the index finger movement range was not taken into consideration. Not taking into account such a fundamental factor as the amplitude of movement will never lead to comparable results related to the characteristics of the subjects tested. The number of extra tapping compared to the standardized table cannot

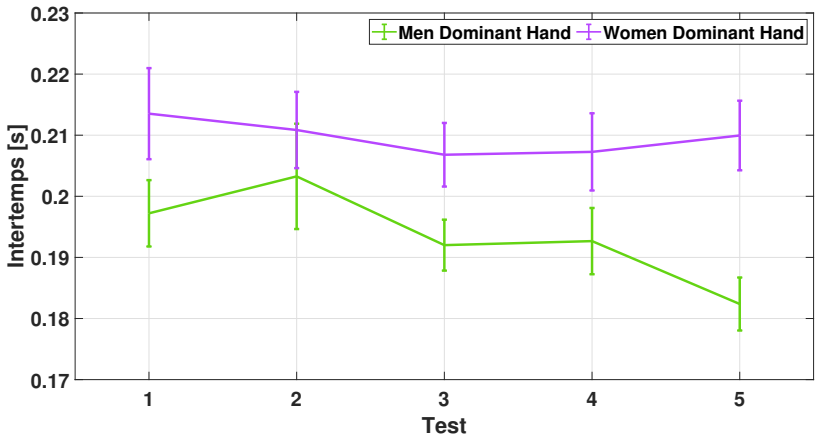

Figure 5.29: Mean and standard deviation of the computed intertemps for all tests performed with the dominant hand

be incriminated to the movement excursion since we imposed the execution of the test at maximum speed and a minimum amplitude to be respected. Although, the amplitude to be maintained was set at a certain height, we obtained a higher mean tap than the reference table. In a second analysis, subjects were analyzed by dividing them by gender. The graphs in Figs. 5.29 and 5.30 show the intertemps mean for the five trials completed with dominant and non-dominant hands, categorized by gender. Upon examination of the graph, it is evident that, for both genders, the trend line declines between the first and final trials. This graph depicts how, on mean, a performance peak is achieved in the fifth trial. The concept of viscoelasticity could explain this phenomenon. Temperature plays a crucial role by improving the viscoelastic properties of the muscle, hence stimulating the recruitment of more muscle fibers [141]. The viscosity reduces as the temperature rises [142]. As the muscle is heated, its viscoelasticity diminishes, resulting in increased flexibility and a reduction in stiffness, which facilitates motions that need rapidity, as in our work. Based on our findings, it is plausible to hypothesize that activation of skeletal muscle fibers may be

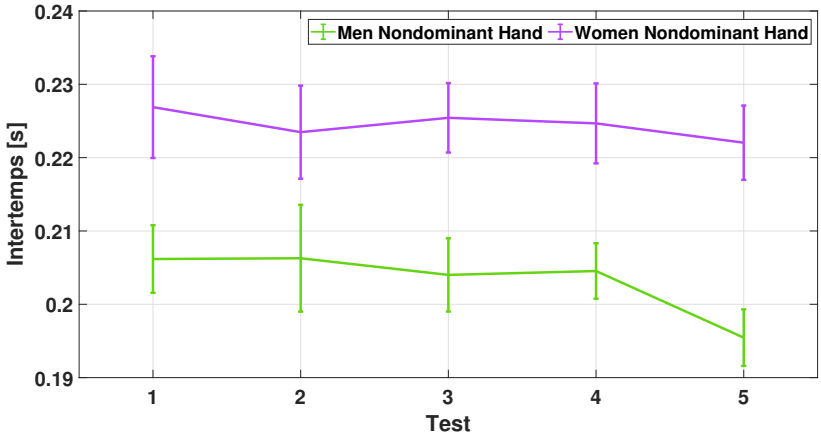

Figure 5.30: Mean and standard deviation of the computed intertemps for all tests performed with the Nondominant hand

responsible for the trend line seen in Figs. 5.29 and 5.30. Muscle fibers convert the chemical energy generated by metabolic processes into mechanical energy, resulting in movement [143]. Myoelectric stimulation generated by repeated activity engages the interosseous and lumbar muscles of the hand during dexterity-requiring tasks, such as in our case [144]. In Tab. 5.13, the mean amplitude of the women gender is higher than that of the male gender for both the dominant and non-dominant hand. These results may be related to women's fundamentally more flexible physical traits than males. Additionally, the literature backs up this theory. Several studies claim that women muscles are less rigid than male [145, 146]. Women have a higher stretching tolerance and contain viscoelastic qualities that make them more flexible [147]. Notwithstanding, the increased joint stiffness in males may be due to fundamental geometric variations, such as lever arm length. Men generally have longer arms than women. The muscles are more stressed during stretching because more power is needed when a specific action must be performed, acting as a longer lever.

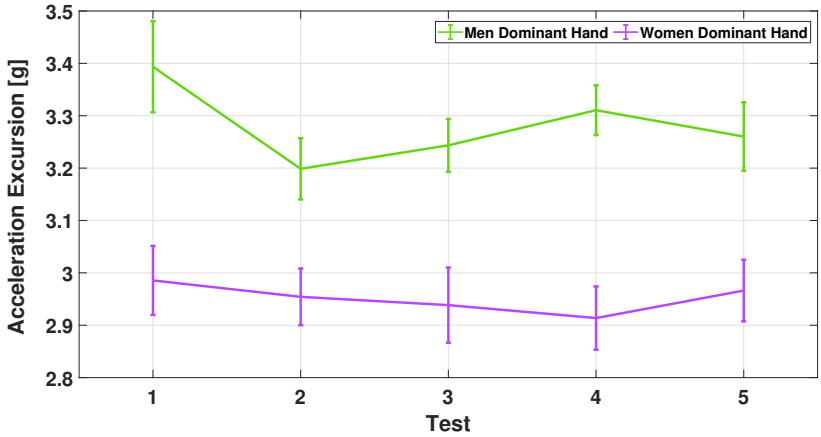

Figure 5.31: Mean and standard deviation of the computed acceleration excursion for all tests performed with the dominant hand

5.6 Final Observation

Wearable sensors are becoming increasingly successful in motion analysis and are being used in more and more different fields. These devices are capable of conducting movement analysis that may be used in sports, clinical environments, and even as remote home care devices. Owing to these devices, it is simple to obtain fundamental data for analyzing the spatial and temporal behavior of different body districts. Non-intrusiveness with the topic being investigated is the characteristic that brought to light the effectiveness of IMU-sensor-based systems. This key effect arises from the natural analysis of motor data without causing discomfort to the user. As a result of technological innovation, these devices could serve as important aids in a wide range of investigations. In particular, this work focused on the application of an IMU sensor as a tool for motion analysis during the assessment of reaction time. The assessment of reaction time may offer in-depth information about the features of a subject of whatever age, which is also essential for enhancing cognitive and physical performance. In partic-

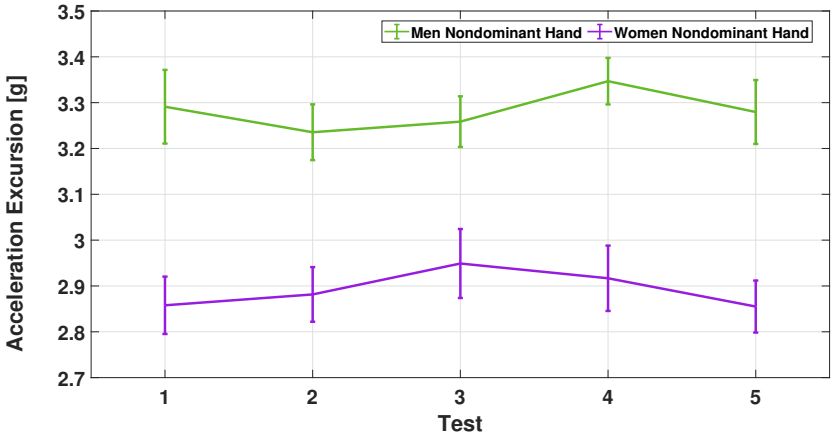

Figure 5.32: Mean and standard deviation of the computed acceleration excursion for all tests performed with the nondominant hand

ular, in this section, the study focused on the application of an IMU sensor as a movement analysis tool for the assessment of reaction time and oculo-manual coordination. The assessment of reaction time can provide in-depth information on the characteristics of a subject of any age, which is also essential for improving cognitive and physical performance. The importance and validity of RT and TT measurements obtained with an IMU sensor are also confirmed by the literature cited in this section. The reported results demonstrate how these coordination tests evaluated by IMU sensors and specific algorithms are capable of rapidly assessing the physical state of athletes. It is also shown how adopting specific measurement protocols before a sports performance can help improve athletes' concentration and thus improve their performance.

Conclusions and future developments

The digitisation process has involved not only the world of industry but also the health sector, bringing to the fore the need to streamline bureaucratic processes, make health services accessible to all and improve diagnosis using *ad hoc* technologies. A scenario in which the main actors are doctors and engineers, working together to bring medical needs and innovative technologies. The challenge has been taken up by the scientific community, which has approached the issue by proposing various innovative solutions, from telemedicine to electronic medical records, to small, wearable sensors capable of monitoring vital parameters or even analysing human movement. Technologies that aim to improve people's quality of life and be valuable aids for doctors in diagnosing illnesses. In this thesis, suitable methodologies, measurement instrumentation and scientific protocols have been proposed for the assessment of movement in relation to both medical applications concerning neuromotor deficits and, in sporting applications, about the assessment and improvement of athletes' performance. At an early stage of the work, an inertial data simulator was designed, implemented and validated which, given a trajectory and the metrological features of the sensor to be simulated, is able to generate accelerometer and angular velocity data from the desired inputs. The simulator allows designing the minimum characteristics of the sensor that should be adopted and, on such basis, generating

inertial data useful for verifying measurement performance under specific metrological conditions.

The validation phase of the simulator performed by means of classification algorithms and data analysis, was followed by a testing phase of the algorithms with the aim of identifying pathological movements, first generated in a laboratory environment and then analysed from an online dataset with pathological data.

The promising results obtained both in simulation and in the laboratory conditions were also confirmed in pathological data acquired in real-life scenario. These steps have progressively led to demonstrating how inertial sensors and data analysis algorithms can be valuable tools for remote monitoring of motion disturbances. This evidence leads to propose, as future development, an automatic measurement system that can monitor movements in real-time, analyse the patient's state and drug adherence, and send all this information to the doctor.

A system that is able to reschedule the medication dosage according to need, to have personalised and increasingly precise diagnoses. The versatility of the sensors and the generality of the algorithms have proved to be such that they can be applied not only in the medical environment but also in sports field. Conducted studies have shown how it is possible to automate exercises used for reaction time and coordination assessments and obtain information that can be useful during training or to determine motor performance. Here again, an automatic, real-time system would allow coaches or personal trainers to check the athletes' performance live, without waiting for the end of the exercise. An integrated measurement system, characterised by several wearable sensors and combined with data analysis algorithms can be a valuable support tool for both doctors and trainers. Technological innovation combined with a common purpose can create tools that can improve people's quality of life.

Bibliography

[1] ONU. *Agenda 2030*. https://unric.org/it/agenda-2030/. Online; accessed 10 September 2023. 2023.

[2] Ministero della Salute. *E-Health*. https://www.salute.gov.it/portale/ehealth/homeEHealth.jsp. Online; accessed 10 September 2023. 2023.

[3] World Health Organization. *Ageing and health*. https://www.who.int/en/news-room/fact-sheets/detail/ageing-and-health. Online; accessed 15 September 2023. 2023.

[4] Abid Haleem et al. "Telemedicine for healthcare: Capabilities, features, barriers, and applications". In: *Sensors International* 2 (2021), p. 100117.

[5] Ronald S Weinstein et al. "Telemedicine, telehealth, and mobile health applications that work: opportunities and barriers". In: *The American journal of medicine* 127.3 (2014), pp. 183–187.

[6] Gianluca Tornese et al. "Telemedicine in the Time of the COVID-19 Pandemic: Results from the First Survey among Italian Pediatric Diabetes Centers". In: *Healthcare* 9.7 (2021). ISSN: 2227-9032. URL: https://www.mdpi.com/2227-9032/9/7/815.

[7] Daniele Giansanti et al. "A Narrative Review of the Launch and the Deployment of Telemedicine in Italy during the COVID-19 Pan-

demic". In: *Healthcare* 10.3 (2022). ISSN: 2227-9032. URL: https://www.mdpi.com/2227-9032/10/3/415.

[8] 2010. World Health Organization: Geneva Switzerland. "Telemedicine: Opportunities and Developments in Member States. Report on the Second Global Survey on eHealth. Geneva". In: (2010).

[9] Michael G Erkkinen, Mee-Ohk Kim, and Michael D Geschwind. "Clinical neurology and epidemiology of the major neurodegenerative diseases". In: *Cold Spring Harbor perspectives in biology* 10.4 (2018), a033118.

[10] Csaba Váradi. "Clinical features of Parkinson's disease: the evolution of critical symptoms". In: *Biology* 9.5 (2020), p. 103.

[11] Christopher G Goetz et al. "Movement Disorder Society-sponsored revision of the Unified Parkinson's Disease Rating Scale (MDS-UPDRS): process, format, and clinimetric testing plan". In: *Movement disorders* 22.1 (2007), pp. 41–47.

[12] Filippo Milano et al. "Parkinson's Disease Patient Monitoring: A Real-Time Tracking and Tremor Detection System Based on Magnetic Measurements". In: *Sensors* 21.12 (2021), p. 4196.

[13] Cristina Cortis et al. "Home is the new gym: Exergame as a potential tool to maintain adequate fitness levels also during quarantine". In: *Human Movement* 21.4 (2020), pp. 79–87.

[14] Muhammad Yahya et al. "Motion capture sensing techniques used in human upper limb motion: a review". In: *Sensor Review* (2019).

[15] Abdul Haleem Butt et al. "Leap motion evaluation for assessment of upper limb motor skills in Parkinson's disease". In: *2017 international conference on rehabilitation robotics (ICORR)*. IEEE. 2017, pp. 116–121.

[16] Nicolas Valencia-Jimenez et al. “A comparative study of markerless systems based on color-depth cameras, polymer optical fiber curvature sensors, and inertial measurement units: Towards increasing the accuracy in joint angle estimation”. In: *Electronics* 8.2 (2019), p. 173.

[17] Sumit Majumder, Tapas Mondal, and M Jamal Deen. “Wearable sensors for remote health monitoring”. In: *Sensors* 17.1 (2017), p. 130.

[18] Abhishek Singh Dahiya et al. “Energy autonomous wearable sensors for smart healthcare: a review”. In: *Journal of The Electrochemical Society* 167.3 (2019), p. 037516.

[19] Bradley N Axelrod, John E Meyers, and Jeremy J Davis. “Finger tapping test performance as a measure of performance validity”. In: *The Clinical Neuropsychologist* 28.5 (2014), pp. 876–888.

[20] Tommaso Di Libero et al. “Assessment of coordinative abilities through upper extremity wearable device technology”. In: *2022 IEEE International Workshop on Sport, Technology and Research (STAR)*. IEEE. 2022, pp. 175–179.

[21] Woosuk Kim and Myunggyu Kim. “Sports motion analysis system using wearable sensors and video cameras”. In: *2017 International Conference on Information and Communication Technology Convergence (ICTC)*. 2017, pp. 1089–1091. DOI: 10.1109/ICTC.2017.8190863.

[22] Johan Marinus et al. “A short scale for the assessment of motor impairments and disabilities in Parkinson’s disease: the SPES/SCOPA”. In: *Journal of Neurology, Neurosurgery & Psychiatry* 75.3 (2004), pp. 388–395.

[23] Eduardo Tolosa, Gregor Wenning, and Werner Poewe. “The diagnosis of Parkinson’s disease”. In: *The Lancet Neurology* 5.1 (2006), pp. 75–86.

[24] Roozbeh Atri et al. “Deep Learning for Daily Monitoring of Parkinson’s Disease Outside the Clinic Using Wearable Sensors”. In: *Sensors* 22.18 (2022), p. 6831.

[25] Patricia Bet, Paula C Castro, and Moacir A Ponti. “Fall detection and fall risk assessment in older person using wearable sensors: A systematic review”. In: *International journal of medical informatics* 130 (2019), p. 103946.

[26] Shyamal Patel et al. “Monitoring motor fluctuations in patients with Parkinson’s disease using wearable sensors”. In: *IEEE transactions on information technology in biomedicine* 13.6 (2009), pp. 864–873.

[27] Sanghee Moon et al. “Classification of Parkinson’s disease and essential tremor based on balance and gait characteristics from wearable motion sensors via machine learning techniques: a data-driven approach”. In: *Journal of NeuroEngineering and Rehabilitation* 17.1 (2020), pp. 1–8.

[28] Alexandros Papadopoulos et al. “Detecting parkinsonian tremor from IMU data collected in-the-wild using deep multiple-instance learning”. In: *IEEE Journal of Biomedical and Health Informatics* 24.9 (2019), pp. 2559–2569.

[29] Jean-Francois Daneault et al. “Accelerometer data collected with a minimum set of wearable sensors from subjects with Parkinson’s disease”. In: *Scientific Data* 8.1 (2021), pp. 1–13.

[30] Sakorn Mekruksavanich and Anuchit Jitpattanakul. “Multimodal wearable sensing for sport-related activity recognition using deep learning networks”. In: *Journal of Advances in Information Technology* (2022).

[31] Minh H Pham et al. “Validation of a step detection algorithm during straight walking and turning in patients with Parkinson’s disease and

older adults using an inertial measurement unit at the lower back". In: *Frontiers in neurology* 8 (2017), p. 457.

[32] Roth, Nils and Wieland, et al. "Do We Walk Differently at Home? A Context-Aware Gait Analysis System in Continuous Real-World Environments". In: *2021 43rd Annual International Conference of the IEEE Engineering in Medicine & Biology Society (EMBC)*. IEEE. 2021, pp. 1932–1935.

[33] Aldeer, Murtadha and Javanmard, et al. "A review of medication adherence monitoring technologies". In: *Applied System Innovation* 1.2 (2018), p. 14.

[34] Sama, Albert and Pérez-López, et al. "Dyskinesia and motor state detection in Parkinson's disease patients with a single movement sensor". In: *2012 Annual International Conference of the IEEE Engineering in Medicine and Biology Society*. IEEE. 2012, pp. 1194–1197.

[35] Hssayeni, Murtadha D and Adams, Jamie L et al. "Deep learning for medication assessment of individuals with Parkinson's disease using wearable sensors". In: *2018 40th Annual International Conference of the IEEE Engineering in Medicine and Biology Society (EMBC)*. IEEE. 2018, pp. 1–4.

[36] Pfister, Franz MJ and Um, et al. "High-resolution motor state detection in Parkinson's disease using convolutional neural networks". In: *Scientific reports* 10.1 (2020), p. 5860.

[37] Manju Rana and Vikas Mittal. "Wearable sensors for real-time kinematics analysis in sports: A review". In: *IEEE Sensors Journal* 21.2 (2020), pp. 1187–1207.

[38] Julian Varghese et al. "Sensor validation and diagnostic potential of smartwatches in movement disorders". In: *Sensors* 21.9 (2021), p. 3139.

[39] Carissimo, Chiara et al. "Development and assessment of a movement disorder simulator based on inertial data". In: *Sensors* 22.17 (2022), p. 6341.

[40] Mathworks. *imuSensor*. `https://it.mathworks.com/help/nav/ref/imusensor-system-object.html`. Online; accessed 30 September 2023. 2022.

[41] Rodger J Elble. "Tremor: clinical features, pathophysiology, and treatment". In: *Neurologic clinics* 27.3 (2009), pp. 679–695.

[42] Bryan T Cole et al. "Dynamical learning and tracking of tremor and dyskinesia from wearable sensors". In: *IEEE Transactions on Neural Systems and Rehabilitation Engineering* 22.5 (2014), pp. 982–991.

[43] SBG. *Elipse-E*. `https://www.sbg-systems.com/products/ellipse-series/`. Online; accessed 30 August 2023. 2023.

[44] MbientLab. *METAMOTIONRL*. `https://mbientlab.com/metamotionrl/`. Online; accessed 30 August 2023. 2023.

[45] Henderi Henderi, Tri Wahyuningsih, and Efana Rahwanto. "Comparison of Min-Max normalization and Z-Score Normalization in the K-nearest neighbor (kNN) Algorithm to Test the Accuracy of Types of Breast Cancer". In: *International Journal of Informatics and Information Systems* 4.1 (2021), pp. 13–20. ISSN: 2579-7069. DOI: `10.47738/ijiis.v4i1.73`. URL: `http://ijiis.org/index.php/IJIIS/article/view/73`.

[46] Paul F Crawford III and Ethan E Zimmerman. "Differentiation and diagnosis of tremor". In: *American family physician* 83.6 (2011), pp. 697–702.

[47] Mehdi Delrobaei et al. "Towards remote monitoring of Parkinson's disease tremor using wearable motion capture systems". In: *Journal of the neurological sciences* 384 (2018), pp. 38–45.

[48] Habib-ur-Rehman, MRCP. "Diagnosis and management of tremor". In: *Arch Intern Med* 160 (2000), pp. 2438–2444.

[49] Mi Zhang and Alexander A Sawchuk. "A feature selection-based framework for human activity recognition using wearable multimodal sensors." In: *BodyNets*. 2011, pp. 92–98.

[50] Serge H Roy et al. "Resolving signal complexities for ambulatory monitoring of motor function in Parkinson's disease". In: *2011 Annual International Conference of the IEEE Engineering in Medicine and Biology Society*. IEEE. 2011, pp. 4836–4839.

[51] Jenna E Thorp et al. "Monitoring motor symptoms during activities of daily living in individuals with Parkinson's disease". In: *Frontiers in neurology* (2018), p. 1036.

[52] Matlab. *Elipse-E*. `https://it.mathworks.com/help/matlab/ref/double.normalize/`. Online; accessed 1 September 2023. 2023.

[53] Huma Mughal et al. "Parkinson's disease management via wearable sensors: a systematic review". In: *IEEE Access* 10 (2022), pp. 35219–35237.

[54] Angelo Antonini et al. "Toward objective monitoring of Parkinson's disease motor symptoms using a wearable device: wearability and performance evaluation of PDMonitor®". In: *Frontiers in Neurology* 14 (2023), p. 1080752.

[55] MbientLab. *Sensor Fusion*. URL: `https://mbientlab.com/tutorials/SensorFusion.html`. (accessed: 31.01.2023).

[56] Carissimo, Chiara et al. "Parkinson's disease aided diagnosis: online symptoms detection by a low-cost wearable Inertial Measurement Unit". In: *2022 IEEE International Symposium on Medical Measurements and Applications (MeMeA)*. IEEE. 2022, pp. 1–6.

[57] BOSH. *BMI160*. URL: `https://www.bosch-sensortec.com/products/motion-sensors/imus/bmi160/`. (accessed: 30.01.2023).

[58] James Diebel. "Representing attitude: Euler angles, unit quaternions, and rotation vectors". In: *Matrix* 58.15-16 (2006), pp. 1–35.

[59] Parkinson's Foundation. *Bradykinesia*. URL: `https://www.parkinson.org/Understanding-Parkinsons/Symptoms/Movement-Symptoms/Bradykinesia-Slowness-of-Movement`. (accessed: 20.09.2023).

[60] Lina Tong et al. "A Parkinson's Bradykinesia Recognition System Based on Deep Learning Method". In: *2022 12th International Conference on CYBER Technology in Automation, Control, and Intelligent Systems (CYBER)*. IEEE. 2022, pp. 1005–1008.

[61] Ekaterina Kovalenko et al. "Detecting the Parkinson's Disease Through the Simultaneous Analysis of Data From Wearable Sensors and Video". In: *IEEE Sensors Journal* 22.16 (2022), pp. 16430–16439.

[62] Murtadha D Hssayeni et al. "Dyskinesia severity estimation in patients with Parkinson's disease using wearable sensors and a deep LSTM network". In: *2020 42nd Annual International Conference of the IEEE Engineering in Medicine & Biology Society (EMBC)*. IEEE. 2020, pp. 6001–6004.

[63] JL Adams et al. "PD-BioStampRC21: Parkinson's disease accelerometry dataset from five wearable sensor study". In: *IEEE Dataport. https://doi. org/10.21227/g2g8-1503* (2020).

[64] Melissa J Armstrong and Michael S Okun. "Diagnosis and treatment of Parkinson disease: a review". In: *Jama* 323.6 (2020), pp. 548–560.

[65] Peter A LeWitt. "Levodopa therapy for Parkinson's disease: pharmacokinetics and pharmacodynamics". In: *Movement Disorders* 30.1 (2015), pp. 64–72.

[66] Werner Poewe and et al. Antonini. "Levodopa in the treatment of Parkinson's disease: an old drug still going strong". In: *Clinical interventions in aging* 5 (2010), p. 229.

[67] Stanley Fahn. "The history of dopamine and levodopa in the treatment of Parkinson's disease". In: *Movement disorders: official journal of the Movement Disorder Society* 23.S3 (2008), S497–S508.

[68] Ali H Rajput. "Levodopa prolongs life expectancy and is non-toxic to substantia nigra". In: *Parkinsonism & related disorders* 8.2 (2001), pp. 95–100.

[69] Straka, Igor et al. "Adherence to pharmacotherapy in patients with Parkinson's disease taking three and more daily doses of medication". In: *Frontiers in Neurology* 10 (2019), p. 799.

[70] Del Din, Silvia et al. "Validation of an accelerometer to quantify a comprehensive battery of gait characteristics in healthy older adults and Parkinson's disease: toward clinical and at home use". In: *IEEE journal of biomedical and health informatics* 20.3 (2015), pp. 838–847.

[71] Di Libero, Tommaso and Langiano, Elisa et al. "Technological support for people with Parkinson's disease: a narrative review". In: *JOURNAL OF GERONTOLOGY AND GERIATRICS* (2022), pp. 1–15.

[72] Del Din, Silvia and Elshehabi et al. "Gait analysis with wearables predicts conversion to parkinson disease". In: *Annals of neurology* 86.3 (2019), pp. 357–367.

[73] Del Din, Silvia and Godfrey, Alan et al. "Free-living gait characteristics in ageing and Parkinson's disease: impact of environment and ambulatory bout length". In: *Journal of neuroengineering and rehabilitation* 13.1 (2016), pp. 1–12.

[74] Joshi, Rajeshree and Bronstein, et al. "PKG movement recording system use shows promise in routine clinical care of patients with Parkinson's disease". In: *Frontiers in neurology* 10 (2019), p. 1027.

[75] Giannakopoulou, Konstantina-Maria et al. “Internet of Things Technologies and Machine Learning Methods for Parkinson’s Disease Diagnosis, Monitoring and Management: A Systematic Review”. In: *Sensors* 22.5 (2022), p. 1799.

[76] Patel, Shyamal and Lorincz, Konrad et al. “Monitoring motor fluctuations in patients with Parkinson’s disease using wearable sensors”. In: *IEEE transactions on information technology in biomedicine* 13.6 (2009), pp. 864–873.

[77] Carissimo, Chiara et al. “Parkinson’s disease aided diagnosis: online symptoms detection by a low-cost wearable Inertial Measurement Unit”. In: *2022 IEEE International Symposium on Medical Measurements and Applications (MeMeA)*. IEEE. 2022, pp. 1–6.

[78] Del Din, Silvia and Kirk, Cameron et al. “Body-worn sensors for remote monitoring of Parkinson’s disease motor symptoms: vision, state of the art, and challenges ahead”. In: *Journal of Parkinson’s disease* 11.s1 (2021), S35–S47.

[79] Robert A Hauser, Frieda Deckers, and Philippe Lehert. “Parkinson’s disease home diary: further validation and implications for clinical trials”. In: *Movement Disorders* 19.12 (2004), pp. 1409–1413.

[80] Aich, Satyabrata and Youn, et al. “A supervised machine learning approach to detect the on/off state in Parkinson’s disease using wearable based gait signals”. In: *Diagnostics* 10.6 (2020), p. 421.

[81] Mikolaizak, A. Stefanie et al. “Connecting real-world digital mobility assessment to clinical outcomes for regulatory and clinical endorsement–the Mobilise-D study protocol”. In: *PLOS ONE* 17.10 (Oct. 2022), pp. 1–21. DOI: 10.1371/journal.pone.0269615. URL: https://doi.org/10.1371/journal.pone.0269615.

[82] COSMIN. *COSMIN*. URL: https://www.cosmin.nl/. (accessed: 30.01.2023).

[83] General Assembly of the World Medical Association et al. "World Medical Association Declaration of Helsinki: ethical principles for medical research involving human subjects". In: *The Journal of the American College of Dentists* 81.3 (2014), pp. 14–18.

[84] Postuma, Ronald B and Berg, et al. "MDS clinical diagnostic criteria for Parkinson's disease". In: *Movement disorders* 30.12 (2015), pp. 1591–1601.

[85] Jette, Alan M and Haley, Stephen M et al. "Late life function and disability instrument: I. Development and evaluation of the disability component". In: *The Journals of Gerontology Series A: Biological Sciences and Medical Sciences* 57.4 (2002), pp. M209–M216.

[86] Fried, Linda P and Tangen, Catherine M et al. "Frailty in older adults: evidence for a phenotype". In: *The Journals of Gerontology Series A: Biological Sciences and Medical Sciences* 56.3 (2001), pp. M146–M157.

[87] Sebastian Schade, Brit Mollenhauer, and Claudia Trenkwalder. "Levodopa equivalent dose conversion factors: an updated proposal including opicapone and safinamide". In: *Movement disorders clinical practice* 7.3 (2020), p. 343.

[88] Hoehn, Margaret M et al. "Parkinsonism: onset, progression, and mortality". In: *Neurology* 50.2 (1998), pp. 318–318.

[89] Goetz, Christopher G and Tilley, et al. "Movement Disorder Society-sponsored revision of the Unified Parkinson's Disease Rating Scale (MDS-UPDRS): scale presentation and clinimetric testing results". In: *Movement disorders: official journal of the Movement Disorder Society* 23.15 (2008), pp. 2129–2170.

[90] Nieuwboer, Alice and Rochester, Lynn et al. "Reliability of the new freezing of gait questionnaire: agreement between patients with Parkin-

son's disease and their carers". In: *Gait & posture* 30.4 (2009), pp. 459–463.

[91] Nasreddine, Ziad S. and Phillips, et al. "The Montreal Cognitive Assessment, MoCA: A Brief Screening Tool For Mild Cognitive Impairment". In: *Journal of the American Geriatrics Society* 53.4 (2005), pp. 695–699. DOI: https://doi.org/10.1111/j.1532-5415.2005.53221.x. eprint: https://agsjournals.onlinelibrary.wiley.com/doi/pdf/10.1111/j.1532-5415.2005.53221.x. URL: https://agsjournals.onlinelibrary.wiley.com/doi/abs/10.1111/j.1532-5415.2005.53221.x.

[92] Carissimo, Chiara, Gianni Cerro, and et al. "Enhancing remote monitoring and classification of motor state in Parkinson's disease using Wearable Technology and Machine Learning". In: *2023 IEEE International Symposium on Medical Measurements and Applications (MeMeA)*. IEEE. 2023, pp. 1–6.

[93] Aodhán Hickey et al. "Detecting free-living steps and walking bouts: validating an algorithm for macro gait analysis". In: *Physiological Measurement* 38 (2017), N1–N15.

[94] Evers, Luc JW and Raykov, et al. "Real-life gait performance as a digital biomarker for motor fluctuations: the Parkinson@ Home validation study". In: *Journal of medical Internet research* 22.10 (2020), e19068.

[95] Tianjian Ji and Aikaterini Pachi. "Frequency and velocity of people walking". In: *Struct. Eng* 84.3 (2005), pp. 36–40.

[96] *Normalize data - MATLAB normalize*. https://www.mathworks.com/help/matlab/ref/double.normalize.html [accessed: 2023-03-24].

[97] Marianna Alesi et al. “Improving children’s coordinative skills and executive functions: the effects of a football exercise program”. In: *Perceptual and motor skills* 122.1 (2016), pp. 27–46.

[98] Harpreet Singh and Ashwani Saini. “Relationship of coordinative ability with the skills of basketball”. In: *İnternational Journal of Yoga, Physiotheraphy and Physical Education* 2.3 (2017), pp. 56–59.

[99] PV Arjun and KB Sunitha. “Effect of yoga training on coordinative abilities of high school students”. In: *International Journal of Yogic, Huan Movement and Sports Sciences* 4.2 (2019), pp. 63–65.

[100] Francesca Latino, Stefania Cataldi, and Francesco Fischetti. “Effects of a coordinative ability training program on adolescents’ cognitive functioning”. In: *Frontiers in Psychology* 12 (2021), p. 620440.

[101] Iconomescu Teodora-Mihaela, Mindrescu Veronica, and Talaghir Laurentiu-Gabriel. “An investigation into the neuromuscular control at the level of the upper limbs of junior handball girls players”. In: *SHS Web of Conferences*. Vol. 26. EDP Sciences. 2016, p. 01039.

[102] Pankhuri Vairagade and Geeta Bhatt. “International Journal of Allied Medical and Clinical Research (IJAMSCR)”. In: *system* 7 (), p. 0.

[103] Lene H. Jakobsen et al. “Validation of reaction time as a measure of cognitive function and quality of life in healthy subjects and patients”. In: *Nutrition* 27.5 (2011), pp. 561–570. ISSN: 0899-9007. DOI: https://doi.org/10.1016/j.nut.2010.08.003. URL: https://www.sciencedirect.com/science/article/pii/S0899900710002509.

[104] Rafael E Reigal et al. “Relationships between reaction time, selective attention, physical activity, and physical fitness in children”. In: *Frontiers in Psychology* 10 (2019), p. 2278.

[105] Mina Keshavarz and Jalal Dehghanizade. "The Effects of Gender and Type of Stimulus Presentation on Serial Reaction Time". In: *International Journal of Motor Control and Learning* 2.4 (2020), pp. 20–29.

[106] Sandeep Kumar Biswas, Maman Paul, and Jaspal Singh Sandhu. "Role of sports vision and eye hand coordination training in performance of table tennis players". In: *Brazilian Journal of Biomotricity* 5.2 (2011), pp. 106–116.

[107] Rafael E Reigal et al. "Relationships between reaction time, selective attention, physical activity, and physical fitness in children". In: *Frontiers in Psychology* 10 (2019), p. 2278.

[108] Kimberley S van Schooten et al. "Catch the ruler: concurrent validity and test–retest reliability of the ReacStick measures of reaction time and inhibitory executive function in older people". In: *Aging Clinical and Experimental Research* 31.8 (2019), pp. 1147–1154.

[109] Noreen Akram et al. "Developing and assessing a new web-based tapping test for measuring distal movement in Parkinson's disease: a Distal Finger Tapping test". In: *Scientific reports* 12.1 (2022), pp. 1–11.

[110] Pio Alfredo Di Tore and Gaetano Raiola. "Exergames in motor skill learning". In: *Journal of physical education and sport* 12.3 (2012), p. 358.

[111] Nancy Laurenson. "Physical Education and the Study of Sport". In: *British Journal of Sports Medicine* 25.4 (1991), p. 246.

[112] Richard W Bohannon and Inga Wang. "Measurement of finger tapping performance using a smartphone application: a pilot study". In: *Journal of Physical Therapy Science* 33.8 (2021), pp. 618–620.

[113] Mackenzie. *Ruler Drop Test*. URL: `https://www.brianmac.co.uk/rulerdrop.htm`. (accessed: 31.05.2022).

[114] MbientLab. *MetaBase App*. URL: https://mbientlab.com/tutorials/MetaBaseApp.html. (accessed: 06.02.2022).

[115] Carissimo, Chiara et al. "Objective evaluation of coordinative abilities and training effectiveness in sports scenarios: an automated measurement protocol". In: *IEEE Access* (2023).

[116] Matlab. *Find abrupt changes*. URL: https://it.mathworks.com/help/signal/ref/findchangepts.html. (accessed: 08.02.2022).

[117] Matlab. *Find Peaks*. URL: https://it.mathworks.com/help/signal/ref/findpeaks.html. (accessed: 08.02.2022).

[118] Milton Friedman. "A Comparison of Alternative Tests of Significance for the Problem of m Rankings". In: *The Annals of Mathematical Statistics* 11.1 (1940), pp. 86–92. DOI: 10.1214/aoms/1177731944. URL: https://doi.org/10.1214/aoms/1177731944.

[119] *Practical Nonparametric Statistics, 3rd Edition — Wiley*. URL: https://www.wiley.com/en-us/Practical+Nonparametric+Statistics%5C%2C+3rd+Edition-p-9780471160687 (visited on 05/26/2023).

[120] Amanda Ross and Victor L. Willson. "Paired Samples T-Test". In: *Basic and Advanced Statistical Tests: Writing Results Sections and Creating Tables and Figures*. Rotterdam: SensePublishers, 2017, pp. 17–19. ISBN: 978-94-6351-086-8. DOI: 10.1007/978-94-6351-086-8_4. URL: https://doi.org/10.1007/978-94-6351-086-8_4.

[121] John Rothwell et al. "Central nervous system physiology". In: *Clinical Neurophysiology* 132.12 (2021), pp. 3043–3083.

[122] TF Calvin, Alison C McDonald, and Peter J Keir. "Adaptations to isolated shoulder fatigue during simulated repetitive work. Part I: Fatigue". In: *Journal of Electromyography and Kinesiology* 29 (2016), pp. 34–41.

[123] Divya Srinivasan and Svend Erik Mathiassen. "Motor variability in occupational health and performance". In: *Clinical biomechanics* 27.10 (2012), pp. 979–993.

[124] Elena Madinabeitia-Mancebo et al. "Peripheral-central interplay for fatiguing unresisted repetitive movements: a study using muscle ischaemia and M1 neuromodulation". In: *Scientific reports* 11.1 (2021), pp. 1–13.

[125] Aranza Vila-Villar et al. "Exploring the role of the left DLPFC in fatigue during unresisted rhythmic movements". In: *Psychophysiology* (2022), e14078.

[126] Elena Madinabeitia-Mancebo et al. "Peripheral-central interplay for fatiguing unresisted repetitive movements: a study using muscle ischaemia and M1 neuromodulation". In: *Scientific reports* 11.1 (2021), pp. 1–13.

[127] Antonio Madrid et al. "Effects of a finger tapping fatiguing task on M1-intracortical inhibition and central drive to the muscle". In: *Scientific reports* 8.1 (2018), pp. 1–10.

[128] Callum G Brownstein et al. "Fatigue-induced changes in short-interval intracortical inhibition and the silent period with stimulus intensities evoking maximal versus submaximal responses". In: *Journal of Applied Physiology* 129.2 (2020), pp. 205–217.

[129] Pablo Arias et al. "Validity of the finger tapping test in Parkinson's disease, elderly and young healthy subjects: Is there a role for central fatigue?" In: *Clinical Neurophysiology* 123.10 (2012), pp. 2034–2041.

[130] Rizwan Qaisar, Shylesh Bhaskaran, and Holly Van Remmen. "Muscle fiber type diversification during exercise and regeneration". In: *Free Radical Biology and Medicine* 98 (2016), pp. 56–67.

[131] Gøran Paulsen et al. “Maximal eccentric exercise induces a rapid accumulation of small heat shock proteins on myofibrils and a delayed HSP70 response in humans”. In: *American Journal of Physiology-Regulatory, Integrative and Comparative Physiology* 293.2 (2007), R844–R853.

[132] Elwood Henneman, George Somjen, and David O Carpenter. “Functional significance of cell size in spinal motoneurons”. In: *Journal of neurophysiology* 28.3 (1965), pp. 560–580.

[133] TAR Schreuders, JW Brandsma, and HJ Stam. “The intrinsic muscles of the hand”. In: *Physikalische Medizin, Rehabilitationsmedizin, Kurortmedizin* 17.01 (2007), pp. 20–27.

[134] Ivana Pajic-Lijakovic. “The basic concept of viscoelasticity”. In: *Viscoelasticity and collective cell migration*. Elsevier, 2021, pp. 21–46.

[135] David G Behm et al. “Acute effects of muscle stretching on physical performance, range of motion, and injury incidence in healthy active individuals: a systematic review”. In: *Applied physiology, nutrition, and metabolism* 41.1 (2016), pp. 1–11.

[136] Frank G Shellock and William E Prentice. “Warming-up and stretching for improved physical performance and prevention of sports-related injuries”. In: *Sports medicine* 2.4 (1985), pp. 267–278.

[137] Jules Opplert and Nicolas Babault. “Acute effects of dynamic stretching on mechanical properties result from both muscle-tendon stretching and muscle warm-up”. In: *Journal of sports science & medicine* 18.2 (2019), p. 351.

[138] Ralph M Reitan and Deborah Wolfson. “3/The Halstead-Reitan neuropsychological test battery and aging”. In: *Clinical Gerontologist* 5.1-2 (1986), pp. 39–61.

[139] Ronald M Ruff and Stephen B Parker. "Gender-and age-specific changes in motor speed and eye-hand coordination in adults: normative values for the Finger Tapping and Grooved Pegboard Tests". In: *Perceptual and motor skills* 76.3_suppl (1993), pp. 1219–1230.

[140] T Di Libero et al. "Motor abilities analysis using a standardized tapping test enhanced by a detailed processing stage: gender and age comparison". In: *2023 IEEE International Symposium on Medical Measurements and Applications (MeMeA)*. IEEE. 2023, pp. 1–6.

[141] Jules Opplert and Nicolas Babault. "Acute effects of dynamic stretching on mechanical properties result from both muscle-tendon stretching and muscle warm-up". In: *Journal of sports science & medicine* 18.2 (2019), p. 351.

[142] Ivana Pajic-Lijakovic. "The basic concept of viscoelasticity". In: *Viscoelasticity and collective cell migration*. Elsevier, 2021, pp. 21–46.

[143] Elwood Henneman, George Somjen, and David O Carpenter. "Functional significance of cell size in spinal motoneurons". In: *Journal of neurophysiology* 28.3 (1965), pp. 560–580.

[144] TAR Schreuders, JW Brandsma, and HJ Stam. "The intrinsic muscles of the hand". In: *Physikalische Medizin, Rehabilitationsmedizin, Kurortmedizin* 17.01 (2007), pp. 20–27.

[145] April L McPherson and Takashi Nagai. "High school male basketball athletes exhibit greater hamstring muscle stiffness than females as assessed with shear wave elastography". In: *Skeletal radiology* 49 (2020), pp. 1231–1237.

[146] Hoge, Katherine M and Ryan, Eric D. "Gender differences in musculotendinous stiffness and range of motion after an acute bout of stretching". In: *The Journal of Strength & Conditioning Research* 24.10 (2010), pp. 2618–2626.

[147] Yu, Suiqing and Lin, Lihua. “Gender difference in effects of proprioceptive neuromuscular facilitation stretching on flexibility and stiffness of hamstring muscle”. In: *Frontiers in Physiology* (2022), p. 1480.